Lateral Buckling of On-bottom Pipelines in Sand

Yongwei Li

The University of Oxford

St Hugh's College

A thesis submitted for the degree of

Master of Science

Trinity 2015

Table of Contents

ABSTRACT

Recent oil and gas developments in remote offshore locations require the construction of long seabed pipelines that operate under high temperature and pressure. Stress induced by thermal expansion of unburied seabed pipelines causes buckling and lateral deformation of the pipeline, which can damage the pipe and affect its overall integrity. A cost-effective design is to relieve the stress through controlled lateral buckling, which requires accurate and reliable assessment of the lateral resistance of pipe-soil interface.

Previous investigating of pipe-soil interface behaviour refers to the following 4 aspects: 1) the initial embedment of pipeline at installation, 2) breakout resistance during buckle formation, 3) Large amplitude displacement as buckle takes place; and 4) reduction effect in stability due to cyclic loading. This study aims at developing a better understanding of the pipe-soil interaction system in terms of lateral stability. To analyse and predict the pipe-soil response, a series of laboratory tests were conducted on a loose dry sand bed. Three types of load-controlled/displacement-controlled tests, namely 1) penetration test, 2) side swipe test and 3) probe test were designed and conducted to estimate the influence of the key parameters on the lateral buckling resistance of a shallowly embedded pipe in sand.

ACKNOWLEDGEMENT

I would like to show my gratitude to the following people for their help and support in my mater by research project over the past years.

First of all, my deepest thanks must go to my supervisor, Prof Byron Byrne, whose encouragement, guidance and support enabled me to complete this research study. Every discussion with him, not only on the research, but also on any other aspects, has been very useful and inspirational.

I am also thankful to the technical support in the University of Oxford. During my research, Mr Bob Sawala and Mr Clive Baker provided solid and sound help in building up the experimental apparatus, which has been a key success to this study.

I would also like to acknowledge to my friends and fellow research students in the Civil Engineering Group in the University of Oxford for valuable discussion and suggestions. They include Mr Deqiong Kong, Mr Boshu Zhang, Dr Boon Chia, Dr Laith Tapper, Mr Weerasinghe M. I am particullay greatful to Dr Boon Chia, Dr Laith Tapper for their help in proof reading my thesis.

Finally, I have dedicated this dissertation to my parents and Miss Qian Lei for their love, encouragement and endless emotional support.

LIST OF FIGURES AND TABLES

CHAPTER 1 INTRODUCTION

1 . 1 Background

As the demand for oil and gas increases, the focus of fuel energy extraction has gradually shifted from close to shore to much further offshore. Pipelines have been proved to be efficient for transporting oil and gas, especially in deep water. It is reported that the energy consumption for crude oil trunk lines is about half of what is needed for tankers (Kennedy 1993). Tens of thousands of kilometres of offshore pipelines have been installed in various water depths as well as different soil conditions (Zhang, 2001). However, as the temperature and pressure experienced by the pipeline changes greatly between operation cycles, the pipeline will naturally relieve the resulting high compressive axial stress through the pipe by buckling. This may be even more severe as most of the pipeline projects are of a large length. The uncontrolled lateral buckling can greatly affect the integrity of the pipeline with resulting cracks and excessive deformation, and therefore cause the failure of the project.

A common practice that has been applied in shallow water (typically refer to the projects with water depths under 300m) is to bury the pipeline in a pre-cut trench, which is backfilled afterwards such that the excessive lateral buckling can be fully restrained. These measures are performed such that the pipeline installed underwater remains stable against

wave and current-induced force, and that protect the pipe against potential damage from anchors and/or fishing gears. However, this solution tends to be less effective when the offshore development gradually shifts to deeper water. These pipeline projects are often tens of kilometers from shore, with water depths of over 1000m where more extreme conditions are encountered. The high surrounding pressure requires trenching and jetting to take place at even higher working pressure, which consequently increases the cost considerably. Therefore, a far more elegant and also cost-effective approach is required.

An alternative solution to this is work with rather than against the pipeline by controlling the formation of lateral buckling along the pipeline (Bruton *et al.*, 2006). At the point of lateral buckling, the resistance against excessive lateral movement can only be resisted by the surrounding soil. This soil mainly consist of sands, soft clay and weak sediments, which may be easily liquefied or weakened under cyclic loading such as wave and current loads. As a result, it is important to develop an accurate and sound assessment to address the lateral breakout resistance of pipelines.

1 . 2 Pipeline Upheaval and Lateral Buckling

Pipelines are considered as long and slender members, and they tend to buckle in either vertical or horizontal directions (shown in Figure 1.1 and 1.2) when subjected to

compressive forces. In the case of buried pipelines, lateral restraint is provided by the surrounding soils, and typical failure of pipeline buckle tends to form in the vertical direction, causing an upheaval buckling (Figure 1.1). On the other hand, the on-bottom pipelines are less laterally restrained and hence they tend to develop displacement in the lateral direction (Figure 1.2). Because of the direct exposure of the pipelines against water, on-bottom pipelines may be subjected to considerable cyclic hydrodynamic loads resulting from current, waves and other environmental forces. These cyclic loads degrade the engineering properties which makes a critical point of lateral instability. Moreover, the temperature and pressure of the oil and gas that are transported through the pipe are significantly higher than those outside the seawater. Typical values of the pressure and temperature within the pipeline were 21MPa and 140℃ respectively, recorded from an offshore project of Borneo (Kristiansen *et al.*, 2005); meanwhile, the normal pressure and temperature of the surrounding seawater were merely 500kPa and 2℃, respectively. The increase of internal pressure and temperature due to heat transfer from the fluid induces axial stresses in the pipeline wall. Because of the heating up and cooling down processes inside the pipeline during and after operation, excessively extensive deformations are expected to occur, and as a result an increase in the compressive stress throughout the pipeline. Therefore pipelines are susceptible to buckle much more easily due to the large slenderness ratio of a typical pipeline. The lateral buckling design approach allows pipe to

break out from its as-laid position and move across seabed, typically by several diameters (Bruton, 2007). In this way the excessive compressive axial stress can be relived through the controlled lateral displacement and hence achieves the economic design.

Figure 1.1 Pipeline buckles in vertical direction (Upheaval Buckle), Mitsuya 2013

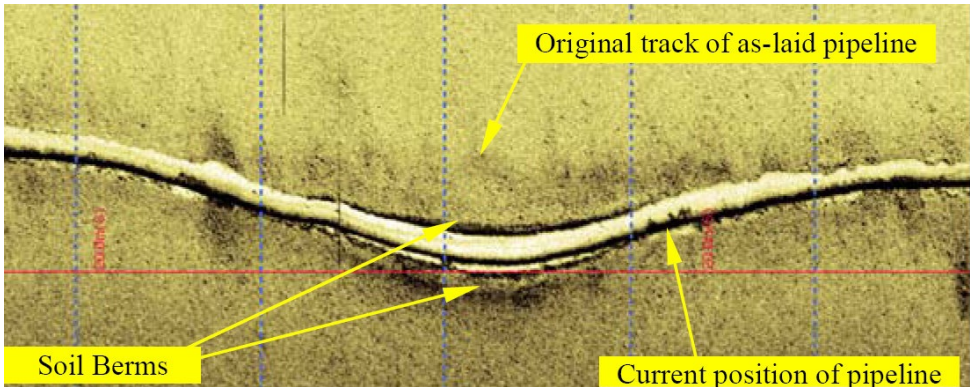

Figure 1.2 Pipeline buckles in horizontal direction (Lateral Buckle), Bruton 2007

According to the installation method, the loading condition on the pipe can be classified into two groups: 1) Over Penetrated, and 2) Normally Penetrated, regarding the loading history on the soil. The over penetrated condition is defined as the range under which the loads applied on the pipe-soil interface are smaller than the maximum load that was applied onto the soil in its loading history; whereas the normally penetrated condition indicates that the current load which the soil surface is experiencing is the maximum load in the loading

history of the surrounding soil. In the design of a pipeline system with certain allowable lateral buckling the pipe-soil relationship would be the largest and most challenging uncertainty. With lateral displacement it is vital to understand the soil behavior at large displacements and through many cycles beyond the point of break-out. An improvement in soil stability is expected under the over penetrated condition where the soil is compacted and consolidated so that the engineering properties are reinforced.

1 . 3 Pipe-soil interaction

In an offshore engineering design, seabeded soil often treated as a material with large uncertainty. Therefore it is reasonable to believe that the critical failure will occur at pipe-soil interface, or somewhere in the soil near the pipe surface (This may happen to pipe buried in clay with high cohesion). For a long pipeline, the problem can be simplified by imaginarily cutting the pipeline into small segments along the length of pipe, and for each segment analysing the individual pipe-soil relationship based on local friction properties that may be obtained by laboratory testing.

Due to similar source of loading and behaviour of shallow foundations and pipelines, the modelling of pipe-soil interactions in previous work is based on an assumption that the pipelines under investigation were idealised as an equivalent infinitely long strip footing

with modified width and other properties. However, pipelines with circular cross section have high torsion rigidity compared that of a rectangular shallow foundation/strip footing (Zhang, 2001). Therefore pipeline stability against torsion is considered to be less crucial.

The embedment ratio associated with a pipeline is likely to have significant influence on the stability given that the typical embedment ratio of a pipeline ranges from 5% of its diameter up to half of its diameter. More importantly, the largest difference between the two cases are that much larger lateral displacements will be expected to occur when a pipeline is subjected to dynamic environmental and internal loads, causing a major change in the geometry of seabed (lateral walking of pipeline will swipe the surrounding soil away and thus alter the seabed geometry and possibly affecting its engineering properties). These issues should be addressed in the model which is being developed for the behaviour of the pipe-soil interaction system. The characteristic combination of the (V:H:M) vertical: horizontal: moment loads are given in Figure 1.3.

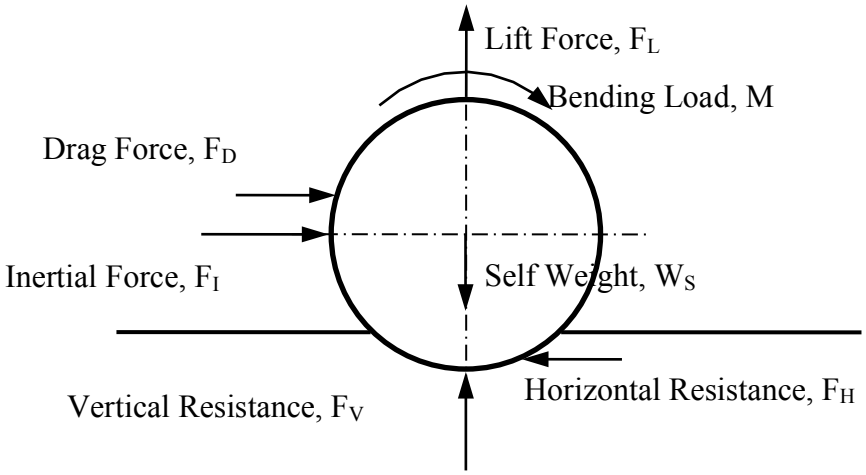

Figure 1.3 Force Balance Diagram of a Typical Pipeline (Zhang, 2001)

1 . 4 Objectives

The primary aim of the research is to develop a rigorous model which captures the key characteristics of the load-displacement response of the lateral pipe-soil interaction system, so that it can be applied to assess the performance of an on-bottom pipeline design on lateral buckling behaviour. In addition, the small and large displacement tests involved in the research are carried out carefully such that they will provide a sound and accurate database for parametric analysis in monitoring the important parameters which govern the overall lateral stability of the pipeline.

CHAPTER 2 LITERATURE REVIEW

2. 1 Introduction

Physical modelling of pipe-soil interaction behaviour for untrenched pipeline has been carried out in clay and sand, since these materials are found on most seabeds where pipeline are installed. A large number of experiments have been carried out with respect to different testing conditions (summarised in Table 2.1), and considerable insights have been drawn to investigate the key parameter on the lateral pipeline instability.

2. 2 Vertical Resistance of Pipeline

2.2.1 Pipe Penetration in Clay

In order to achieve a more economic design, the recent offshore pipelines projects tend to be implemented with the on-bottom pipelines that are laid on the seabed without burial. In this case, the pipeline embedment is related both to the self-weight of the pipeline and to the surrounding hydrodynamic forces that act on the pipeline during installation. This embedment is an important factor to affect the stability of the entire pipe-soil system, as it provides an initial barrier against the subsequent lateral movement when the pipe buckles due to thermal expansion. A pipeline with deeper initial embedded depth is expected to receive more stable and sufficient lateral resistance; however it would reduce the convective heat loss during operation, and thus would result in higher temperature and a more severe

buckling problem. This concern is of vital importance in pipeline projects with a clayey surrounding (Lee, 2012), though less significant for pipelines operating on sand.

During real pipe laying process, the pipe was often pushed into soil, and this could inevitably create heaves that may induce some changes to the pipe-soil stability system (Figure 2.1). In early studies the effect of heave was neglected due to the large slenderness ratio (L/D) of a typical pipeline, and therefore this simplified the problem to a limited plane strain condition (Murff *et al.*, 1989). However, considering the buoying effect of pipeline that were penetrated into clayey soil underwater, Randolph *et al.* included the effect of heave to the analysis, which will be discussed further in this chapter.

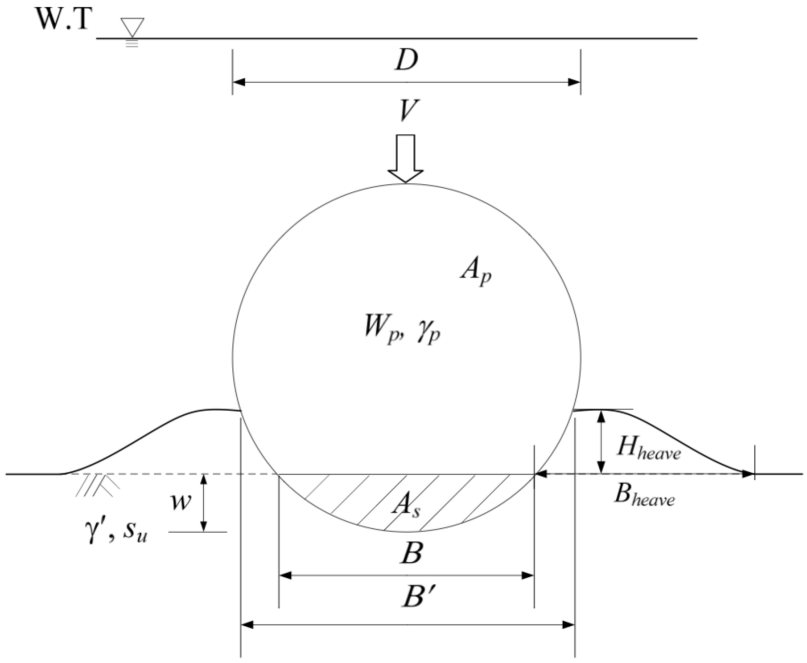

Figure 2.1 Partially Embedded Pipeline and Heave Generated due to Push-in (Lee, 2012)

The early analysis of vertical resistance of pipeline were mainly based on considering the pipe as a slender stripe footing with an equivalent base length of its chord length B' (see Figure 2.1). Based on an extensive laboratory-testing program, Verley and Lund (1995) proposed an empirical equation to estimate the vertical resistance of pipelines on clay:

$$\frac{w}{D} = 0.0072\left(\frac{V}{Ds_u}\left(\frac{s_u}{D\gamma}\right)^{0.3}\right)^{3.2} + 0.062\left(\frac{V}{Ds_u}\left(\frac{s_u}{D\gamma}\right)^{0.3}\right)^{0.7}, \qquad 2\text{-}1$$

where γ is the unit weight of soil. This formula is adopted for the pipeline design in the recommended practice DNV-RP-F109.

Murff *et al.* (1989) used a lower bound and upper bound plasticity solution to link the vertical penetration resistance with the pipe embedment less than half of its diameter (w/D < 0.5). Aubeny *et al.* (2005) then introduced a dimensionless indicator $\eta = kD/s_u$ to track the strength variation. A curve fit was proposed to examine the vertical resistance in the form of the following:

$$\frac{V}{Ds_u} = a\left(\frac{w}{D}\right)^b, \qquad 2\text{-}2$$

where s_u is the undrained shear strength of soil, and a, b are shape factors obtained from curve-fitting and are found to be dependent on the relative roughness of the pipe-soil interface. For a fully smooth pipe, the simulation gave an estimation of a =4.97 and

$b = 0.23$; whilst for a fully rough pipe, the corresponding values are 6.73 and 0.29 respectively.

Referring to the laboratory testing data from the Safebuck Joint Industrial Project, Bruton *et al.* (2006) also proposed an empirical fit in the form of the above equation. The vertical resistance is expressed as follows:

$$\frac{w}{D} = \frac{S_s}{15}\left(\frac{V}{Ds_u}\right)^2, \qquad 2\text{-}3$$

where S_s is introduced as a factor that accounts for the effect of soil sensitivity.

As mentioned above, the effect of heave in fact may not be neglected. Recalling Figure 2.1, if the pipe was considered penetrated into the soil without creating a heave, the submerged weight of the pipe would be reduced due to the buoyancy effect of soil, such that

$$V' = V - \gamma' A_s, \qquad 2\text{-}4$$

where γ' is the effective unit weight of soil, and A_s is the cross-section area of the submerged pipe segment (assuming a pipe segment of unit length), shown in Figure 2.1. A_s can be calculated using the following equation:

$$A_s = \frac{D^2}{4}\left[sin^{-1}\left(2\sqrt{\frac{w}{D}\left(1-\frac{w}{D}\right)}\right) - 2\left(1-\frac{2w}{D}\right)\sqrt{\frac{w}{D}\left(1-\frac{w}{D}\right)}\right]. \qquad 2\text{-}5$$

It is clear form Figure 2.1 that the existence of the heave increases the submerged area A_s,

which in turn increases the buoyancy effect. Randolph *et al.* (2008) introduced a factor, i.e. f_b, to account for the effect of heave:

$$\frac{V}{Ds_u} = a\left(\frac{w}{D}\right)^b + f_b\frac{\gamma' A_s}{Ds_u}, \qquad 2\text{-}6(a)$$

which can be re-written in the form of dimensionless group:

$$\frac{V}{Ds_u} = a\left(\frac{w}{D}\right)^b + f_b\frac{A_s}{D^2}\left(\frac{\gamma' D}{s_u}\right). \qquad 2\text{-}6(b)$$

Results of large displacement finite element analyses indicate a good fit value of f_b to be 1.5, where the heave can contribute to as high as approximately 16% of the total resistance for a pipe with 0.5D of embedment. Note that the early method can be integrated by taking f_b as 1.0, representing a plane strain condition where the effect of initial heave is neglected.

Alternatively, the American Gas Association (AGA) pipeline design guideline suggested that the partially embedded pipelines could be regarded as strip footings with a circular cross-section. Merifield *et al.* (2009) conducted the analytical solutions for the vertical resistance by adopting this concept. The ultimate bearing capacity for strip footing is:

$$q_u = N_c s_u + N_{sw}\gamma' w, \qquad 2\text{-}7$$

where $q_u = \frac{V}{D}$, N_c is the bearing capacity factor, and N_{sw} is self-weight factor respectively. Therefore

$$\frac{V}{Ds_u} = N_c + \frac{wN_{sw}}{D}\frac{\gamma' D}{s_u}. \qquad 2\text{-}8$$

By comparing this equation to the Randolph formula (Equation 2-7), it can be obtained that

$$N_c = a\left(\frac{w}{D}\right)^b, \qquad 2\text{-}7(a)$$

$$N_{sw} = f_b \frac{A_s}{Dw}. \qquad 2\text{-}7(b)$$

2.2.2 Pipe Penetration in Sand

2.2.2.1 Vertical Response under Monotonic Loading

Unlike clay, sand has high initial void ratio and compressibility, and this implies a different failure mode of shallow foundations to be the punching shear failure. However, similar insights can still be obtained from the modelling of shallow foundations in sand under vertical loading. Zhang (2009) proposed a model for vertical response of pipelines on calcareous sand, which is based on a plain-strain pipe-soil system. Due to high compressibility, the plastic vertical load-displacement behaviour is found to be quasi-linear with an application of a plastic stiffness factor k_{vp}:

$$V = k_{vp} w. \qquad 2\text{-}8$$

When the pipe reaches equilibrium, the vertical resistance of soil should be equal to the sum of its self-weight and other vertical components of hydraulic forces. By introducing the concept of plastic displacement as $w_p = w - w_e$, where the elastic displacement is simply

$w_e = {}^{V}/_{k_{ve}}$, the maximum vertical resistance can be expressed as the following:

$$V_{max} = \frac{k_{ve}k_{vp}}{k_{ve}-k_{vp}} w_p. \quad 2\text{-}9$$

For an untrenched pipeline being laid on sand surface underwater, gradual settlement occurs, and the pipeline will continue to be self-pushed into the underlying soil until the soil gains sufficient bearing capacity and forms equilibrium against the pipe self-weight. The AGA guidelines also suggests a generalised equation of ultimate bearing capacity for strip footings on sand:

$$q_u = 0.5\gamma B N_\gamma + \gamma' w_0 N_q, \quad 2\text{-}10$$

where B is the contact width of the strip footing, and N_γ and N_q are the bearing capacity factors. However the geometry of the pipe bottom has determined a different contact surface other than that of shallow foundations. The soil displaced by the pipe will generate an initial berm that helps to increase the contact area. The increase of this contact area as the pipe penetrates will result in a different load distribution on the surrounding soils. In terms of pipelines with a circular cross-section (Figure 2.2), the contact width B is replaced by an equivalent contact width B' that can be calculated based on the pipe diameter D and the embedded depth w_0:

$$B' = 2\sqrt{Dw_0(1 - w_0)}. \quad 2\text{-}11$$

The size of the displaced soil is calculated as:

$$V_{disp} = \frac{D^2}{8}(2\theta - sin2\theta), \quad 2\text{-}12$$

where the angle θ can be defined as

$$sin\theta = B/D = 2\sqrt{w_0/D - (w_0/D)^2}. \quad 2\text{-}13$$

The height of the heaved soil zone h_t can be derived as the following:

$$h_t = \frac{D^2}{4B}(2\theta - sin2\theta). \quad 2\text{-}14$$

Therefore the equivalent width of the contact area can be estimated using

$$B' = 2\sqrt{D(w_0 + h_t) - (w_0 + h_t)^2}. \quad 2\text{-}15$$

This approach shows that the bearing capacity, or the pipe self-weight, appears to be in an approximately linear relation with the embedded depth, and can be used to roughly estimate the preliminary penetration of pipelines.

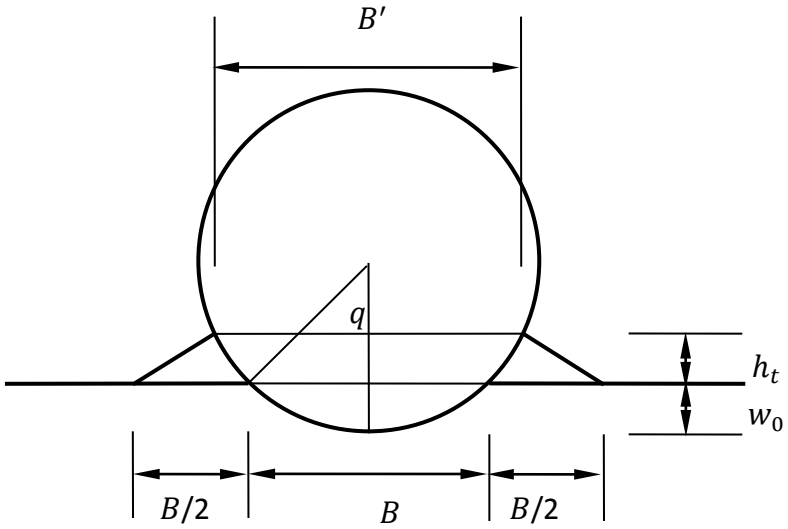

Figure 2.2 Equivalent Width of Pipeline (Zhang, 2009)

2.2.2.2. Load-unload-reload Process

As shown in Figure 2.3, when the pipeline reaches the maximum vertical capacity and then unloads, an excessive component of the displacement can be observed, often termed as the plastic displacement, w_p. The vertical response for unloading can be described as the following:

$$w = w_{pmax} + w_e \qquad 2\text{-}16(a)$$

$$w = \frac{k_{ve}-k_{vp}}{k_{ve}k_{vp}} V_{max} + \frac{V}{k_{ve}}, \qquad 2\text{-}16(b)$$

where V_{max} remains unchanged. The transition portion of the reload curve joining the plastic response can be expressed as:

$$w_p = V_{max}\left(\frac{1}{k_{vp}} - \frac{1+s\alpha}{(1+\alpha)k_{ve}}\right) \qquad 2\text{-}17(a)$$

$$V'_{max} = k_{vp}\frac{w - V/k_{ve}}{1-(1+s\alpha)/(1+\alpha)(k_{vp}/k_{ve})}, \qquad 2\text{-}17(b)$$

where α is the parameter that controls the curvature of the reloading curve, and s is an indicator that defines the extent of the elastic zone ($0 < s \leq 1$).

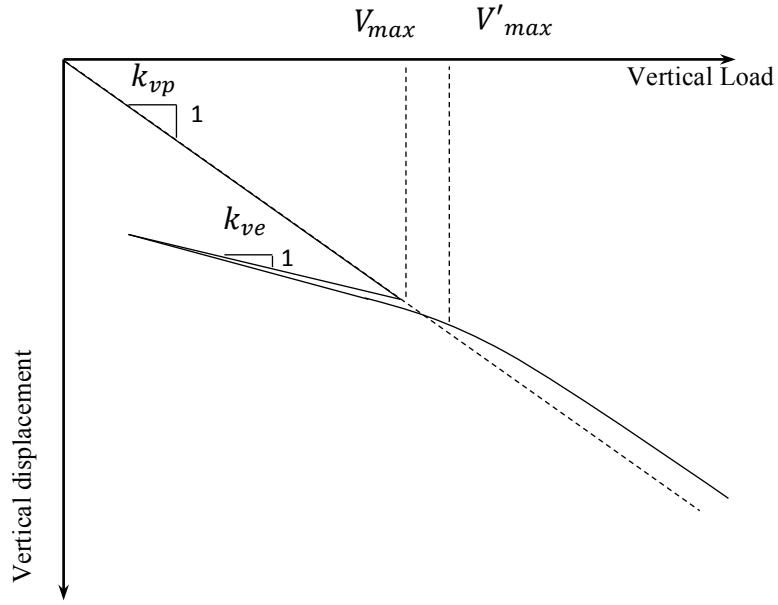

Figure 2.3 Elastic-to-plastic Behaviour of Load-unload-reload Process

Note that the above equation reverts back to the unloading curve for $\alpha = 0$ and $s = 1$. This implies that the reloading process is under pure elastic behaviour, and no transit is observed at the point of unloading.

2.2.2.3 Cyclic Loading under Drained Condition

Due to high void ratio of sand, soil may become more compact during cyclic loading, and hence bearing capacity is improved. In Zhang's model (2001, 2009), a multiplier c is applied to the formula to describe the unloading-reloading process:

$$V'_{max} = c\left(\frac{1+\alpha}{1+s\alpha}\right)V_{max}, \qquad 2\text{-}18$$

and the multiplier is expressed as

$$c = c_{max} - (c_{max} - 1)e^{-(\lambda w_{pc}/D)}, \qquad 2\text{-}19$$

where λ is an empirical parameter derived from calibration tests and w_{pc} is the accumulated plastic displacement over cycles.

2. 3 Lateral Resistance of Pipeline

2.3.1 Friction Model

In the very first stage of this research area, Lyons (1973) put forward a "friction model" based on the coulomb friction theory. In this approach the horizontal resistance of a pipe-soil interface was assumed proportional to its vertical load. The ratio of lateral load to vertical load, i.e. the friction coefficient μ, has become the most critical parameter in the small amplitude experiments that were carried out thereafter. Peak horizontal resistance was observed to occur at around 10% of pipe diameter, and it remained constant throughout the test. Lyons explained that this was a result of the accumulated soil berm in the initial stage of pipe movement, and consequently a maximum resistance against the pipe segment was achieved near the point where the pipe climbed over the soil mound. The maximum friction coefficients in the model were calculated through various tests (listed in Table 2.1), and had values between 0.45 and 0.75. It is worth mentioning that the value of this pipe-soil interface friction factor was found to be almost equal to the tangent of the internal friction

angle of sand. In this model, the ultimate horizontal resistance was simply represented as a direct multiplication of the vertical load acting on the pipeline and this friction coefficient, i.e. $H = \mu V$.

However, the friction model above is not sufficient to represent the real case of pipeline lateral behaviour in deeper water depth, where a more sophisticated model is required to describe the pipe-soil response at larger penetration depth. The maximum penetration can reach as high as 0.5D in some preliminary experimental studies of model pipeline under combined loadings. Among these tests, the strain hardening was recorded after lateral cyclic loading test of shallowly embedded pipelines, whereas softening occurred on pipelines for deeper embedment (Brennodden *et al.,* 1986). According to large-scale test results, under cyclic lateral loading the friction factors increased to 0.85 for dense sand and 1.3 for loose sand respectively, in comparison to around 0.75 for both sand conditions under simple lateral loading. The inconsistency of the friction factor under different loading conditions has limited the accuracy and reliability to evaluate soil lateral resistance.

Further experiment has been carried out, and a modified friction model was put forward. This approach concluded that the increase of pipeline penetration during its loading history would cause a rise in its lateral resistance (Wagner *et al.,* 1987). The lateral buckling

behaviour of pipeline was therefore proposed by adding an additional component – a term that represents the effectiveness of further penetration – to the original expression. The proposed modified friction model is written in terms of the friction factor μ, the penetration and soil strength of the surrounding seabed, as follows:

$$H = H_f + H_p, \qquad 2\text{-}20$$

where H is the ultimate lateral resistance of pipeline; H_f is the friction component which is given by $H_f = \mu \times V$; H_p is known as a passive component that is contributed by the penetration of the pipeline, and is expressed as a function of unit weight γ and cross-sectional area of the resultant soil berm A.

$$H_p = 0.5\beta_p \gamma' A\ (sand), and \qquad 2\text{-}21(a)$$

$$H_p = 0.5\beta_p S_u DA\ (clay). \qquad 2\text{-}21(b)$$

The modified friction model is a rather rigorous model in determining the capacity of the soil seabed where the pipelines were installed. However, the evaluation of the factor β_p was not clear, and the suggested model only used empirical solutions obtained from the tests under specific loading and soil conditions. In other words, the aim of fully understanding such relationship between pipe wall and surrounding soil is merely partly achieved. An adequate design work should not be restricted to a simple stability problem, and an additional modelling of the pipe movement over a considerable lateral displacement

(of the order of 10D) is required.

From the previous published data, it is shown that under lateral loading the pipe also moved vertically (known as penetration) either downward or upward, which indicates the coupling of the horizontal and vertical responses. The vertical movement of the pipeline during lateral loading defines the additional passive component of the modified friction factor H_p. This can be related to the additional embedment from horizontal loading, which is in fact an accumulation of vertical displacement.

Additionally, Wagner *et al.* (1987) conducted a series of finite element analyses to examine the lateral resistance of a partially embedded pipe at large displacement. Results showed that the lateral resistance of the pipe at large displacement was largely dependent on the pipe embedment. They proposed the concept of an effective embedment w'/D to account for the height of the berm ahead of the pipe. This was different from the conventional use of pipe embedment w/D that was defined as the elevation of the soil surface relative to the pipe invert. Based on the finite element results, they proposed a power law function to link the lateral resistance with the effective embedment w'/D.

White and Cheuk (2007) used a kinematic hardening model and presented a design

framework that allows the existing pipe-soil interaction models to be extended to capture the large displacement effect. Typically the effects of the active soil berm created during the lateral walking of pipeline were addressed in the model. A series of large displacement tests were carried out on Kaolin Clay to verify the model, and the suction effect on the pipe was also studied. It is found that the lateral breakout force and residual strength of pipeline on Kaolin Clay can be expressed as:

$$H_{breakout} = 0.2V + \frac{3}{\sqrt{s_u/\gamma' D}}\frac{z_{ini}}{D} \qquad 2\text{-}22$$

$$\frac{H_{res}}{V} = 1 - 0.65\left[1 - exp\left(-\frac{s_u}{2\gamma' D}\right)\right]. \qquad 2\text{-}23$$

These equations are somehow similar to the corresponding ones in the modified friction model (Equation 2-20), with a friction factor μ of value 0.2 applied to the vertical load. Soils are constantly being scratched forward as the pipe moves laterally and creates an accumulated soil berm, and this phenomenon is believed to provide significant additional resistance to the lateral displacement of the pipe. This feature was studied and captured in the model that White and Cheuk (2007) put forward by considering the conservation of volume of the displaced soil mound. By introducing an average thickness of the soil ploughed away by the advancing pipe (defined in Figure 2.4 and denoted as t_{plough}), a relationship can be found to address such parameter:

$$t_{plough} = \alpha \left(\frac{V}{Ds_u}\right)^{\beta}, \qquad 2\text{-}24$$

where indices α and β are empirical coefficients. The value of α is 0.0015 and the value of β is 2.3 , and this is found to give good predictions in estimating the solutions for pipe embedment ratios (z/D) less than 0.5.

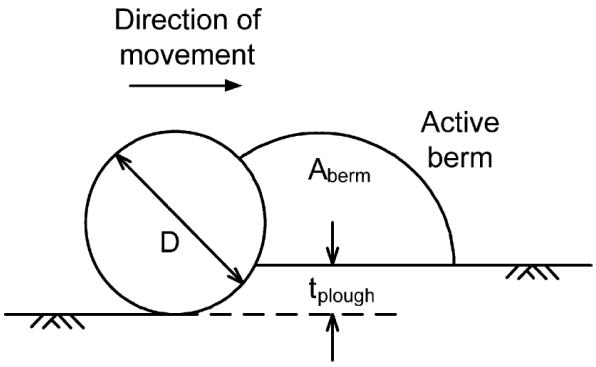

Figure 2.4 Idealised Growth of an Active Berm (White and Cheuk, 2007)

On the other hand, according to the conservation of volume of the soil mound the following can be interpreted:

$$\frac{dA_{berm}}{du} = t_{plough}. \qquad 2\text{-}25$$

The increase in the area of the accumulated berm will result in a rise in lateral resistance as the pipe must push harder on the soil mound to displace it forward. In practice, shear stress against any soil berm ahead of the pipe will provide additional support, and any rebound behind the pipe will reduce the plough depth. In addition, horizontal force creates additional loading within the soil and thus leads to greater plough depth. The additional lateral

resistance can be then linked to the increased volume of the soil mound created:

$$H_{berm} = \lambda \left(\frac{A_{berm}}{D^2}\right)^{\delta}. \qquad 2\text{-}26$$

Substituting the berm area with Equations 2-24 and 2-25, the passive terms contributing to lateral resistance through the accumulation of soil mound is given by the following:

$$H_{berm} = \lambda \left[\alpha \left(\frac{V}{Ds_u}\right)^{\beta} \times \frac{u}{D}\right]^{\delta}. \qquad 2\text{-}27$$

And hence the total lateral resistance of a pipeline is addressed.

In this way, the peak and residual lateral resistances of the pipeline can be calculated based on the respective breakout and residual lateral displacements ($u_{breakout}$ and $u_{residual}$), and by linear proportion the results can be summarised as a tri-linear model shown in Figure 2.5.

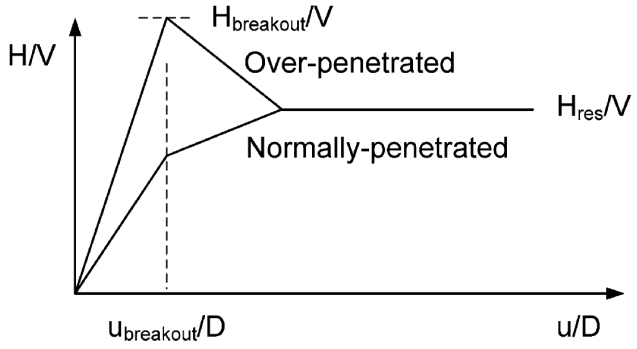

Figure 2.5 Tri-linear Model (White and Cheuk, 2007)

However, the model does not account for the variation in vertical penetration with

horizontal displacement. Though the framework has a simple and clear format, the determination of the four parameters (α, β, γ and δ) is not clearly defined. More importantly, the model fails in modelling the hardening effect of pipe-soil system as the pipe penetrates further into the soil bed. Besides, the equation of evaluating residual strength has to base on the precise prediction of the position where breakout, suction and residual condition took place, in order to address the tri-linear model that adopted in this theory (Figure 2.5). The model suggests magnitudes of a 10% diameter and a 25% diameter for the breakout and residual displacements respectively, where the explanation has not been clear yet. As a result, this raises doubts over the model.

2.3.2 Energy-Based Model

Verley and Sotberg proposed a new model in 1994 based on the original friction and an additional approach through the view of energy consumed during lateral movement of the pipeline on sandy soils. Improvement was made in estimating H_p, the passive term that contributes to the lateral resistance. Derived from dimensionless analyses, the model was concluded to be capable of predicting the development of pipe penetration into the soil and the associated soil resistance that may be mobilized against horizontal pipe motions. The vertical contact force is given by subtracting the self-submerged weight of pipeline W_s by an uplift force F_L (usually caused by the floating effect of water). This gives the vertical

effective force F_C:

$$F_C = W_s - F_L. \tag{2-28}$$

It is of worth noting that the uplift force F_L could be varying, for instance in a form of hydrodynamic force (Verley and Sotberg, 1994). Hence the first component of the friction model H_f can be expressed as:

$$H_f = \mu F_C. \tag{2-29}$$

Furthermore, the penetration-dependent resistance may be expressed as a function of the following parameters at breakout:

$$H_p = f(F_C, \gamma', D, z, a, u), \tag{2-30}$$

where z is pipe penetration, a is the average amplitude of pipeline movements over several cycles, and u is known as the lateral displacement. The normalized form of the above equation gives:

$$\frac{H_p}{\gamma' D^2} = f\left(\frac{\gamma' D^2}{F_C}, \frac{z}{D}, \frac{a}{D}, \frac{u}{D}\right), \tag{2-31}$$

where we can denote that $\frac{\gamma' D^2}{F_C} = \kappa$, and $\frac{a}{D} = \alpha$. Particularly, the parameter α represents the effect of overburden, i.e. the excess soil in front of the pipeline due to the cyclic lateral movement with constant amplitude. However, when considering the maximum resistance force, u/D may be omitted as the lateral breakout of pipelines is observed mostly for small

lateral movement, which is typically 5%-10% of its pipe diameter. In addition, the overburden effect α should also be of minor importance. The reason is that the maximum resistance occurs for fairly large displacement of pipe when the overburden is a small portion of the soil involved in the iteration (Verley and Sotberg, 1994). Thus the main contributors regarding the passive component of lateral resistance is given by

$$\frac{H_p}{\gamma' D^2} = f\left(\kappa, \frac{z}{D}\right). \qquad 2\text{-}32$$

Considering the penetration development over n cycles of lateral loading, the final vertical displacement could be linked to the following factors. The normalised equation is given as:

$$\frac{z}{D} = f\left(\frac{\gamma' D^2}{H}, \frac{u}{D}, \mu, \kappa, \frac{s}{D}, n\right), \qquad 2\text{-}33$$

where s represents the total distance travelled by the pipe.

The energy-based model assumed that work done by the pipe is the cause of the vertical displacement, and the effect of friction force is neglected. Therefore according to Equation 2-20, H may be replaced by H_p and the work done is thus the integral of $H_p(s)ds$ (Verley and Sotberg, 1994). The terms $\frac{\gamma' D^2}{H_f}$ and s/D in Equation 2-33 can be combined in the form of energy consumed during the process, which was defined as $\xi = \frac{E}{\gamma' D^3}$, where E relates to the work done by the horizontal force H_p on the soil. By omitting the term u/D

and replacing s/D and n with ξ and $\alpha = a/D$ respectively, the above equation transforms into

$$\frac{w}{D} = f(\xi, \kappa, \alpha). \qquad 2\text{-}34$$

Through iteration on estimating H_p and w, a final converged solution could be generated from the model. Although no actual testing was carried out to verify the model, Verley and Sotberg used several databases, such as AGA (Brennodden *et al.*, 1986; Wagner *et al.*, 1987), PIPESTAB (Brennodden *et al.*, 1989), and DHI (Palmer *et al.*, 1988) tests, to calibrate and develop an empirical relationship based on the concept mentioned above. By incorporating the data into a spreadsheet program, the estimated passive component of the horizontal resistance and the resultant penetration is shown in the following equations:

$$\frac{H_p}{\gamma' D^2} = \begin{cases} (5 - 0.15\kappa_{ini})\left(\frac{w_2}{D}\right)^{1.25} & for\ \kappa \leq 20 \\ 2\left(\frac{w_2}{D}\right)^{1.25} & for\ \kappa > 20 \end{cases} \qquad 2\text{-}35\text{(a) and (b)}$$

$$\frac{w_2 - w_i}{D} = k\left(\xi {\kappa_{avg}}^{-1} \alpha^{-\frac{1}{2}}\right)^{0.31}, \qquad 2\text{-}35\text{(c)}$$

where w_2 is the maximum pre-breakout penetration, w_i is the initial embedment, and k is an empirical constant defined by the test results.

Note that the above equations are expressed to solve the lateral resistance at breakout. To

map a horizontal force-displacement model for pipe behaviour, the energy model gives definition to the residual lateral force H_p in the similar form of breakout lateral resistance, which is believed to be relative to a different variable w_3. This factor w_3 can be viewed as an equivalent penetration after breakout, which may be approximated by the following equation:

$$\frac{w_3}{w_2} = \begin{matrix} 0.82 - 3.2\,(w_2/D) & w_2/D \le 0.1 \\ 0.5 & w_2/D > 0.1 \end{matrix}. \qquad \text{2-36(a) and (b)}$$

Through iteration process with penetration and the solved lateral resistance, a final force-displacement relationship can be mapped, as shown in Figure 2.6 below.

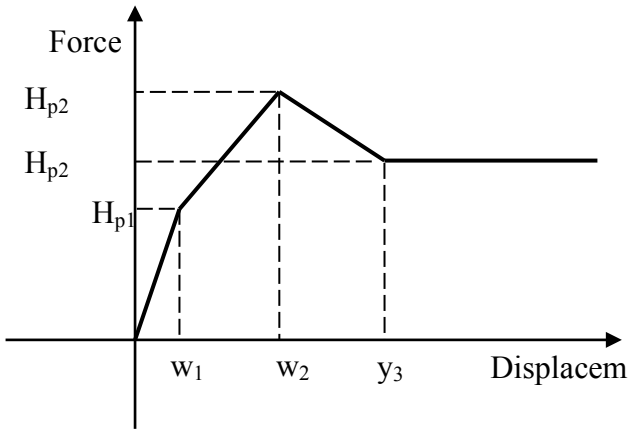

Figure 2.6 Force Displacement Model (Verley and Sotberg, 1994)

The iteration process (Figure 2.7) begins with an initial dummy vertical displacement, based on which the corresponding lateral load can be calculated with the known vertical load factor κ. The increment of vertical displacement can be further calculated by $\frac{z}{D} = f(\xi, \kappa, \alpha)$, where the work done by the pipeline can be calculated by integrating the

obtained horizontal resistance. The newly obtained penetration can solve the corresponding horizontal resistance and hence address the next point in mapping the lateral load – displacement curve. The required iterative calculation process can be achieved by computer coding, either in MATLAB language or using an Excel spreadsheet.

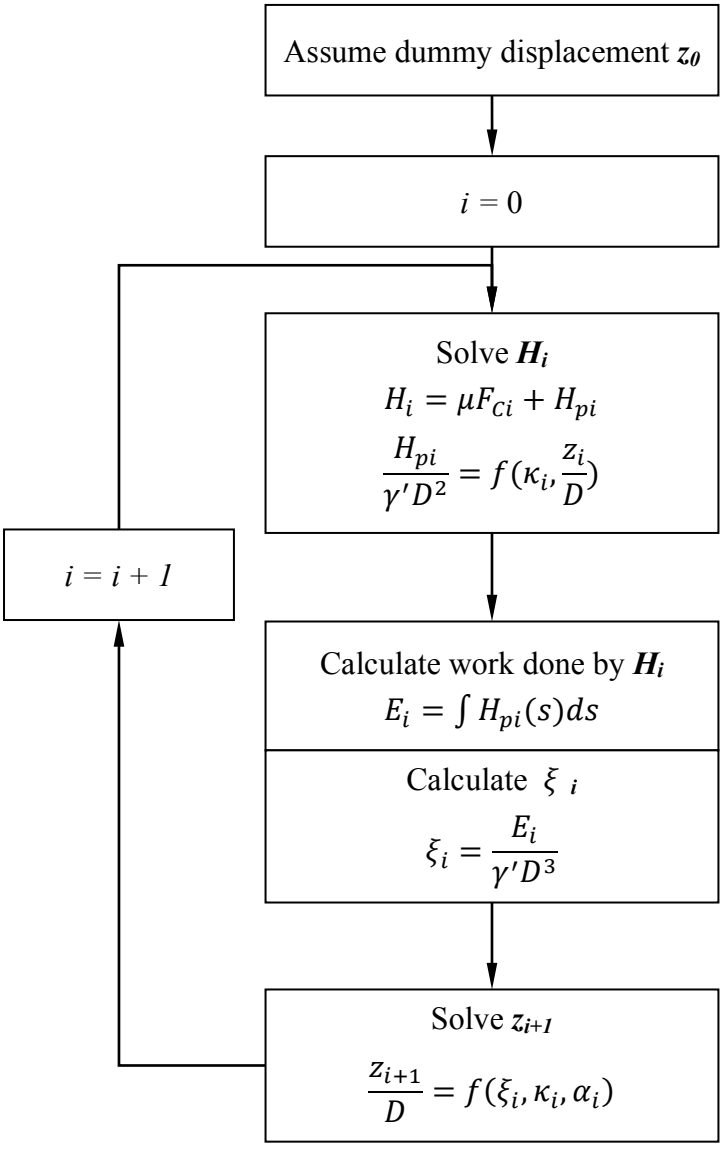

Figure 2.7 Flow chart of iteration process described in Verley and Sotberg's model (1994)

According to the dimensionless analyses detailed by Verley and Sotgerg (1994), the lateral

buckling behaviour can be described by a total horizontal soil resistance F_h for a unit length of pipe (diameter D and submerged weight W_s). The pipe is oscillated with relatively small amplitude on a sand soil (density ρ_s) because of the fluctuating horizontal (F_x) and vertical forces (F_t) (e.g. hydrodynamic forces). In the proposed research plan the tests will be carried out on a dry loose sand bed. In the work presented by White and Cheuk (2007) the key parameters include vertical load V, breakout horizontal resistance $H_{breakout}$, residual horizontal resistance $H_{residual}$, and respectively corresponding displacements $u_{breakout}$ and $u_{residual}$.

The model fitted the incorporated data well yet doubts may be rised due to the lack of relevant test result having high κ values larger than 30. As shown in Figure 2.8, the value of κ is distributed around 10 or less, with only a few points are located in the area greater than 20. This indicates a limited validity of the energy model to a small overburden load that can be fitted into the proposed expressions. Though Verley and Sotberg adopted dimensionless analyses to investigate the problem, yet the equations drew are empirical expressions with little theoretical basis. The coefficients of the model were calculated from the soil strength, pipe weights and dimensions, and loading rates used in the experiments, and were therefore limited to a small scale. As a result, these equations were capable to model the soil response with certain level of accuracy, which may not be applicable with

different soil conditions. This may cause difficulties when attempting to evaluate pipe behaviour under conditions other than those originally tested. Moreover, the model linked the passive component of lateral resistance directly to the penetration of the pipeline, and this would underestimate the capacity. Heaving occurred in the forward direction of the pipe movement during most of the tests. This created considerably larger embedment depths, which afforded the additional resistance adding up to the ultimate lateral capacity.

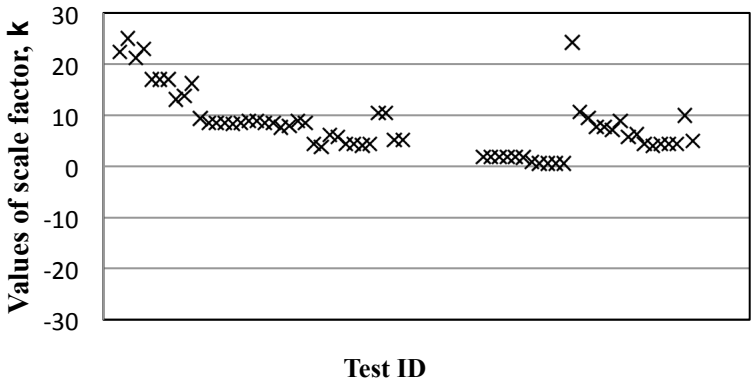

Figure 2.8 Relative Scale of Energy Model

2.3.3 Plasticity Model

The load-displacement response of shallow foundations is a classic geotechnical problem, and has been introduced to the offshore engineering applications because of the involved complex loading conditions. Recent investigations have been focused on the construction of the load interaction relationship in order to describe the combined vertical and horizontal capacity of foundations and, similarly, of pipelines. In the vertical and horizontal load space, the combination of loads forms a path and can be describe by a function $F_u = f(V, H, V_u)$, where F_u is the failure surface with a size determined by its peak vertical load V_u. The

possible combinations of the load points therefore have to exist within the surface, while any point reaching the surface indicates failure or yielding of the interface. To describe the full load-displacement response, the theory of plasticity has been introduced to include the following features (Martin, 1994; Montrasio and Nova, 1997):

1) a yield surface which defines all possible combinations of load at failure;

2) elastic equations that predict the response when the load point lies within the yield surface;

3) a hardening rule that describes the growth of the envelope after soil has been remolded;

4) a flow rule that indicates the direction of the plastic deformation upon yielding.

2.3.3.1 Yield Surface

The yield surface defines the boundary of the possible combinations of lateral and vertical load points on the V- H plane. The shape of the yield envelope was found to be parabolic, with the maximum lateral load being estimated by applying an h_0 factor to the maximum vertical load, i.e. $H_{max} = h_0 \times V_u$. Similar to what has been studied for shallow foundation, the failure envelope for pipeline under combined $V : H$ loading is described by the

following function:

$$f = H - \mu_s V\left(1 - \frac{V}{V_{max}}\right)^{\upsilon} = 0, \qquad 2\text{-}37$$

where μ_s is the initial slope of the yield surface at the origin, and the exponent υ is the shape factor. Values of μ_s are calculated at around 0.5 from previous studies, and the shape factor υ was taken as 1 by Butterfield *et al.* (1979). This led to a simple parabolic yield envelope that could be used to describe the behaviour of the pipe under combined $V:H$ loadings. A series of sideswipe tests were conducted by Gottardi *et al.* in 1999 to suggest a normalised parabolic failure surface as follows:

$$\frac{h}{h_0} - 4v(1 - v) = 0, \qquad 2\text{-}38$$

where $h = H/V_{max}$, $v = V/V_{max}$, and V_{max} is the peak vertical load level. The fitting of the results suggested an empirical value of h_0 of 0.1213. It is also noted that a single test was conducted under the overloaded condition. The pipe was first loaded to a certain level and then unloaded to perform sideswipe at a lower load level. The result indicates that the lateral load increased at a constant vertical load before reaching the edge of failure surface. In this case, V_{max} may not be able to reflect the size of the failure envelope, and it is preferable to consider peak load in the loading history to determine the size of the associated failure surface. In the latter studies, this is reflected in the term of overloading

ratio V/V_m, where V_m is the maximum load that was applied to the pipe during its loading history.

The effect of embedment depth of footings under combined loading in sand was investigated by researchers such as Montrasio and Nova (1997), Gadre and Dobry (1998), Byrne and Housby (1999), etc. It is developed that the parameter μ_s is related to the embedment depth z_0 and footing width B:

$$\mu_s = \mu_{s0} + \kappa_\mu \frac{z_0}{B}, \qquad 2\text{-}39$$

where μ_{s0} equals 0.35 for smooth surface footing and 0.48 for rough surface footing respectively, and κ_μ equals 0.72. When adopting this relationship to pipeline behaviour, z_0 can be represented by initial embedment, and B can be expressed as an equivalent width (B'), which can be obtained from the following Figure 2.9

To account for the effect on moment loading so as to study the pipeline response under combined $V:H:M$ loadings, Martin (1994) suggested the following relationship based on tests that was carried out on Kaolin Clay:

$$f = \left[\left(\frac{M}{M_{max}}\right)^2 + \left(\frac{H}{H_{max}}\right)^2 - 2\alpha\left(\frac{M}{M_{max}}\right)\left(\frac{H}{H_{max}}\right)\right]^{1/2} - 4\left(\frac{V}{V_{max}}\right)\left(1 - \frac{V}{V_{max}}\right), \qquad 2\text{-}40$$

where H_{max} and M_{max} are the loading capacities of pipeline along corresponding axis. Specifically, considering only $V:H$ space, the yield surface can be reduced to

$$f = H - 4h_0 V_{max}\left(\frac{V}{V_{max}}\right)\left(1 - \frac{V}{V_{max}}\right), \qquad 2\text{-}41$$

where h_0= 0.137. This is very similar to the studies of Zhang (2001) and Tian and Cassidy (2008):

$$F_u = \left(\frac{H}{H_{max}}\right)^2 - {\beta_f}^2\left(\frac{V}{V_0} + \eta\right)^{2\beta_1}\left(1 - \frac{V}{V_0}\right)^{2\beta_2}, \qquad 2\text{-}42$$

where η represents the tensile capacity of the pipe, and $\beta_1, \beta_2, \beta_f$ are the shape factors.

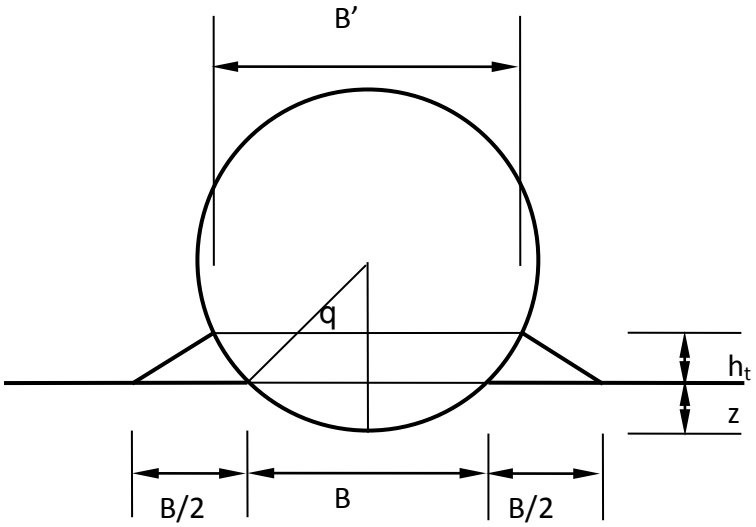

Figure 2.9 Equivalent Width of Pipeline (Zhang, 2001)

2.3.3.2 Elasticity

The model assumes elasticity within the yield surface defined above. With the estimation of vertical and horizontal elastic stiffness from testing data, the elasticity matrix can be

established as follows:

$$\Delta F = \begin{Bmatrix} \Delta V \\ \Delta H \end{Bmatrix} = \begin{bmatrix} k_{ve} & 0 \\ 0 & k_{he} \end{bmatrix} \begin{Bmatrix} \Delta w_e \\ \Delta u_e \end{Bmatrix}. \quad \text{2-43}$$

2.3.3.3 Hardening Law

The size of the yield surface expends or contracts in response to the increase or decrease of the maximum vertical load V_u and the vertical plastic displacement w_p. The model gives the following estimation for the development of V_0:

$$V_0 = k_p\left(-\zeta + \sqrt{\zeta^2 + \omega^2}\right) \quad \text{2-44}$$

$$\omega = w_p + c \cdot |u_p|, \quad \text{2-45}$$

where k_p represents the plastic stiffness of sand, and ζ is defined as the plastic displacement of pipe when the slope of the $V - w_p$ curve equals $k_p/\sqrt{2}$. Besides, ω is the plastic displacement factor contributed by the vertical plastic displacement w_p and lateral plastic displacement u_p with a multiplying factor c.

2.3.3.4 Flow Rule

The flow rule, which is regarded as the direction of the plastic deformation at the loading point of yielding, is given by the following formula by taking the derivative of the yield envelope:

$$\frac{\partial f}{\partial V} = -\mu_s \left(1 - \frac{2V}{V_{max}}\right). \qquad 2\text{-}46$$

And hence a displacement vector can be determined.

The study of Zhang and Tian (2009) explained the model in details and defined a plastic potential with a normal vector indicating the direction of the plastic displacement. The plastic potential was established in the similar form of the yield surface and was written as:

$$g = \left(\frac{H\prime}{\alpha H_{max}}\right)^2 - \beta_g{}^2 \left(\frac{V}{V_0} + \eta\right)^{2\beta_3} \left(1 - \frac{V}{V_0}\right)^{2\beta_4}, \qquad 2\text{-}47$$

where H' stands for the ordinate value of the corresponding points on the plastic potential with a given vertical load on the V-H plane. Also, α, β_3, β_4 and β_g are shape factors those are similar to what are defined in constructing the yield surface.

This model is in the similar form as the model presented by Zhang (2001). Zhang carried out a series of centrifuge tests in Calcareous sand under different loading conditions:

$$f = H - \mu_s V_{max} \left(\frac{V}{V_{max}} + \beta\right)\left(1 - \frac{V}{V_{max}}\right), \qquad 2\text{-}48$$

where β = 0.06.

2.3.3.5 Summary

It should be noted that in the Martin (1994) approach the size of yield surface is defined by the peak loads during the tests, which limits the model to simulate only isotropic hardening of the yield surface, i.e. that it expands in the same shape with the original envelope and consequently leads to a mutually proportional relationship between horizontal and vertical capacities. In addition, as mentioned above, a linear relationship can be found to express the factor μ_s. This allows the envelope to vary independently of the peak vertical load, and instead to directly respond to pipe vertical penetration (recall that μ_s is determined by pipe embedment and equivalent width of pipeline).

As shown in Figure 2.10, the pipe is believed to perform elastically before breakout, which is denoted by the point within the yield surface (Figure 2.10a). Elastoplastic deformation commences when the load point reaches the boundary of the yield envelope (Figure 2.10b). On continual loading, the load point is expected to remain on the yield surface as a result expands or contracts to account for work hardening or softening resulted from the downward or upward movement of the pipe respectively (Figure 2.10c). The framework enables a link between the applied loads and the penetration and lateral displacement of the pipeline, and thus is able to capture the response of penetration and berm formation.

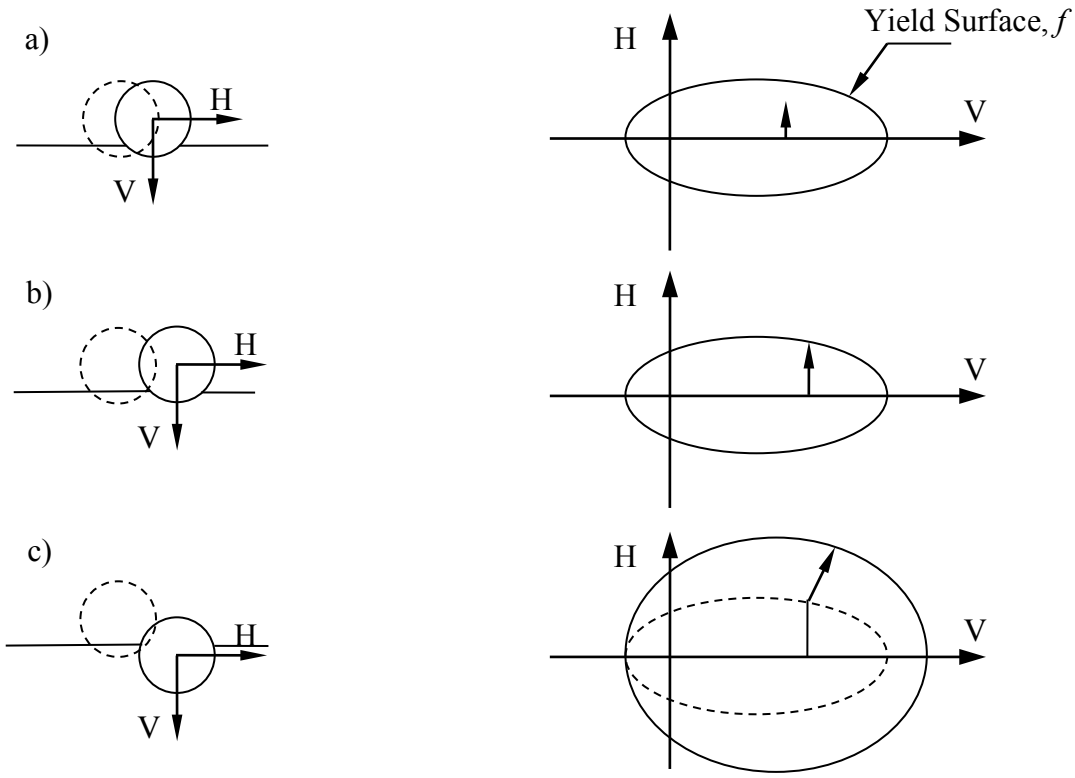

Figure 2.10 Work Hardening for Plasticity Model (Sanford, 2007)

Note: a) Small elastic deformation occurred at the beginning;
b) yielding condition was met at breakout point as pipe kept moving forward; and
c) growth of new yield envelope after breakout and soil remold.

2.4 Concluding Remarks

Several models are discussed in this review, and corresponding basis can be divided into the friction model or plasticity model (the energy model put forward under the assumption of a friction model, where passive components were expressed in the view of work done by the pipeline over lateral movement). The friction model introduced a simple friction factor assuming linear combination to simulate the V:H response of a pipeline. Cheuk (2007) provided a way to model pipelines with large displacement behaviour including berm

formation. However, though a passive term was added into the formula to account for the additional resistance that is contributed by the active soil berm, the model did not capture the response of hardening or softening process as the pipe penetrated further or moved up from the soil. The work of Zhang (2001) provided a rigorous framework with the influence of the penetration on the capacity of the pipeline by performing centrifuge tests of pipeline in calcareous sand. Plasticity theory not only provided a sound basis to capture the characteristics of the lateral capacity of the pipeline under combined loading, but also described the behavior of the pipe-soil system when the pipe reached its yielding state

Reference	Soil Condition		Pipe Parameter		Loading Condition	Formulas and remark
	Soil Type	Density	D (m)	L (m)		
Lyons, 1973	Sand	-	0.025, 0.229, 0.406	0.305 1.372	Monotonic load controlled horizontal loading	Friction factor μ is recommended at 0.65 for sands. However coulomb friction model is not suitable for pipeline in clays.
Lambrakos, 1985	Fine sand	Dense	0.6096	3.05	Monotonic load controlled horizontal loading	
Brennodden *et al.,* 1986	Silty fine sand	loose	0.5, 1.0, 1.5	1.6	Monotonic and cyclic displacement controlled horizontal loading	$P_u = \mu W_s$, where $\mu = 0.75$ for simple break-out behaviour. This increased after cyclic loding.
	Medium-coarse sand	Loose/dense				
	Clay	Soft & stiff				
Wagner *et al.*, 1987	Silty fine sand	loose	0.5, 1.0	1.6	Monotonic and cyclic displacement controlled horizontal loading	$P_u = 0.6(W_s - F_L) + \beta\gamma A$, where β is the empirical coefficient and A is half of the mound area displaced by the pipeline.
	Medium-coarse sand	Loose/dense				
	Clay	Soft & stiff				
Palmer *et al.*, 1988	Coarse sand	dense, Medium dry	0.295	1	Monotonic and cyclic inclined controlled load	$\mu = 0.5$ for breakout; vertical penetration is linked to initial embedment.
Jorgensen *et al.*, 1988	Fine sand	Dense	0.295	1	Monotonic and cyclic inclined controlled load	μ is found to be related to embedment depth; cyclic loading induces densification of the surrounding soil.
Morris *et al.*, 1988	Calcium bentonite mixture	Soft	0.15	1.5	Cyclic lateral loading, load/displacement control	Shielding effect is observed during cyclic testing with a accumulation of an active berm.
Brennodden *et al*., 1989	Medium-coarse sand	Loose/dense	0.5, 1.0, 1.5	1.6	Cyclic loading, displacement control	$P_u = 0.6(W_s - F_L) + 0.72\alpha W_s k_{D_r}$, where $\alpha = k_1(z/D)^{k_2}$, and k_1, k_2 and k_{D_r} are empirical function of sand density, pipe weight and diameter
	Clay	Soft				
Dunlap *et al.*, 1990	Calcium bentonite mixture	Soft	0.15	1.5	Cyclic vertical loading, load/displacement control	Small amplitude vertical cyclic loading induces a vertical penetration, which was close to same level of horizontal loading
Wallace, 1995	Calcareous sand	Loose	0.02	0.16	Centrifuge monotonic loading	$dz/dx = \tan\delta\,(2V/V_{max} - 1)$, where z and x are vertical and horizontal displacements respectively.
Cooper, 1997	Calcareous sand	Loose	0.02	0.16	Centrifuge cyclic loading	
Zhang, 2001	Calcareous sand	Loose & dense	0.02, 0.07	0.16, 0.35	Centrifuge monotonic and cyclic loading	$F_b = H - \mu(V/V_{max} + \beta)(V_{max} - V)$, F_b being the function of yield surface.
Lee *et al.*, 2011	Kaolin clay	Consolidated	0.05	0.2	Cyclic vertical loading, load/displacement control	Horizontal breakout resistance is dependent on the initial embedment and the undrained shear strength.

Table 2.1 Summary of Previous Physical Modelling Tests

CHAPTER 3 TEST SET UP

3 . 1 Introduction

In order to provide a better understanding of the behavior of lateral pipe-soil interaction, a series of model tests will be conducted to examine the lateral breakout resistance of a shallowly-embedded model pipe in sand. The cyclic loads are exerted using mechanical actuators to simulate the actual wave-induced and thermally induced forces upon pipes.

3 . 2 Scale Effect

The soundness of a valid physical model of pipe-soil interaction system requires identification of key parameters within reasonable range of scale. The following variables describe the possible parameters involved in a lateral buckling event:

$$F_h, F_l, V, \mu, \gamma_g, \gamma_s, D, W_s, y, w, n$$

where F_h and V [MT^{-2}] are the lateral and vertical load (per unit length) of the pipeline respectively, F_l [MT^{-2}] is the lift force of pipeline underwater, μ is the Coulomb friction factor of soil (sand in this study), γ_g and γ_s [$ML^{-2}T^{-2}$] are the unit weight of pipe and soil respectively, D [L] is the diameter of the pipe, W_s [MT^{-2}] is the self-weight of pipe segment, y and w [L] are the lateral and vertical displacement of the pipe segment and n is the cycle of loading. For simplicity of study these

parameters are combined and divided into several non-dimensional groups:

$$\frac{F_h}{\gamma' D^2}, \frac{V}{\gamma' D^2}, \frac{y}{D}, \frac{w}{D}, n.$$

The dimensional analyses performed by Verley suggest that the pipe embedment and the lateral resistance of an on-bottom pipeline are linked to the following dimensionless groups (which are discussed in Chapter 2):

$$\frac{w}{D} = f\left(\frac{F_h}{\gamma' D^2}, \frac{V}{\gamma' D^2}, \frac{y}{D}\right), \quad 3\text{-}1$$

$$\frac{F_h}{\gamma' D^2} = f\left(\frac{V}{\gamma' D^2}, \frac{w}{D}\right). \quad 3\text{-}2$$

Among these non-dimensional groups only the vertical load group ($V/\gamma' D^2$) and lateral displacement group (y/D) can be controlled by performing constant vertical load probe tests and constant penetration swipe tests. In a typical lateral buckling event, the pipeline can be moving laterally up to more than 2D, whilst in extreme cases it even reaches 10D (Zhang, 2001). This indicates a y/D value of less than 10 for the maximum lateral displacement in lateral loading tests. On the other hand, a scaling factor, K, can be defined to indicate a relative load scale of the model pipe, and can be written in the form of $K = V/\gamma' D^2$, where V stands for the vertical line load applied, and γ' is the effective unit weight of sand (14.5kN/m^3 in these tests). This dimensionless group ensures that the model tests are representative of the field case. By adopting the relevant data extracted from existing experiment projects

including AGA, PIPESTAB and DHI, for a model pipe with diameter D of 100mm, an indication of the value of this scaling factor is estimated in the range from 0.05 to 1.67.

3 . 3 Apparatus and Model Preparation

A test tank with inner dimension of 2.5m (length) x 0.5m (width) x 0.5m (height) is used to contain the soil sample. A two dimensional actuation system is attached to the testing tank, and is controlled by two stepper motors in the horizontal and vertical motion of the model pipe. The system can operate at a variety speeds on a range from 0.0125mm/s to 7-8cm/s. A load capacity of up to 1kN can be applied in both horizontal and vertical directions. Details of the actuator system are summarised in the Table 3.1 below. The schematic and actual layout of the combination of actuator system and the sand box is provided in Figure 3.1 and 3.2.

Table 3.1 Details of the Two Dimensional Actuation System

Characteristic	Limits	
	Horizontal	Vertical
Length	1035mm	580mm
Resolution	0.0125mm	0.0125mm
Minimum Speed	0.0125mm/s	0.0125mm/s
Maximum Speed	70mm/s	80mm/s

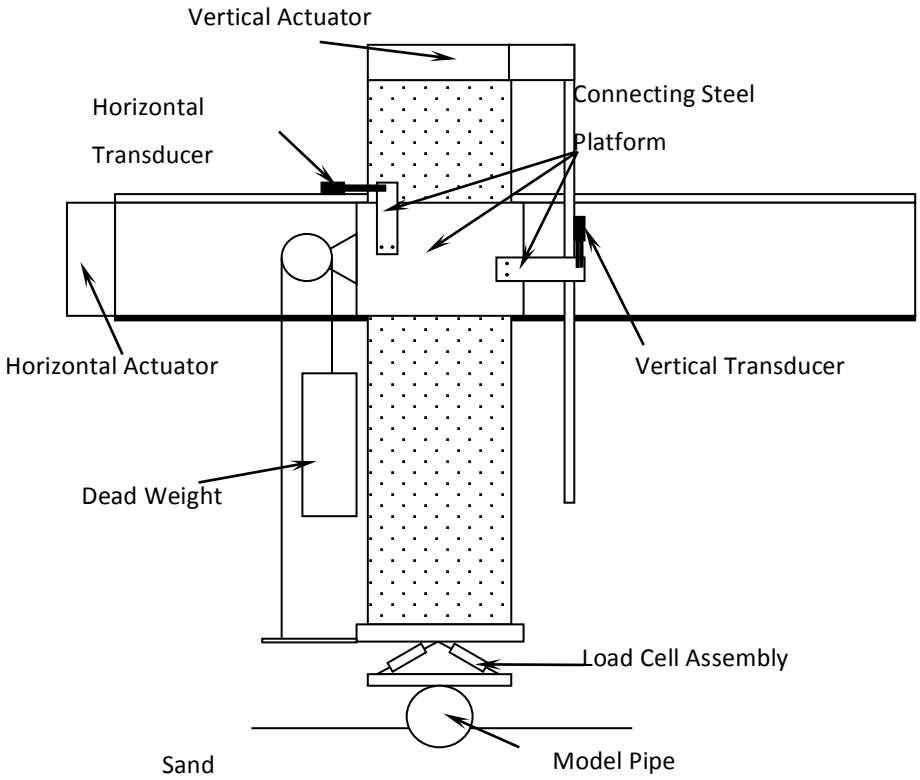

Figure 3.1 Schematic Design of Loading Rigs

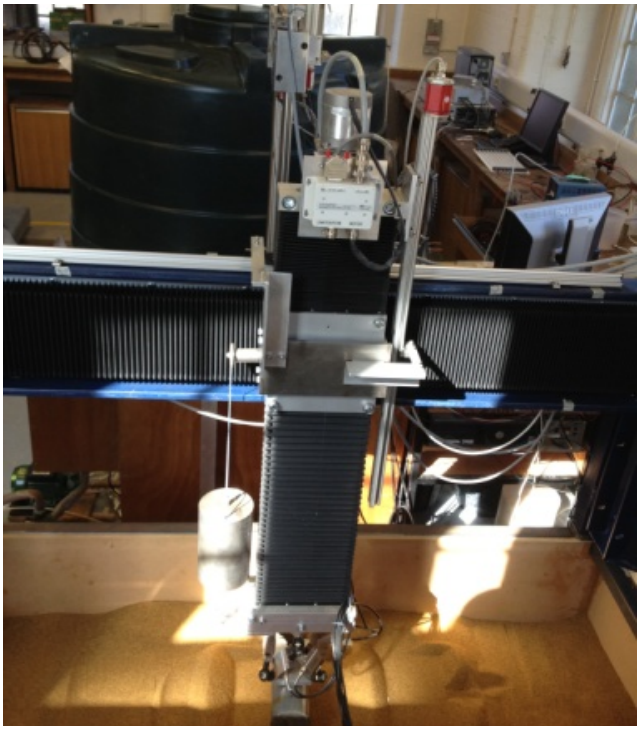

Figure 3.2 General Layout of Actuator System and Sand Box

A 100mm diameter smooth pipe with a length of 300mm (providing a length to diameter ratio L/D of 3) is used, and this was designed to be penetrated to a specific depth before moving laterally under various conditions. The typical sign convention of the model pipe is shown in Figure 3.3. A new counterbalance system for the actuator system was designed, which balances the self-weight of the model pipe alongside with the transducers when it is at rest or under operation so that the motion and response of the two-dimensional stepper motors will not be affected. It consists of a roller connecting one end to the moving arm and the other end to the model pipe, so that the counterbalance system can move horizontally with the model pipe as the moving arm displaces laterally, while the roller can allow the model pipe to move freely in the vertical direction (Figure 3.4).

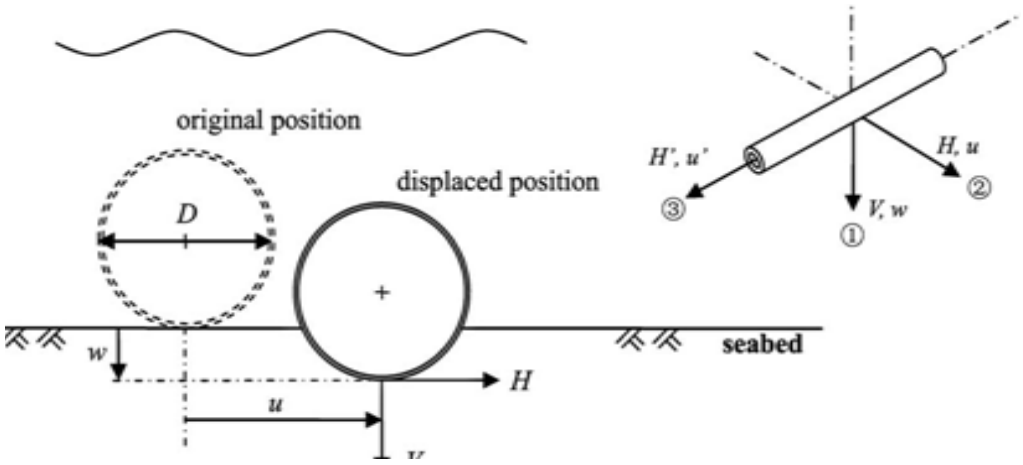

Figure 3.3 Typical Sign Convention (Weerasinghe, 2007)

The movements of the model pipe are captured by two Magnetostrictive linear-position transducers, horizontal transducer and vertical transducer respectively.

The transducers are manufactured by Tempasonics® and have a length of 1400mm and 800mm for horizontal and vertical displacement measurement respectively. Each of the displacement sensors consist of a magnetic slider freely to move along a track which returns different voltages depending to its locations. The time-based voltage was then recorded by the computer and converted to displacements. Instead of combining horizontal and vertical transducers together as a whole part, the new design made them two separate recording systems. Both horizontal and vertical transducers are attached separately to the moving platform of the loading frame, shown in Figure 3.5. In this way less joining effects will be produced due to the inference of either transducer to the other when the pipe moves.

The loads occurred in the experiment are captured by a six degree-of-freedom load cell assembly. Six individual load cells are installed where the recorded response can be translated into a load matrix of a linear equation. With the load cell assembly six independent loads can be determined: 1) Vertical Load V, 2) Horizontal Load H_1 regarding the axial direction, 3) Horizontal Load H_2 regarding the lateral direction, 4) Torque T along the pipe, 5) Moment M_1 regarding the vertical direction, and 6) Moment M_2 regarding the horizontal direction. The value of M_1 and M_2 is to check whether the model pipe is loaded with eccentricity, which should be avoided during

the tests. Ideally these two values should be zero, indicating the load on the pipe is at the centre of its relative axis. Figure 3.6 shows the layout of the load cell assembly which has been built such that it could be fitted between the vertical actuator and the pipe-element. The load cell assembly is able to withstand a maximum vertical force of 2kN and a maximum horizontal force of 1kN. The load voltages detected by each of the 6 load cells are wired to a data acquisition card (DAQ card, PCI-DAS6013), which is then delivered to a connected computer and shown on the front panel in the controlling program.

All the recording devices are calibrated to produce a matrix containing six independent loads and two movements (horizontal and vertical displacement). To achieve this, several calibration tests were carried out where the response voltage from the load cell and the transducers were recorded with a series of known load being applied. The calibration matrix is then generated such that the linear combination of the input voltages gives the smallest sum of the errors E which is calculated by the root mean square of the difference between actually applied load L_a and the calculated load L_c, as shown in the equation below:

$$E = \sum \sqrt{(L_a - L_c)^2} \qquad 3\text{-}3$$

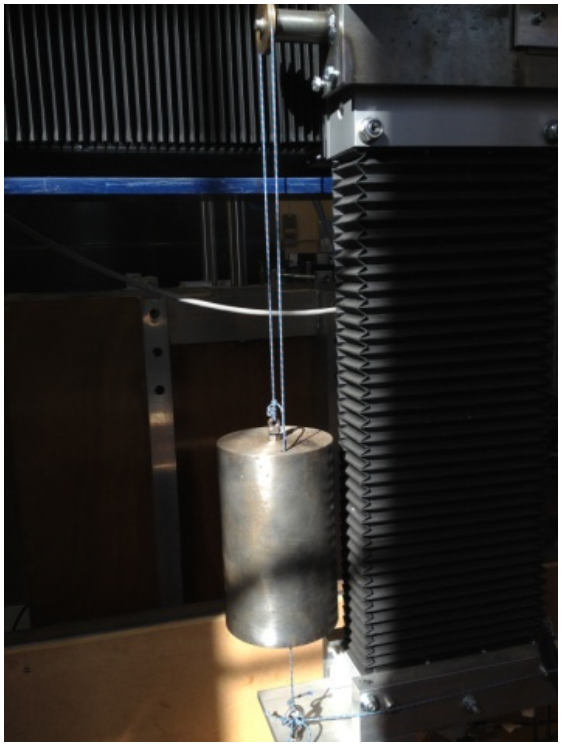

Figure 3.4 Counter-Balance System

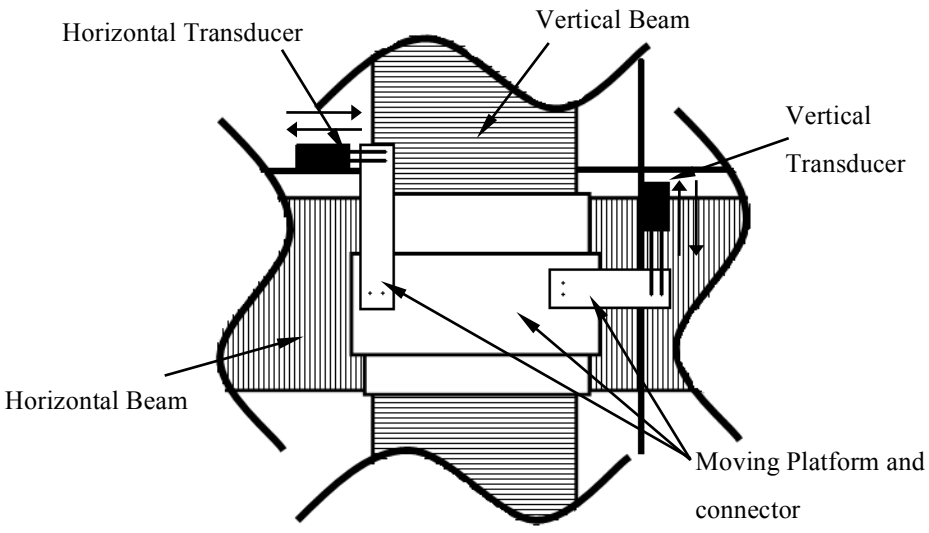

Figure 3.5 Schematic Transducer Design

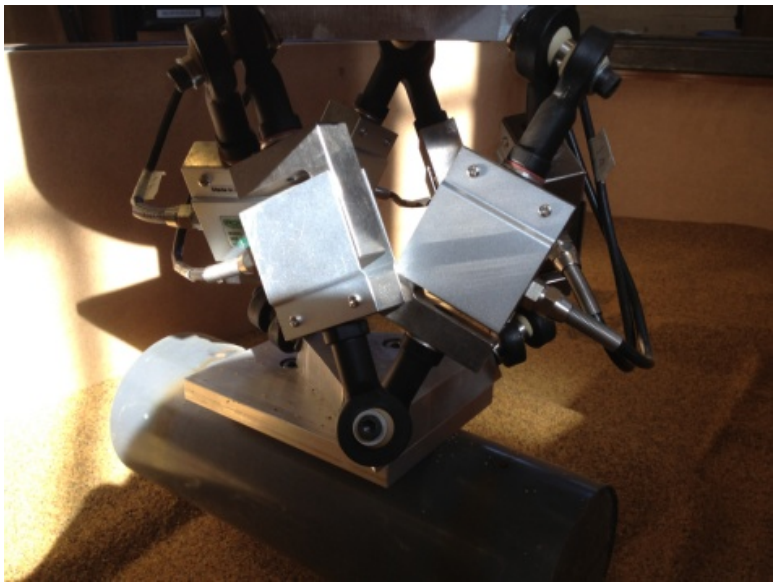

Figure 3.6 Load Cell Assembly

3 . 4 Leighton Buzzard Sand

The primary component of typical beach sand as well as consistence of sea bed is silica sand, which contains a high portion of silica (SiO2) in the form of quartz. The soil adopted in the test is the Leighton Buzzard Sand (14/25), which has high silica content and round-shaped particles, having a maximum and minimum grain size of 1.18mm and 0.6mm respectively. The sand is poured into the sand box prepared in dry condition to create a loose sand “seabed” condition (i.e. sand with low relative density, RD), so that the tests could explore the drained response. The basic engineering properties of the sand adopted in the test are given by the following Table 3.2. Note that the unit weight of sand adopted in the later analyses should be taken as the minimum unit weight due to the loose state condition of sand.

Table 3.2 Details of Sand Properties

Sand Type	Leighton Buzzard Sand (14/25)
Friction angle, φ	33°
Minimum unit weight, γ_{min}	14.65kN/m^3
Maximum unit weight, γ_{max}	17.58kN/m^3
Average depth of sand	300mm

3 . 5 Controlling Program

The experiments are designed to be controlled by computer to acquire higher accuracy, and thus a computing program is required for accurate data acquisition, data logging and control of the stepper motors. A provided program developed by Churchman (2008) based on visual basic makes use of string commands to order the stepper motors, yet it only allows single commands while user-defined codes are still required to perform a series of movement, which are cyclic movements in this case. The program is also limited to the control of the motors and there were no data acquisition or logging mechanisms. An alternative program was developed based on the LabView language, which achieves the three goals for the basis of the experiment. The program consists of three parts: 1) data acquisition, 2) data logging and 3) motor control. However, jam of dealing commands in the stepper motors occurred when several

commands were sent from the computer at the same time, and result in no response and thus failure of testing. In addition, a trial controlling system is required to move the pipe to the desired starting point prior to the commencement of each test. Therefore it is essential to develop a controlling program such that the test procedure and response could be controlled and captured precisely.

In the proposed program response from the load cell assembly in voltage was captured and translated into engineering units of Newton and meters by the data acquisition session. With the application of the calibration matrix these data were transformed and put into the load columns, which were also displayed on the screen and logged into files. Load control panel consists of horizontal and vertical control of motor. Response of the loads and displacements were detected so that the computer can send commands to the stepper motors with respect to the current state of the model pipe. For example, the horizontal control session contains one single loop where horizontal displacement was detected. When a user-defined target lateral displacement was input into the system, the error between the target position and the detected current position of the model pipe was calculated. Whether this error stays within the yields limit will be the primary factor for the computer to determine the moving or stopping states of the stepper motor. In terms of the vertical control session, two loops were designed

with respect to vertical load control and displacement control according to the requirement of tests. Similar to that of horizontal control loop, the vertical control program detects the vertical load and displacement respectively. Further efforts have been put into the load control cycles to avoid jam of commands. This is achieved by applying a more complex conditional case structure. The control code for the vertical stepper motors were separated into two individual parts with one section being shut down while the other being at operation. In addition, a trial control panel was added to the program to enable the user to move the model pipe at a designed speed or to a designed position directly. This is of importance for safety issues as well as convenient for the user to define the starting position of the test. Besides, in order to carry out tests under the same initial condition, a secondary code was written to control the model pipe to move back to the datum after a single test is done.

In the constant load control loop, because the recognizable command that can be sent to the stepper motor should only be related to speed or displacement, a relationship should be established to convey the target vertical load into the required displacement to achieve this load. A proportional gain of stability, k, is introduced by assuming a linear relationship between displacement and load within a small range of movements. The speed of lowering or raising the model pipe, v, is then decided by the following

equation:

$$v = k \times e \qquad 3\text{-}4$$

where e is the error between the target load and the detected current load

The direction of movement can also be determined from the calculated error. Positive error shows the lack of current vertical load and thus requires the pipe to move down (positive speed) and negative error indicates excessive vertical load and hence requires the pipe to move up (negative speed). After calibration the gain, k, is estimated at 0.00015. In this case the speed of movement will be slow to ensure stability of the system, and a safety limit of maximum speed is also pre-set to the program at 0.025mm/s. To acquire accurate simulation the error range was set to be ±5N such that a speed command will be sent to the stepper motor whenever the absolute value of detected load error excesses 5N.

The front panel is shown on Figure 3.7, consisting of five parts.

1) Ultimate control section: A single test starts or ends. The move-to-datum button is also available in this section.

2) Trial control window: Pilot command can be sent to the stepper motor prior to the start of test.

3) Display window: The response of model pipe is shown here. In addition, several data series are plotted for a clearer view, which includes the graphs showing the displacement path, the relationship of penetration against vertical load, and relationship of horizontal load against vertical load.

4) Control window: This detects the response of model pipe and controls the stepper motor.

5) Data logging window: Data will be recorded and output into files for future analyses upon activation of the “log” button.

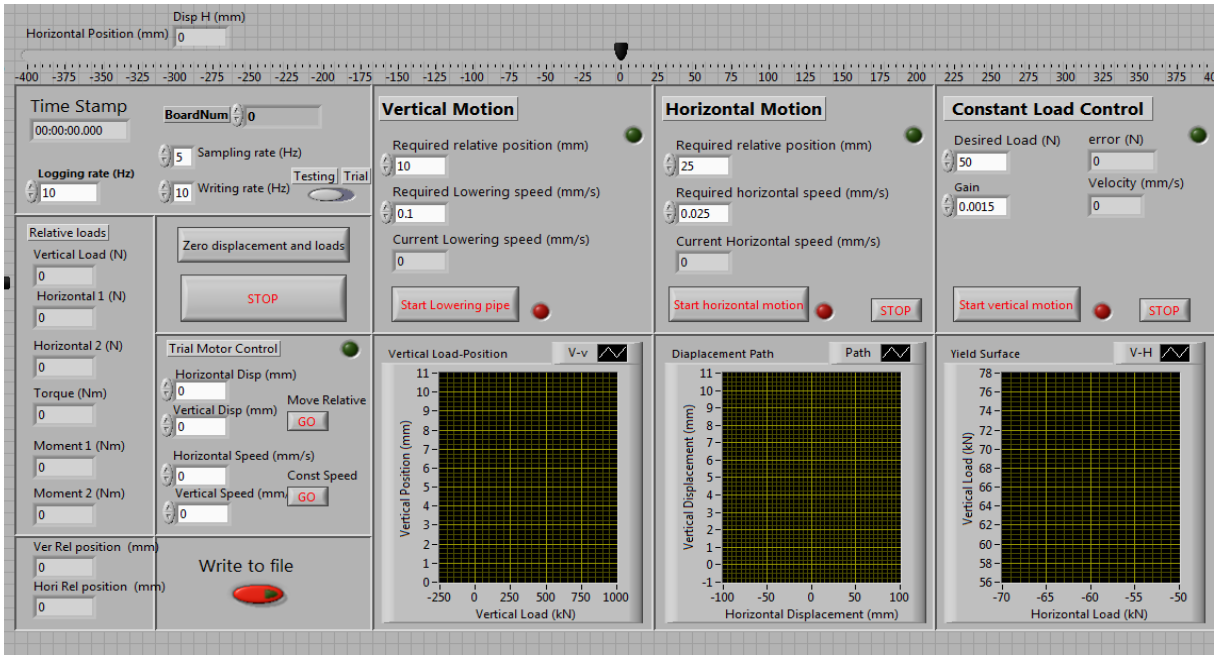

Figure 3.7 Front Panel of Controlling Program

During the test, it is important for the motor control section to detect fast enough before the response rises or drop too much between the two consistent cycles of data sampling. In order to achieve that, the frequency of data sampling rate is set to be

10Hz, whereas the detecting frequency of the motor control loops is preset to be a slightly larger value of 15Hz. The logging rate of recoding data is set to be 10Hz.

3 . 6 Testing Sequence

A testing sequence has been designed involving three types of tests:

1) Vertical Penetration Tests:

The tests involve penetration tests and lateral tests (sideswipe test and probe test) within 1-pipe-diameter of lateral movement. 5 monotonic vertical penetration tests and 9 vertical loading tests with load-unload-reload process were carried out at different locations in the sand tank, i.e. tests were performed at 0, ±100mm and ±200mm on the lateral axis of the tank. The plastic modulus of the sand can be determined from the results (i.e. the slope of the vertical load – displacement curve), which is an important factor in the theoretical model (Verley and Sotberg model, 1994). The schematic layout of the vertical penetration tests performed is shown in Figure 3.8.

2) Constant Penetration Sideswipe Tests

In these tests the model pipe was penetrated to a target initial embedment depth after which the vertical position of the model pipe was held constant throughout the rest of test while lateral movement was applied to the model pipe. The purpose of these tests

is to define the yield envelope of the pipe-soil interface relationship under combined loading.

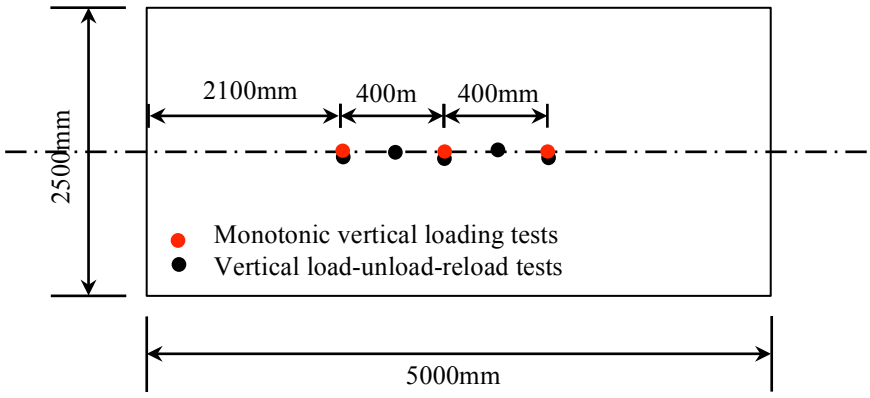

Figure 3.8. Schematic Drawing of the Locations of Vertical Loading Tests

3) Constant Vertical Load Probe tests,

In these test the vertical load was kept constant using load control loops after the pipe reached its initial embedment depth. Then the pipe was pushed laterally and its displacement path and reaction forces were recorded. The purpose of these tests is to examine and estimate the ultimate lateral resistance which the pipe can rely on the sand bed. Plastic behavior and the development of lateral resistance can be analysed from the results of these tests.

In order to achieve sufficient data, the moving speed of the actuator is set at 0.025mm/s. The realistic vertical with respect to the adopted sand and model pipe will be in the range from 7.25N/m to 242.5N/m, which is equivalent to 2N and 73N

respectively (multiply with the length of pipe, 0.3m). The designed tests are therefore conducted at a vertical load with relative scale, specifically under 25N, 50N and 75N as described in Table 3.3.

The loading and displacement history of the model pipe is recorded during the tests, and the loading condition can be described as either normally loaded or overloaded. The normally loaded condition represents the situation where the vertical load acting on the pipe during breakout is always the maximum load that it has experienced throughout its loading history. The overloaded condition is where a higher vertical load has been applied to the pipe prior to the vertical under which the lateral loading is applied. An over-penetration ratio, $R = V_{max}/V$, will be used to indicate the degree of loading history during the tests, which will vary from 1 to 20.

The installation method of the model pipe was push-in, where the pipe was directly penetrated into the sand without pre-trenching. Details of performed tests were given in Table 3.3:

Table 3.3. Tests Performed

Test	No	Penetration w (mm)	Lateral Location O_x (mm)	Vertical load V (N)	Vertical Load (Dimensionless) V/ysD^2L	Initial Penetration w_{ini} (mm)	Over-loading Ratio OLR	Lateral Displacement u_{max} (mm)	Number of Cycles n
Vertical Tests	V1	5	0						
	V2	5	200						
	V3	5	0						
	V4	5	400						
	V5	10	0						
	V6	22	0						
	V7	21	200						
	V8	22	200						
	V9	22	-200						
	V10	24	-200						
	V11	25	400						
	V12	23	400						
	V13	25	-400						
	V14	24	-400						

Table 3.3. Tests Performed Continued

Test	No	Penetration w (mm)	Lateral Location O_x (mm)	Vertical load V (N)	Vertical Load (Dimensionless) V/ysD^2L	Initial Penetration w_{ini} (mm)	Over-loading Ratio OLR	Lateral Displacement u_{max} (mm)	Number of Cycles n
Side Swipe Tests	S01			Vary	NA	5	1	100	1
	S02			Vary	NA	10	1	100	1
	S03			Vary	NA	15	1	100	1
	S04			Vary	NA	20	1	100	1
	S05			Vary	NA	5	1	150	3
	S06			Vary	NA	10	1	150	3
	S07			Vary	NA	15	1	150	3
Probe Tests Probe Tests	P01			24.468	0.56	5.15	24.84	25	3
	P02			25.056	0.58	5.06	21.95	25	3
	P03			49.716	1.14	4.76	10.13	25	2
	P04			74.865	1.72	5.13	5.58	25	4
	P05			74.865	1.72	5.1	5.89	25	3
	P06			75.324	1.73	10.16	14.61	25	3
	P07			76.053	1.75	10.54	14.7	20	2
	P08			26.289	0.60	4.82	28.7	150	3
	P09			25.725	0.59	4.73	23.41	150	3

Table 3.3. Tests Performed Continued

Test	No	Penetration w (mm)	Lateral Location O_x (mm)	Vertical load V (N)	Vertical Load (Dimensionless) V/ysD^2L	Initial Penetration w_{ini} (mm)	Over-loading Ratio OLR	Lateral Displacement u_{max} (mm)	Number of Cycles n
	P10			26.07	0.60	9.95	18.99	150	3
	P11			51.006	1.17	5.24	5.25	150	3
	P12			51.285	1.18	10.23	6.82	150	3
	P13			25.119	0.58	4.84	11.64	450	1
	P14			25.632	0.59	5.23	16.52	800	1
	P15			25.527	0.59	6.67	17.28	350	1
	P16			50.193	1.15	10.21	6.24	450	1
	P17			50.559	1.16	5.4	8.6	600	1
	P18			50.616	1.16	10.59	17.56	800	1
	PC01			49.725	1.14	9.97	8.06	50	10
	PC02			50.217	1.15	11.93	10.13	100	10
	PC03			49.659	1.07	10.76	10.23	200	10
	PC04			25.125	0.58	7.16	8.2	200	10
	PC05			24.801	0.55	8.75	11.34	200	10
	PC06			24.84	0.57	9.72	16	200	10

CHAPTER 4 TEST RESULT AND OBSERVATIONS

4. 1 Introduction

The experimental results of pipe-soil interaction behaviour is presented and discussed in this chapter. The resistances (vertical and lateral resistance) and displacements data (penetration and lateral offset) were divided by the test characteristics (unit weight of soil and diameter of model pipe) so that the results can be plotted and presented in a form of dimensionless groups, e.g. forces are presented using $H/\gamma' D^2, V/\gamma' D^2$ and displacements using $u/D, w/D$. In this way it may be convenient and clear to compare the test results with other sources of testing data. The vertical loading test results and lateral loading test results were discussed in section 4.2 and 4.3, where the response of the model pipeline under monotonic and cyclic loading conditions and of different lateral offset distances were also presented and analysed.

4. 2 Vertical response

4.2.1 Introduction

The resistance of seabed soil against vertical pipe settlement is of vital importance to understand and investigate the development of lateral resistance. The development of vertical resistance when the soil is under loading causes settlement, which compacts the underneath soil and hence improves its strength. This process is defined as

hardening, and the corresponding settlement was considered as an indicator of the hardening capacity of the soil bed, which is explained in detail in Chapter 2.

In order to study the soil-pipe response under vertical loading, a total of 6 monotonic vertical penetration tests and 9 vertical loading-unloading-reloading tests were conducted following the procedures described in Chapter 4. Among all the tests the model pipe was pushed in to the sand box before the vertical loading was applied, and therefore a small heave was observed at the beginning of tests. The soil materials in the experimental sand box were assumed to be homogenous and were verified by these vertical penetration tests taken at different locations in the experimental sand box. The vertical load responses were reported in this chapter, and the data were analysed using the soil model developed by Zhang (2009).

4.2.2 Monotonic Vertical Loading Tests

A total of 5 monotonic vertical loading tests were conducted prior to the lateral probe tests and swipe tests. The test results were presented in Figure 4.1.

From the figure an approximate linear load-displacement response is indicated in all 5 tests, which similar behavior has also been found for flat shallow foundations in sand. 3 levels of constant load were applied on the pipe after the target depth was achieved, which were 25N, 50N and 75N. This gave a equivalent line load Assuming these loads

were uniformly distributed along the pipe segments, the line loads that are put into analyses should be divided by the length of the model pipe. The average vertical loading gradient derived from the graph was calculated at k_{vp} = 285kN/m/m.

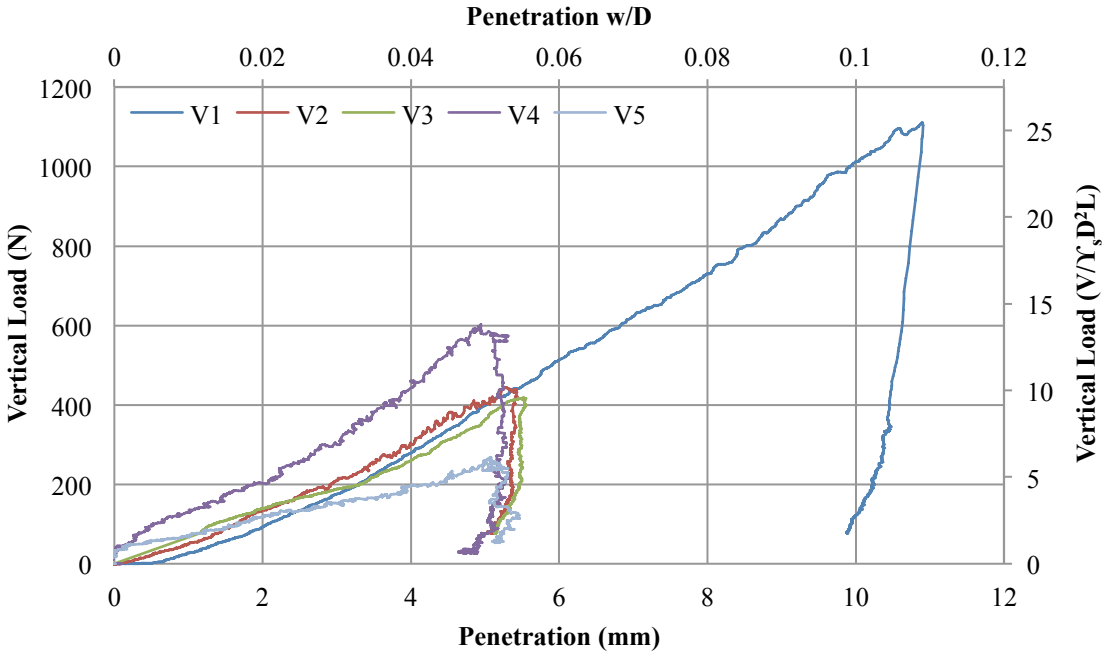

Figure 4.1 Test Results of Monotonic Vertical Loading

Therefore the maximum vertical load on the pipe can be estimated by simply multiplying the plastic modules with the depth of pipe penetrated in future design:

$$V_{max} = k_{vp} \times z. \qquad 4\text{-}1$$

The behavior of pipe movement against penetration can be modified similarly to that of shallow foundations. According to previous research, the plastic modules, $\boldsymbol{k_{vp}}$, can also be obtained from a cone penetration test. Given that

$$k_{vp} \cong BL \times \frac{dq_c}{dz}, \quad 4\text{-}2$$

where $\boldsymbol{B}$ is the contact width and length of the shallow foundation and $\boldsymbol{q_c}$ is the bearing capacity of a shallow foundation. In such case the pipe can be treated as a shallow foundation penetrating into the sand, which has a punching shear failure mode. Given the common equation of estimating bearing capacity of shallow foundation on sand shown below, bearing capacity in the case of pipeline movement can also be applied.

$$q_u = \zeta_{qc} \times q \times N_q, \quad 4\text{-}3$$

where $\boldsymbol{q_u}$ is the ultimate bearing capacity of a shallow foundation, $\boldsymbol{q}$ is the effective stress on the foundation, $\boldsymbol{\zeta_{qc}}$ is the compressibility factor which depends on the soil strength and its shear modulus and $\boldsymbol{N_q}$ is the bearing constant.

For underground structures the effective stress is found to be linearly proportional to the embedment depth where the gradient is found to be the effective unit weight of soil, $\boldsymbol{\gamma'}$. Given that $q = \gamma' z$, the bearing capacity of shallow foundation can be written as

$$q_u = \zeta_{qc} \times \gamma' z \times N_q \quad 4\text{-}4$$

The bearing modulus, denoted as $q_u/\gamma' z$, was found to be around 60 for sandy materials (Finnie, 1993). Recall from Table 3.2, the unit weight of Leighton Buzzard

Sand is taken as 14.65kN/m^3 as the sand was poured into the sand box and should have a low relative density to form a very loose state. As discussed in Chapter 2, the equivalent contact width of pipelines to shallow foundations in the traditional bearing capacity equations can be calculated. Recall that

$$B' = 2\sqrt{D(w_0 + h_t) - (w_0 + h_t)^2}, \quad 4\text{-}5$$

where w_0 and h_t are the embedment and height of heave due to vertical push-in of the pipeline. This indicates a value of 234.4kPa in an estimation of the plastic modulus, k_{vp}, which is close to that obtained from the vertical loading tests. Hence with the above equations the plastic modulus of sand k_{vp} may be estimated using the field data, so that the maxed vertical load on the sand bed can be derived in a clearer and more convenient way.

4.2.3 Vertical Load-unload-reload Tests

A total of 9 vertical loading tests with load-unload-reload process were carried out and the results are shown below in Figure 4.2. The results shared similar gradient, which indicates that the elastic and plastic modulus remain unchanged within the testing area. The plastic modulus calculated from the gradient of the plotted results gave a value of $k_{vp} =$ 148.9kPa. This indicates a looser sand bed with lower bearing capacity. It is worth mentioning that the plastic modulus increased at deeper penetration. This may due to the excess plastic deformation of the sand under repeated load-unload process.

The elastic modulus, showing by the gradient of the load-displacement relationship in the unload-reload process, was calculates at approximately $k_{ve} = 2500$kPa.

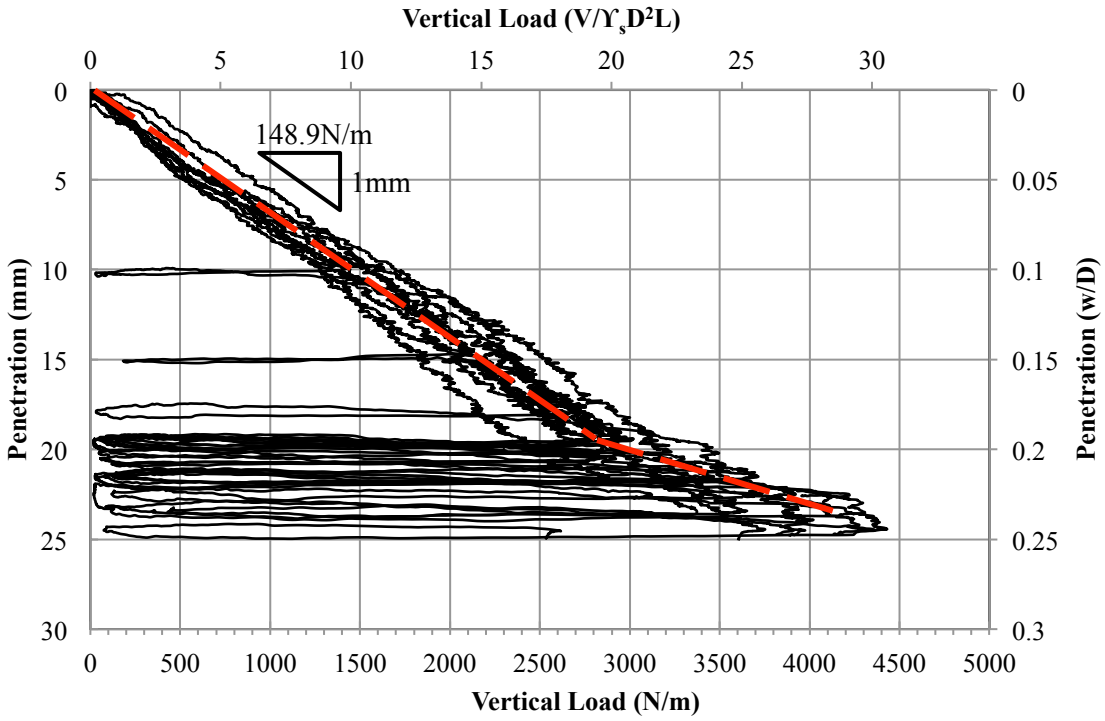

Figure 4.2 Test Results of Vertical Load-unload-reload Process

A model developed by Zhang (2001) was used to simulate the results of the vertical load-unload-reload process with the following equations:

$$w = \frac{k_{ve}-k_{vp}}{k_{ve}k_{vp}} V_{max} + \frac{V}{k_{ve}}, \quad 4\text{-}6$$

$$V'_{max} = k_{vp} \frac{w - V/k_{ve}}{1-(1+s\alpha)/(1+\alpha)(k_{vp}/k_{ve})}, \quad 4\text{-}7$$

where α is the parameter that controls the curvature of the reloading curve, and s is an indicator that defines the extent of the elastic zone ($0 < s \leq 1$). Zhang gave a

value of α = 0.5 and s = 0.1 which showed a good agrement with the data presented, as shown in Figure 4.3.

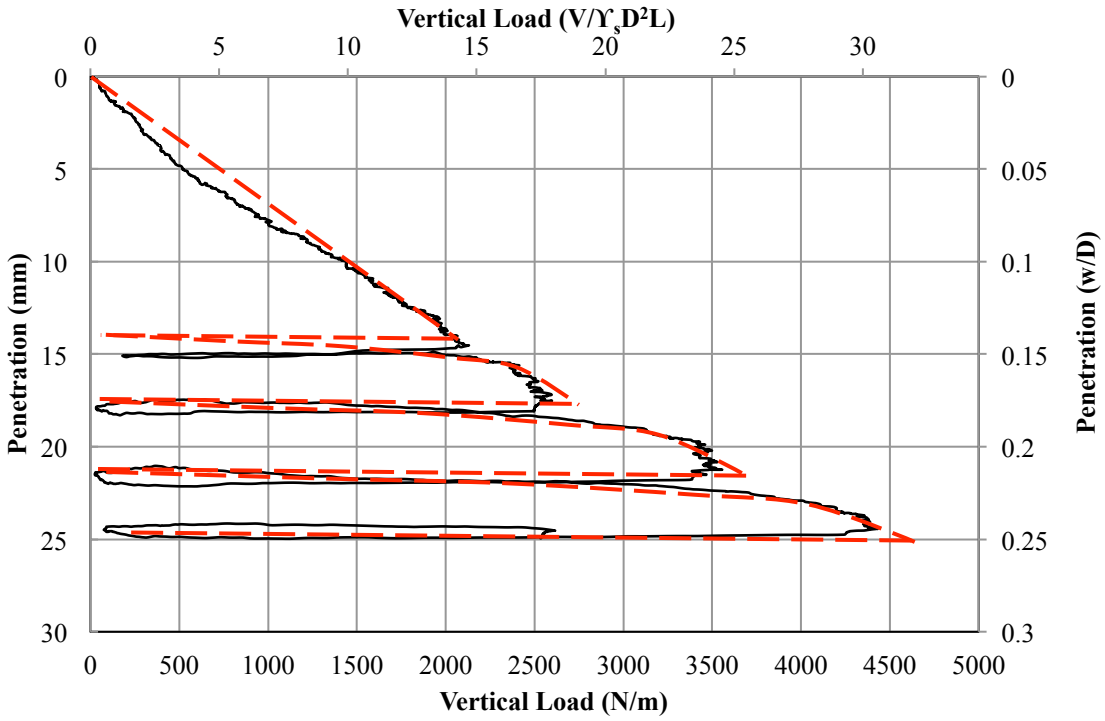

Figure 4.3 Detailed Result of Unload-reload Process (V10)

4. 3 Lateral Response

4.3.1 Introduction

In the analysis of on-bottom pipeline stability the lateral loads (e.g. hydrodynamic loads and excessive stress due to temperature differences between operation/rest periods) are resisted by the supporting soil along the pipe length. To obtain a confident prediction on the stability assessment, an appropriate pipe-soil interaction model is required. Results of previous work have shown that the lateral response of an on-bottom pipeline is dependent on its penetration into the seabed during lateral movement (Verley *et al.*, 1994; Zhang, 2001; and Tian, 2008).

The prediction of the lateral resistance of an on-bottom pipeline is generally based on two types of models. One type of model is built on empirical observation (known as the friction approach, Wagner *et al.*, 1989 and Verley *et al.*, 1994). In this approach the lateral resistance is calculated in terms of two components: i) a friction component which is proportional to the vertical load (self-weight) of the pipe; and ii) a passive component that accounts for the additional supportive force induced by the soil berm created on the direction of pipe lateral movement. This model predicts the maximum lateral load during horizontal movement (referred to as a "break-out" event) which can be calculated using an iteration program based on an assumed and back-calculated maximum penetration during the specific cycle of movement. However, this empirical model is not suitable to predict the pipe response under different loading conditions. Moreover, the loading history of the pipe-soil interaction system is not taken into consideration, making it insufficient for the stability assessment of cyclic loading events.

More recent investigations focus on plasticity solutions to study the pipe-soil interaction relationship. This second approach uses a yield envelope to define the limit combinations of vertical and lateral loads. It provides a possible framework to investigate the pipe-soil interaction system under various loading conditions. In this

approach, the size of the calculated yield envelope is dependent on the plastic displacement of pipeline, which is a function of pipe embedment. The horizontal and vertical behaviour are assumed to be elastic inside the envelope, and can be addressed by introducing two factors: horizontal and vertical elastic modulus. In addition, supplementary hardening equations have been established to define the expansion or contraction of the yield surface, which is directly linked to the plastic vertical displacement of the pipeline. A plastic potential curve was defined with a vector normal to it, and it describes the direction of the relative vertical and horizontal plastic displacements of the pipelines in the elastoplastic region. Some limitations can exist with this model however. For example, the construction of the proposed yield surface is based on an assumed flat seabed, where the berm effect is implicitly considered in the model. Moreover, the hardening law established in the model becomes less accurate when the lateral displacement is greater than two pipe-diameters (Tian, 2010), where the increasing effect from a berm accumulated in front of the pipe cannot be ignored.

To study the pipe-soil interaction relationship for different embedment and load conditions, a series of laboratory tests were carried out. In the lateral loading tests, the model pipe was moved laterally either under constant vertical load or at constant

embedment. Test results under constant vertical load can be analysed to investigate the effect of accumulated soil berm on the total lateral resistance, and the results of tests under constant embedment can be used to map a series of yield envelopes with various initial embedments.

4.3.2 Constant Vertical Load Probe Tests

A number of lateral loading tests under constant vertical load were conducted, as summarised in Table 4.1. During the test, the pipe was initially pushed into the sand to a particular depth z_{ini} with a measured maximum vertical load V_{max}. The pipe was then unloaded to the desired vertical load V_0 which was kept constant during lateral movement. An over-penetration ratio is defined to study the effect of loading history, and is similar to the over-consolidation ratio in geotechnics theory: the ratio of V_{max} to V_0, i.e. $OLR = V_{max}/V_0$.

As shown in Table 4.1, the tests were carried out with different maximum lateral displacements, including i) small displacement test (with a lateral displacement $\leq$ 0.5D), ii) constant vertical load tests with larger lateral displacement (y < 2D); iii) monotonic large displacement lateral loading tests (y > 2D) and iv) cyclic lateral loading tests (with a lateral displacement of up to 2D and 10 cycles of lateral loading). The applied constant vertical load level was varied between about ~25N, ~50N and

~75N. The vertical load is assumed to be uniformly distributed on the pipe segment, corresponding to line loads of ~83.3N/m, ~166.7N/m and ~250N/m respectively over the pipe segment with a length of 0.3m.

Table 4.1 Summary of Constant Vertical Load Tests Performed

Test	Constant Vertical Load			Initial Penetration	OLR	Max. Lateral Displacement	Number of Cycles
	(N)	(N/m)	$V_0/\gamma_s D^2 L$	(mm)		(mm)	
P01	24.5	81.6	0.56	5.15	24.84	25	3
P02	25.1	83.5	0.58	5.06	21.95	25	3
P03	49.7	165.7	1.14	4.76	10.13	25	2
P04	74.9	249.6	1.72	5.13	5.58	25	4
P05	74.8	251.1	1.72	5.10	5.89	25	3
P06	75.3	253.5	1.73	10.16	14.61	25	3
P07	76.1	246.9	1.75	10.54	14.70	20	2
P08	26.3	87.6	0.60	4.82	28.70	150	3
P09	25.7	85.8	0.59	4.73	23.41	150	3
P10	26.1	86.9	0.60	9.95	18.99	150	3
P11	51.0	170.0	1.17	5.24	5.25	150	3
P12	51.3	171.0	1.18	10.23	6.82	150	3
P13	25.1	83.7	0.58	4.84	11.64	450	1
P14	25.6	85.4	0.59	5.23	16.52	800	1
P15	25.5	85.1	0.59	6.67	17.28	350	1
P16	50.2	167.3	1.15	10.21	6.24	450	1
P17	50.6	168.5	1.16	5.40	8.60	600	1
P18	50.6	168.7	1.16	10.59	17.56	800	1
PC01	49.7	165.8	1.14	9.97	8.06	50	10
PC02	50.2	167.4	1.15	11.93	10.13	100	10
PC03	49.7	165.5	1.14	10.76	10.23	200	10
PC04	25.1	83.8	0.58	7.16	8.20	200	10
PC05	24.8	82.7	0.57	8.75	11.34	200	10
PC06	24.8	82.8	0.57	9.72	16.00	200	10

4.3.3 Test Results and Observations

i. Constant vertical load tests with small lateral displacement (y < 0.5D)

Figures 4.4 to 4.6 show the results of constant vertical load tests with small lateral displacement (0.25D) in 2-3 cycles (Tests P01-P07). The tests were conducted with different initial embedment of 5mm and 10mm under a constant vertical load of approximately 25N, 50N and 75N during lateral movement. The results of these tests are recorded in Table 4.2 below. Note that all loads have been normalised by the pipe length (L = 0.3m).

Table 4.2 Results of constant vertical load tests of 0.25D lateral displacement

Test	**P01**	**P02**	**P03**	**P04**	**P05**	**P06**
Maximum vertical load before sweeping, V_{max} (N/m)	2026.3	1833.0	1678.0	1392.0	1477.6	3703.9
Maintained vertical load, V_0 (N/m)	81.6	83.5	165.7	249.6	251.1	253.5
Maintained vertical load (dimensionless), $V_0/\gamma_s D^2 L$	0.56	0.58	1.14	1.72	1.73	1.75
Over-loading ratio, R	24.84	21.95	10.13	5.58	5.89	14.61
Initial embedment, z_0 (mm)	5.15	5.06	4.76	5.13	5.10	10.16
Measured maximum lateral load, H_{max} (N/m)	97.5	90.3	159.1	211.5	223.4	207.6
H_{max}/V_0	1.20	1.08	0.96	0.85	0.89	0.81
horizontal stiffness, k_H (N/m/mm)	30.1	63.1	41.6	33.2	41.2	31.2

It is seen in Figure 4.4 that the response of a lateral load event is dependent on the vertical load level. The lateral load of all tests increased monotonically before moving to the maximum lateral displacement of 0.25D. A peak resistance was observed to be

achieved at the end of each cycle, and was found to grow with the vertical load applied. However, the ratio of maximum horizontal load to vertical load (termed as the maximum friction factor, H_{max}/V), ranging from 0.85 to 1.18, slightly reduced with higher applied vertical load.

Figure 4.4 also shows that the results share similar trends in the first 2%D to 5%D, where the lateral load developed rapidly and almost linearly. During this stage the embedment was nearly unchanged before the lateral resistance reached the yield point (Figure 4.5). Hardening of lateral resistance was observed, and was found to slightly increase with larger initial embedment. This can also be reflected within the first 5mm of lateral displacement in the second cycle where only a small change in the vertical penetration was obtained. Moreover, the over-penetration ratios of the performed tests are ranged from 5 to 25. It was shown in Figure 4.5 that the model pipe with smaller overloading ratio penetrated into the soil at a larger rate and therefore reached to a deeper depth of maximum penetration.

After the rapid growth of lateral resistance, the horizontal stiffness reduced and lateral resistance gradually reinforced as the pipe moved laterally. The hardening caused downward penetration which showed a linear increase with the lateral displacement

before the maximum lateral displacement of the tests was reached (25mm, 0.25D).

The first two tests in Figure 4.5 P01 and P02 shared similar initial embedment (5.15mm and 5.06mm respectively) and vertical loads (81.56N/m and 83.52N/m respectively). The gradient in penetration for P01 was found to be steeper than that of P02 under a smaller overloading ratio. In the meantime, similar trends can also be observed in P04 and P05 where the pipe in P05 penetrated at a slower rate. On the other hand, the penetration of P03 and P06 with similar values of overloading ratio (10.13 and 14.61 respectively) showed a similar gradient in the plot. This may imply that higher overloading ratios lead to pre-compaction of the base soil from initial penetration, and consequently increasing the bearing capacity of the sand. In other tests with a larger over-penetration ratio the pipe went upwards, accompanied by a post-peak drop in horizontal stress. This is shown in the results of large amplitude tests. However, the initial embedment depth did not appear to have a major influence on these parameters.

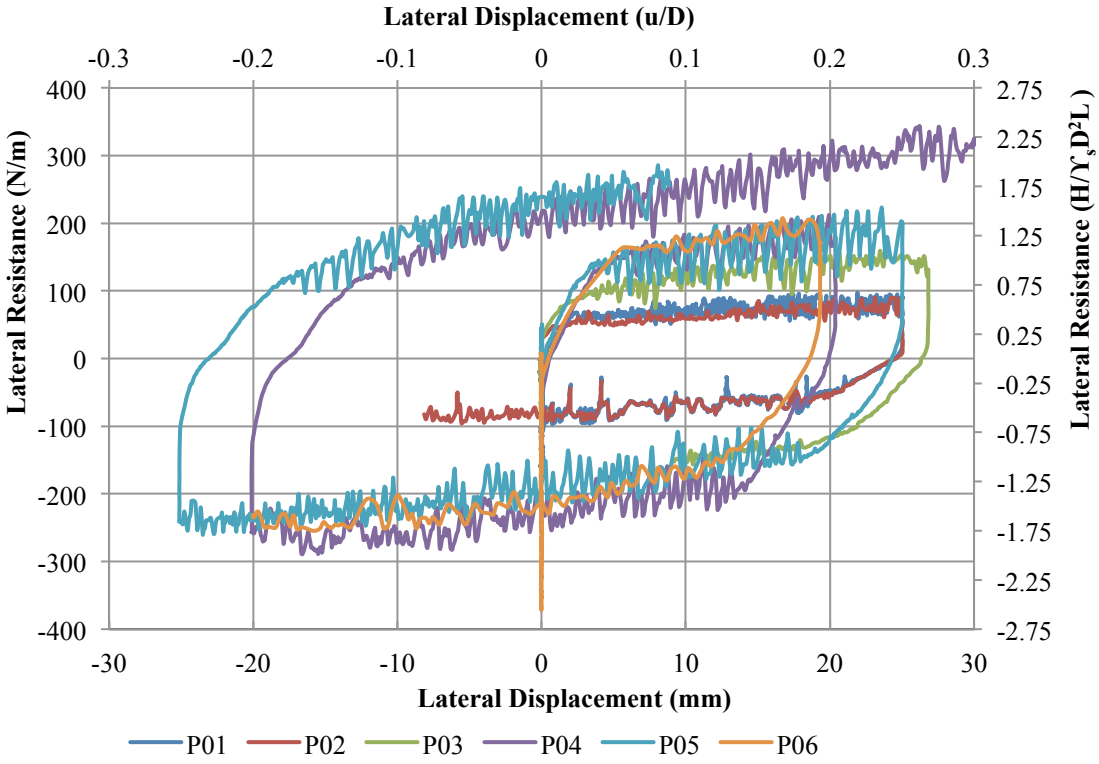

Figure 4.4 Total lateral load (tests with 0.2D-0.25D of lateral displacement)

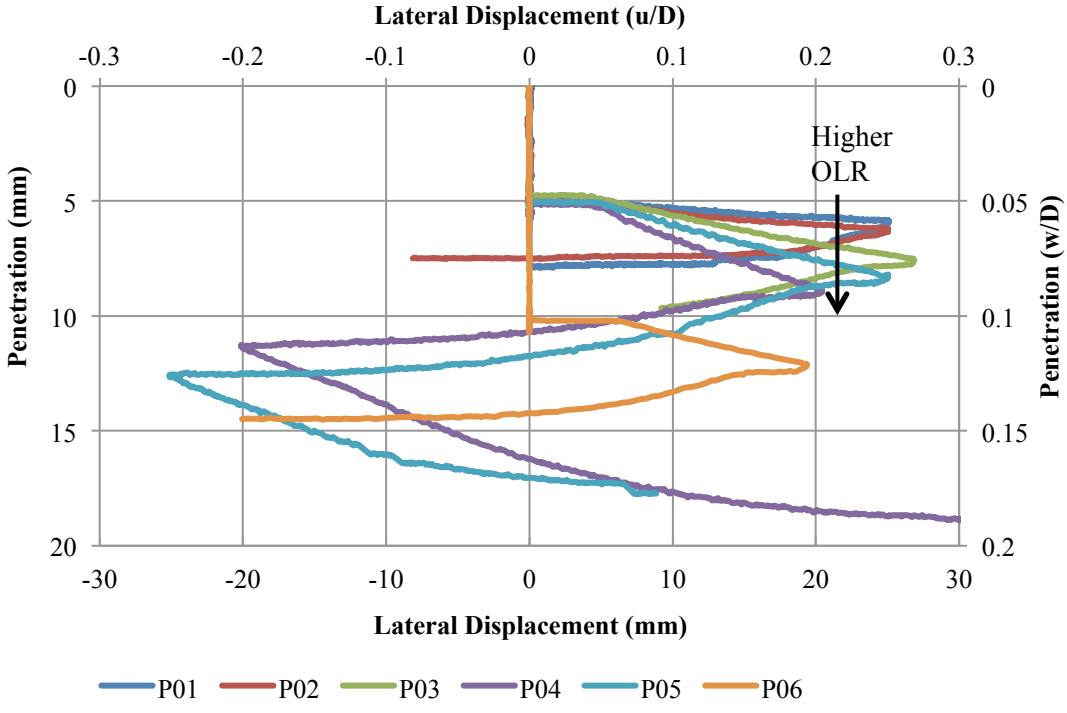

Figure 4.5 Penetration (tests with 0.2D-0.25D of lateral displacement)

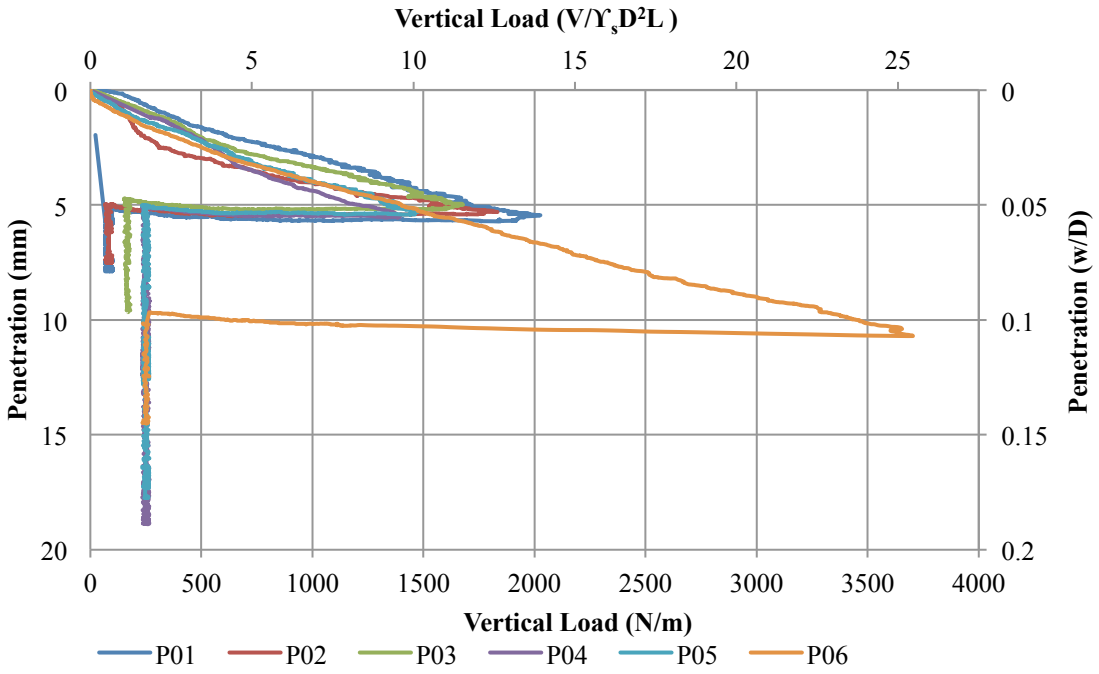

Figure 4.6 Vertical load (test with 0.2D-0.25D of lateral displacement)

ii. Constant vertical load tests with larger lateral displacement (y < 2D)

A series of tests (Test P08, P09, P10, P11, and P12) were conducted with a maximum displacement of 150mm (1.5D) under constant vertical load from ~25N to ~75N. The aim of this tests group is to investigate the influence of large lateral displacement on the lateral response of pipe-soil system as a comparison to that obtained in the tests with small lateral displacement. The normalized results are plotted in Figures 4.7 to 4.10, and characteristic values are summarised in the Table 4.3.

Table 4.3 Results of constant vertical load tests of 1.5D lateral displacement

Test	**P08**	**P09**	**P10**	**P11**	**P12**
Maximum vertical load before sweeping, V_{max} (N/m)	2515.0	2007.2	1650.1	891.8	1165.8
Maintained vertical load, V_0 (N/m)	87.6	85.8	86.9	170.0	171.0
Maintained vertical load (dimensionless), $V_0/\gamma_s D^2 L$	0.60	0.59	0.60	1.17	1.18
Over-loading ratio, OLR	28.70	23.41	18.99	5.25	6.82
Initial embedment, z_0 (mm)	4.82	4.73	9.95	5.24	10.23
Measured maximum lateral load, H_{max} (N/m)	92.0	98.8	110.7	216.4	217.0
H_{max}/V_0	1.05	1.15	1.27	1.27	1.27
Initial horizontal stiffness, k_H (N/m/mm)	31.8	26.5	29.9	48.5	54.4

Figure 4.7 shows the plot of lateral resistance against lateral displacement. The lateral response of the first cycle generally follows a similar trend with tests results of smaller maximum lateral displacement. During the first 0.02-0.05D of lateral displacement, the horizontal resistance developed in sand increased quickly to the yielding point, which is then followed by a hardening behavior. After the first stage, the horizontal resistance developed along the model pipe gradually increased at a rate of 0.18N/m/mm for tests under ~85N/m constant loading condition and 0.75N/m/mm for tests under ~170N/m constant loading condition. This gradual enhancement of lateral resistance resulted from a sand berm being created in front of the pipe as it moved forwards. After the pipe reached 1.5D in lateral displacement, the horizontal load reached maximum, which gives an estimated friction factor ranging from 1.05 to

1.27. The initial horizontal stiffness obtained from the test results show a slight increase with the vertical load level. Pipe with larger initial embedment and higher overloading ratio presents a greater initial horizontal stiffness, indicating a stiffer sand condition. The development of lateral resistance in the second cycle and the initial half part of the third cycle of lateral movement showed a similar growth with that in the first cycle. The lateral resistance was found to be mobilised at a lateral displacement of approximately 0.5D (at around -1D on the lateral displacement axis in Figure 4.7) and was close to the maximum lateral resistance obtained in the first cycle. However the maximum lateral resistance in the third cycle showed a further increase after the pipe passed the origin. This may due to the change in the ground surface. A trench was created during the first and second sweep; in particular a dominant berm was accumulated at the maximum lateral displacement, which provides greater resistance as the active berm created during lateral movement joined the dominant berm. A new peak lateral load was reached at y = -1D on the lateral displacement axis, and then it was found to drop and finally stayed at a slight smaller residual value.

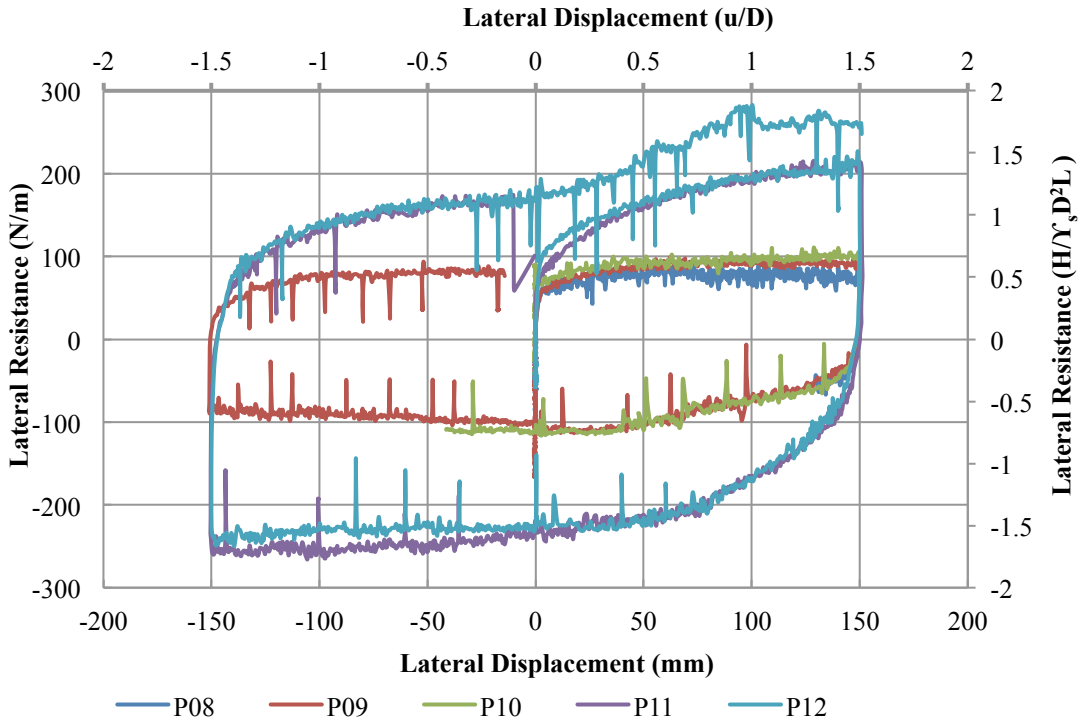

Figure 4.7 Total lateral load (tests with 1.5D of lateral displacement)

The development of penetration is plotted in Figure 4.8. A slight upward movement was observed at the beginning of test. This may have resulted from overloading of the model pipe when the model pipe penetrated into soil. The pipe penetration then remained constant as the initial embedment during the next 0.02D-0.05D of lateral displacement, which corresponds to the assumed "elastic region" of pipe-soil interaction system. After this stage, the pipe penetrated in to the sand at an average initial gradient of 0.1. The gradient however reduced as the pipe displaced laterally, which was different from that obtained in the constant loading tests with 0.2-0.25D of lateral displacement (as shown in Figure 4.5). This effect became more significant after the lateral displacement was greater than 0.5D of lateral displacement (0.25D for

P08 and P09 because of a lower vertical load applied). Furthermore, the pipe penetration tends to remain constant after a lateral displacement of 1D, indicating that the volume of soil that is being displaced increased linearly with lateral displacement thereafter. Accordingly, a linear increase was observed in the lateral resistance after 1D of lateral displacement in all cycles, and the horizontal load stiffness ($\Delta H/\Delta y$) was found to increase with this constant vertical penetration. In the beginning of the second cycle, the pipe penetrated further into the sand with an initial gradient greater than that in the first cycle as it moved backwards. The maximum depth during the second cycle was achieved at a horizontal displacement of approximately 75mm, half of the amplitude that was applied in the tests. Beyond this point the pipe penetration remained unchanged for a small lateral displacement. As the collection of the active berm grew, upward movement was observed and the vertical location of the model pipe even went beyond the initial embedment. As a result, the horizontal resistance of the pipe in the second cycle only showed a small increase or even decreased (refer to test P09, Figure 4.7) after the pipe passed its starting point.

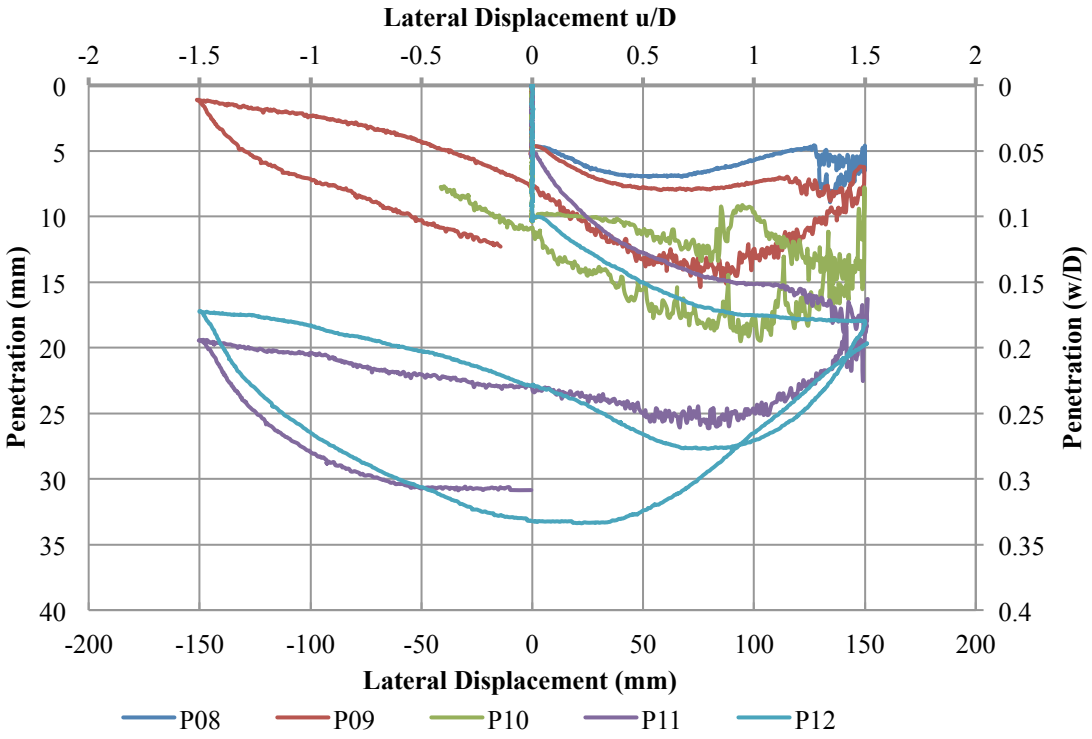

Figure 4.8 Penetration (tests with 1.5D of lateral displacement)

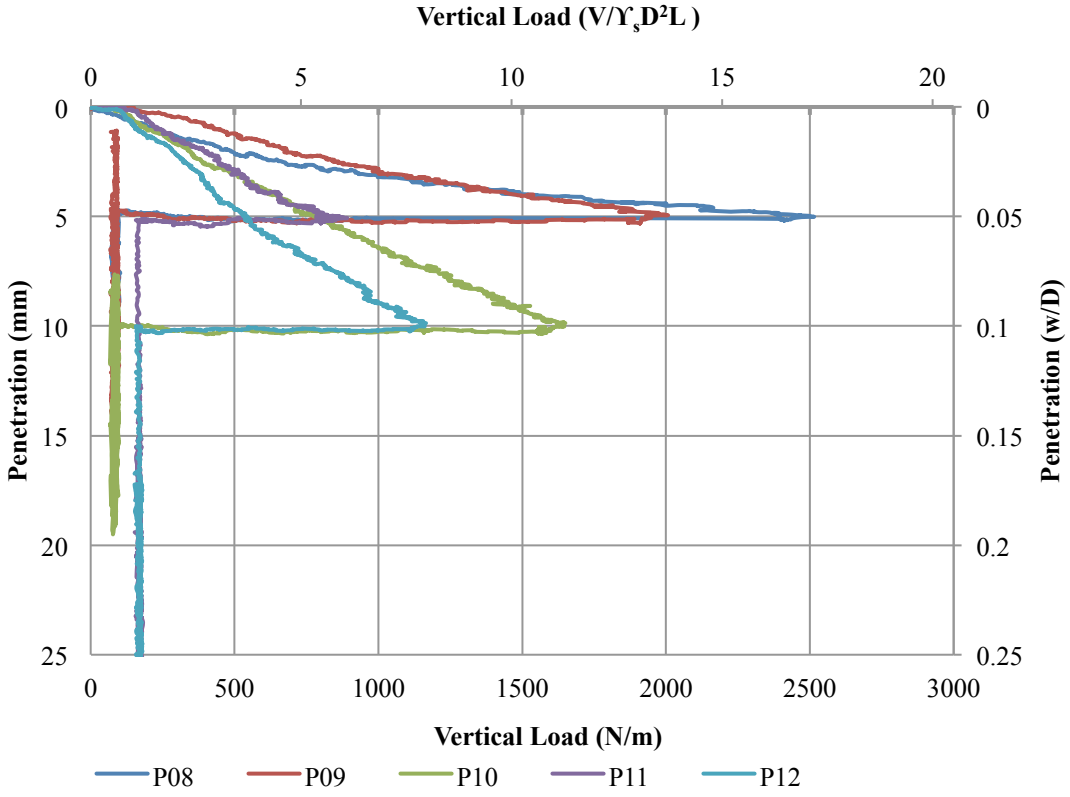

Figure 4.9 Vertical load (tests with 1.5D of lateral displacement)

The maximum global penetration was achieved when the model pipe passed through original lateral position, which is at about a lateral displacement of half the trench width that the pipe created during the first two cycles. This was different from that observed in Figure 4.4 where the lateral resistance increased monotonically. A peak value at a lateral displacement of about 1D was obtained, where the pipe is found to break out of the current ground surface (P09, Figure 4.7). This resulted in a decrease of the soil being displaced and hence reduced the resistance provided by the active soil berm accumulated in front of the pipe while travelling laterally.

iii. Constant vertical loading test of large monotonic displacement (y > 2D)

Test results of the lateral load-displacement response with large lateral displacement (y > 2D) under various constant vertical load at an initial embedment of 0.05D-1D are plotted (test P13-P18). The vertical load-displacement relationship at the beginning of the tests and the development of penetration while the pipe moved laterally was shown in Figures 4.10 and 4.11. The results of each test are summarised in the Table 4.4 below. The model pipe in test P15 and P18 was displaced to a maximum lateral displacement of 8.5D to investigate the influence of very large displacement on the lateral response, whilst in other tests a minimum lateral displacement of 3.5D was attained. The results reveal that the lateral response is dependent on the vertical load

level, with a maximum friction factor (H_{max}/V_0) ranging from 1.12 to 1.84. Comparing the test results of P13 with P14 which both started with similar initial embedment depth of 4.8mm and 5.2mm respectively, it can be seen that the lateral response does not differ much, despite the fact that the pipe in test P15 has a greater overloading ratio (17.3 in P15 against 11.6 in P13). This indicates that the overloading ratio may be a trivial factor and has minimal influence on the lateral response of pipe in sand material. However in test P16 and P18 which share a similar initial embedment of around 10mm, the maximum lateral resistance obtained from test P16 is much greater than that obtained from test P18. This may due to the discrepancy in the initial relative density of sand during preparation leading to a lower bearing capacity. Figure 4.12 shows the vertical load-displacement relationship before the pipe started to move laterally. The response of P16 clearly showed a smaller load-displacement ratio compared with the other tests, which indicates a less stiff sand condition. No significant influence was observed for the initial embedment mobilise the total lateral resistance.

Table 4.4 Results of constant vertical load tests of large lateral displacement

Test	P13	P14	P15	P16	P17	P18
Maximum vertical load before sweeping, V_{max} (N/m)	997.9	1385.4	1443.2	1042.0	1364.4	2923.0
Maintained vertical load, V_0 (N/m)	85	87	83	165	167	166
Maintained vertical load (dimensionless), $V_0/\gamma_s D^2 L$	0.59	0.60	0.57	1.14	1.15	1.14
Over-loading ratio, R	11.6	16.5	17.3	6.2	8.6	17.6
Initial embedment, z_0 (mm)	4.8	5.2	6.6	10.2	5.4	10.5
Measured maximum lateral load, H_{max} (N/m)	109.0	109.7	136.2	306.7	208.6	187.4
H_{max}/V_0	1.31	1.32	1.64	1.84	1.25	1.12
Initial horizontal stiffness, k_H (kPa)	12.0	11.4	10.9	14.3	28.7	14.8

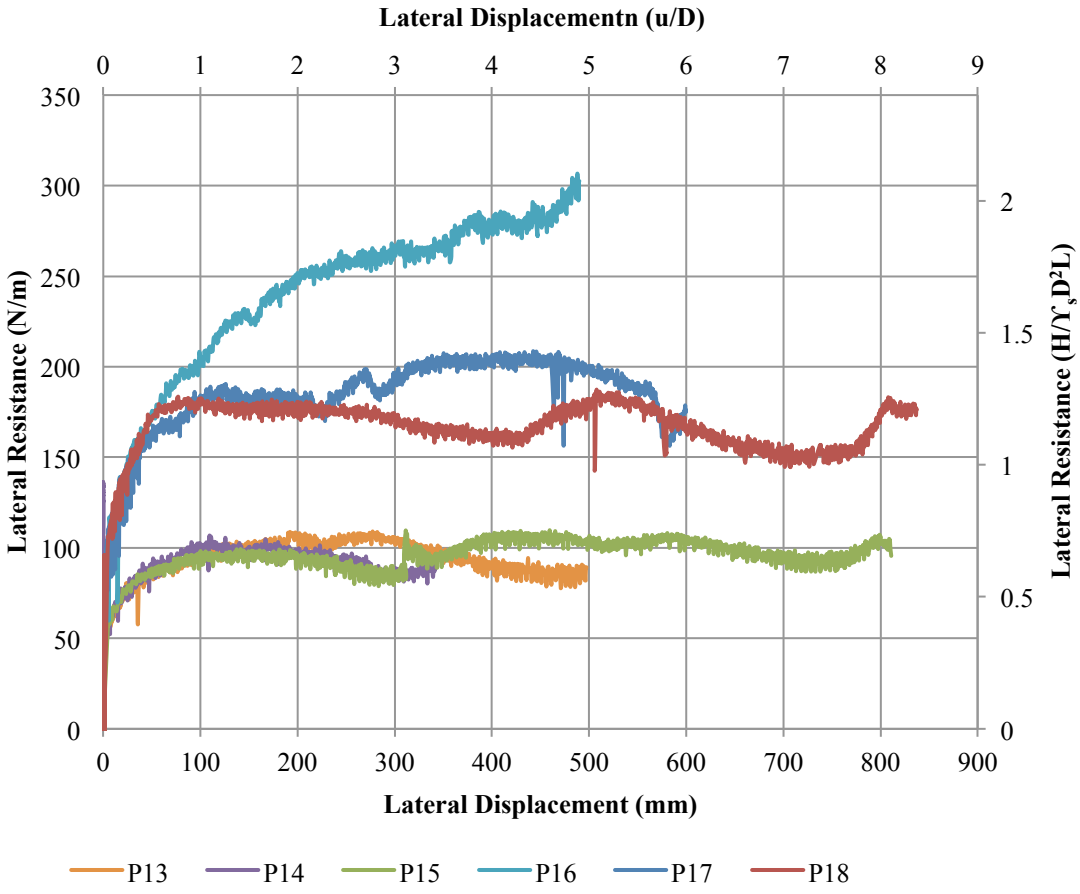

Figure 4.10 Total lateral resistance (tests with large lateral displacement)

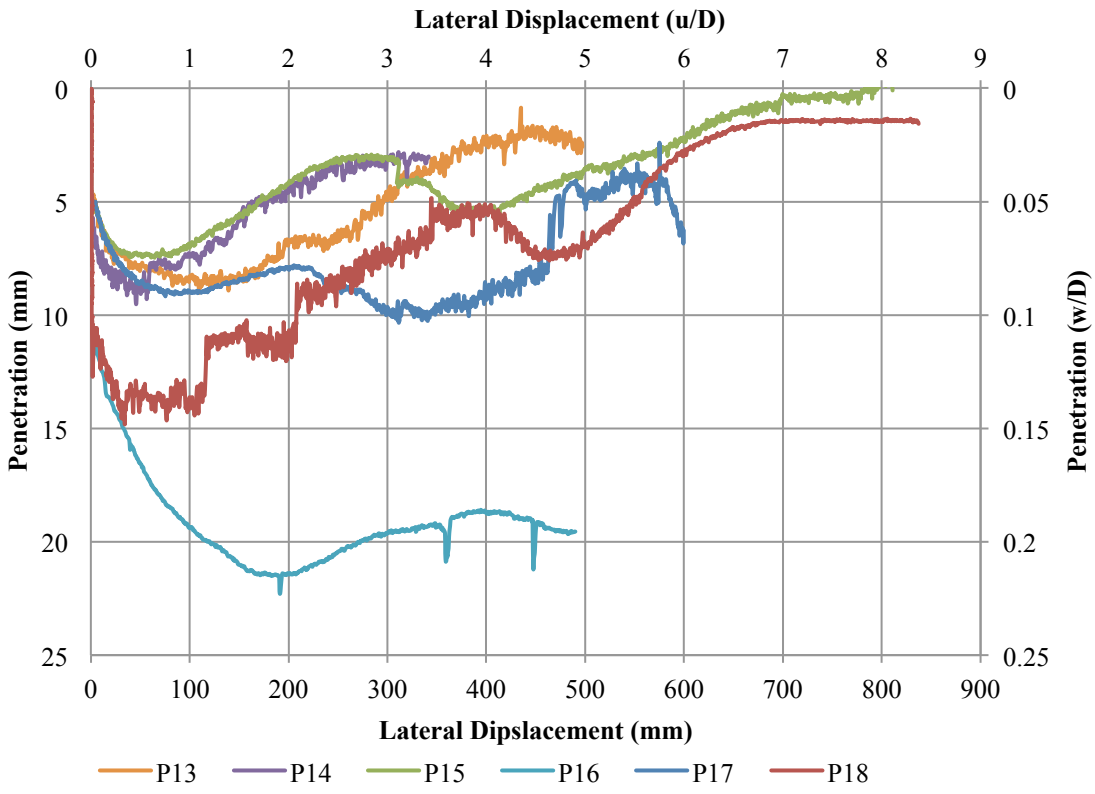

Figure 4.11 Penetration (tests with large lateral displacement)

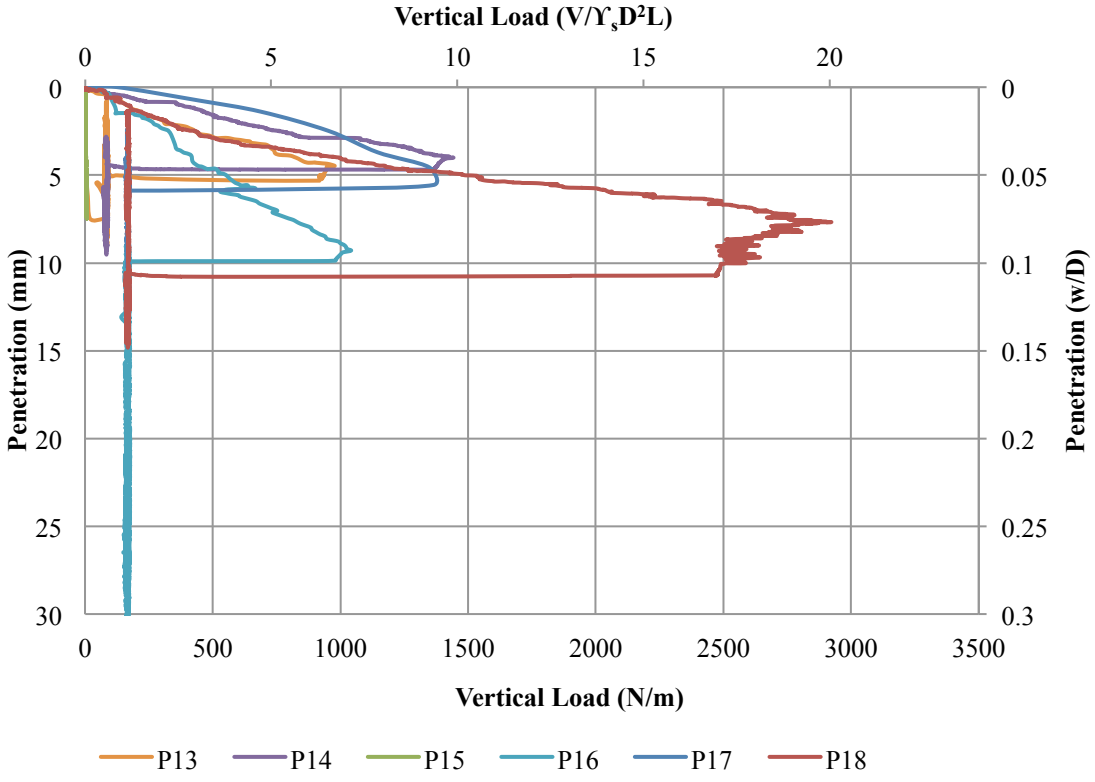

Figure 4.12 Vertical load (tests with large lateral displacement)

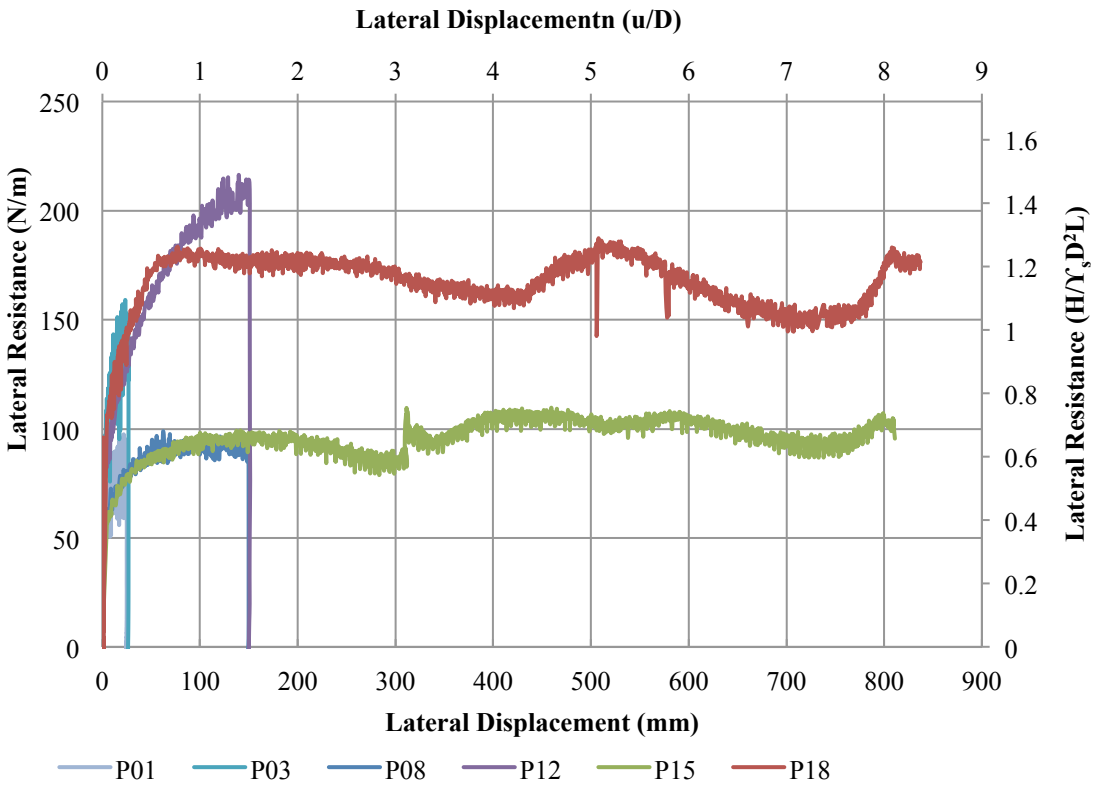

Figure 4.13a Comparison between tests of different lateral displacement in terms of lateral load

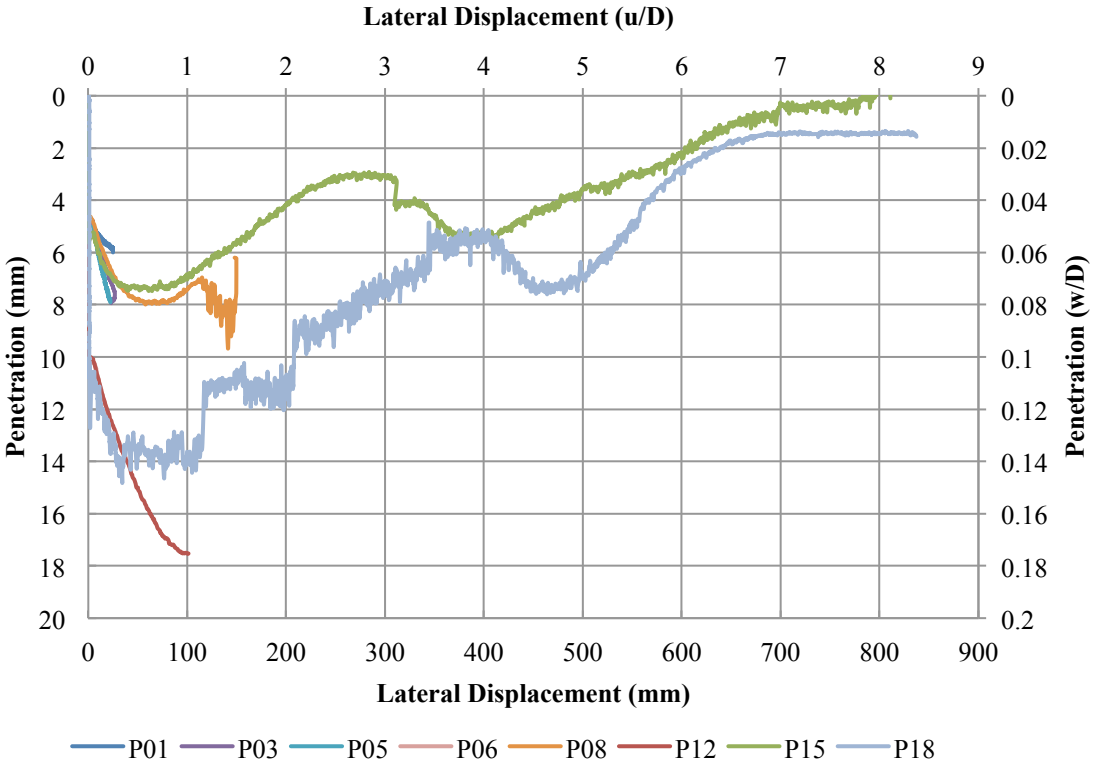

Figure 4.13b Comparison between tests of different lateral displacement in terms of embedment

The pipe trajectories obtained from the tests explain the development of lateral resistance of the partially embedded pipe in Figure 4.11. The penetration of the pipe during lateral movement reached a maximum at a lateral displacement of about 0.5D (test P14, P15, P18) with an overloading ratio around 17. However others were at a lateral displacement of approximately 1D (test P13 and P17) with a much lower overloading ratio. In addition, the corresponding lateral resistance at such lateral displacement also achieved its maximum value. This agrees with the observation obtained in the test with smaller lateral displacement (Figure 4.13), which implies that the overloading ratio may affect the mobilising displacement to obtain the maximum lateral resistance. The pipe movements are approximately similar at the beginning of the lateral movement regardless of the overloading ratio for the test with same initial embedment (see Figure 4.11). A softening in lateral resistance was observed in the post-peak region after the initial breakout of the partially embedded pipe with higher vertical load, which models a “heavy pipe” (simulates pipes that have greater self-weight). However the change in pipe penetration during the sweep creates different profiles of pipe trajectories which subsequently affect the total lateral resistance at larger lateral displacement. Despite the further downward penetration observed after the initial breakout that is probably due to local weakness of the sand, the embedment of both a “heavy” and “light” pipe eventually reached a constant value

(test P14 and P18) of approximately a mere 0.8-1.4mm. The displaced soil is therefore a small amount and has trivial impact on the size of the berm in front of the advancing pipe.

iv) Cyclic constant vertical loading tests

In the tests presented above, a hardening effect is observed in which the lateral resistance was found to enhance with cycles of lateral loading. A series of cyclic tests were conducted to study this cyclic effect on the lateral response of partially embedded pipes. The cyclic tests were performed with an initial embedment of 10mm, and varied in the vertical load as well as maximum lateral displacement. Some additional cyclic tests were conducted to investigate the effect of overloading ratio. The results of cyclic tests are presented in the following Figures 4.14 to 4.19. Figures 4.14 to 4.16 show the results of probe tests (PC01-03) under a constant vertical loading of about 50N (equivalent to a uniformly distributed load of 166.7N/m over the pipe width) with various maximum lateral displacements. The results of other tests with a constant vertical loading of around 25N (equivalent to a uniformly distributed load of 83.3N/m) are subsequently plotted in Figure 4.17 to 4.19. In the test PC01 (Figure 4.14) and PC02 (Figure4.15), the pipe was only laterally displaced by 0.5D and 1.0D for comparison, whereas all of the other cyclic tests were conducted with a maximum lateral displacement of 2D. Table 4.5 summarises the vertical condition and

measured lateral resistance during lateral sweeps.

Table 4.5 Summary of cyclic loading tests

Test	Initial embedment z_{ini} (mm)	Max. vertical load, (N/m)		Vertical load during sweeps (N/m)		Max. lateral resistance in 1st cycle (N/m)	Max. lateral resistance H_{max} (N/m)	Max. penetration z_{max} (mm)
		V_{max}	OLR	V_0	$\frac{V_0}{\gamma_s D^2 L}$			
PC01	9.97	1336.3	8.06	165.8	1.14	189.4	397.5	47.43
PC02	11.93	1696.1	10.13	167.4	1.15	173.6	401.8	63.00
PC03	10.70	1693.6	10.23	165.5	1.14	235.2	414.2	60.33
PC04	7.16	686.7	8.20	83.8	0.58	106.2	186.1	39.42
PC05	8.75	937.6	11.34	82.7	0.57	106.6	177.3	36.14
PC06	9.72	1324.9	16.00	82.8	0.57	96.2	178.2D	33.34

Figure 4.20 and 4.21 demonstrates that the lateral response of shallowly buried pipe is mainly dependent on the vertical load level. Prediction using a model developed by Verley *et al.* (1994) gives an underestimation of the maximum lateral resistance. More importantly, the breakout displacement used in the model (assumed to be 0.5D to obtain maximum lateral capacity) is found to be about 1.5D. The maximum lateral load for the first cycle was obtained at the maximum lateral displacement of 2D for test with constant vertical load of 83.3N/m and 166.7N/m, which was 96.3N/m and 235.3N/m respectively. The corresponding friction factor was calculated as 1.16 and

1.40 with respect to the different vertical load level. In addition, the lateral resistance is found to increase with the number of cycles. A peak can be observed after the second cycle, at which point a trench has been created by the pipe while moving back and forth. The maximum lateral resistance was achieved at the last cycle for both tests, with a peak value of 174.1N/m and 412.4N/m. The respective friction factor increased from 2.14 with lower vertical load to a greater 2.42. Table 4.6 summaries the corresponding maximum friction factor during each cycle.

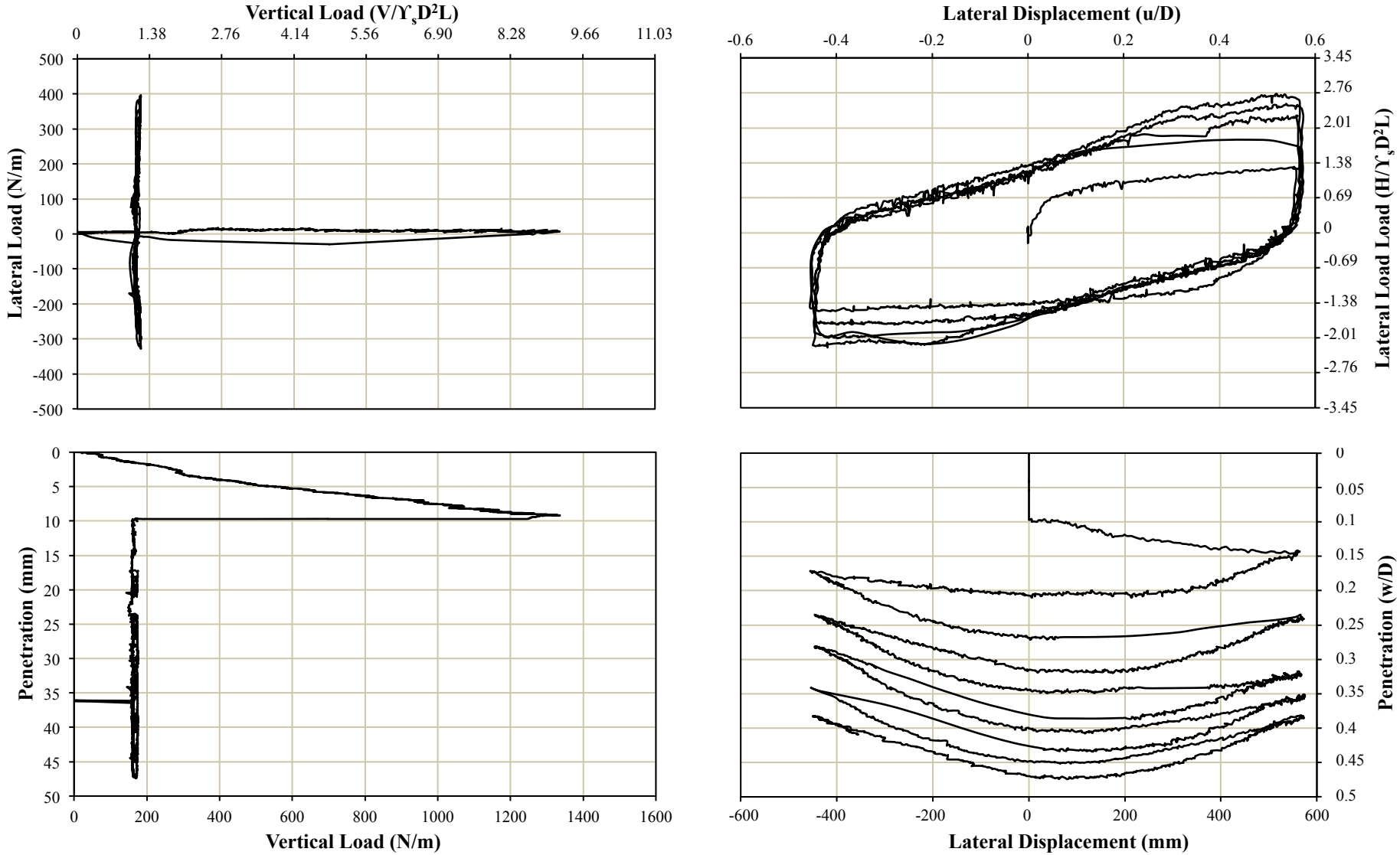

Figure 4.14. Test result of cyclic constant loading test PC01

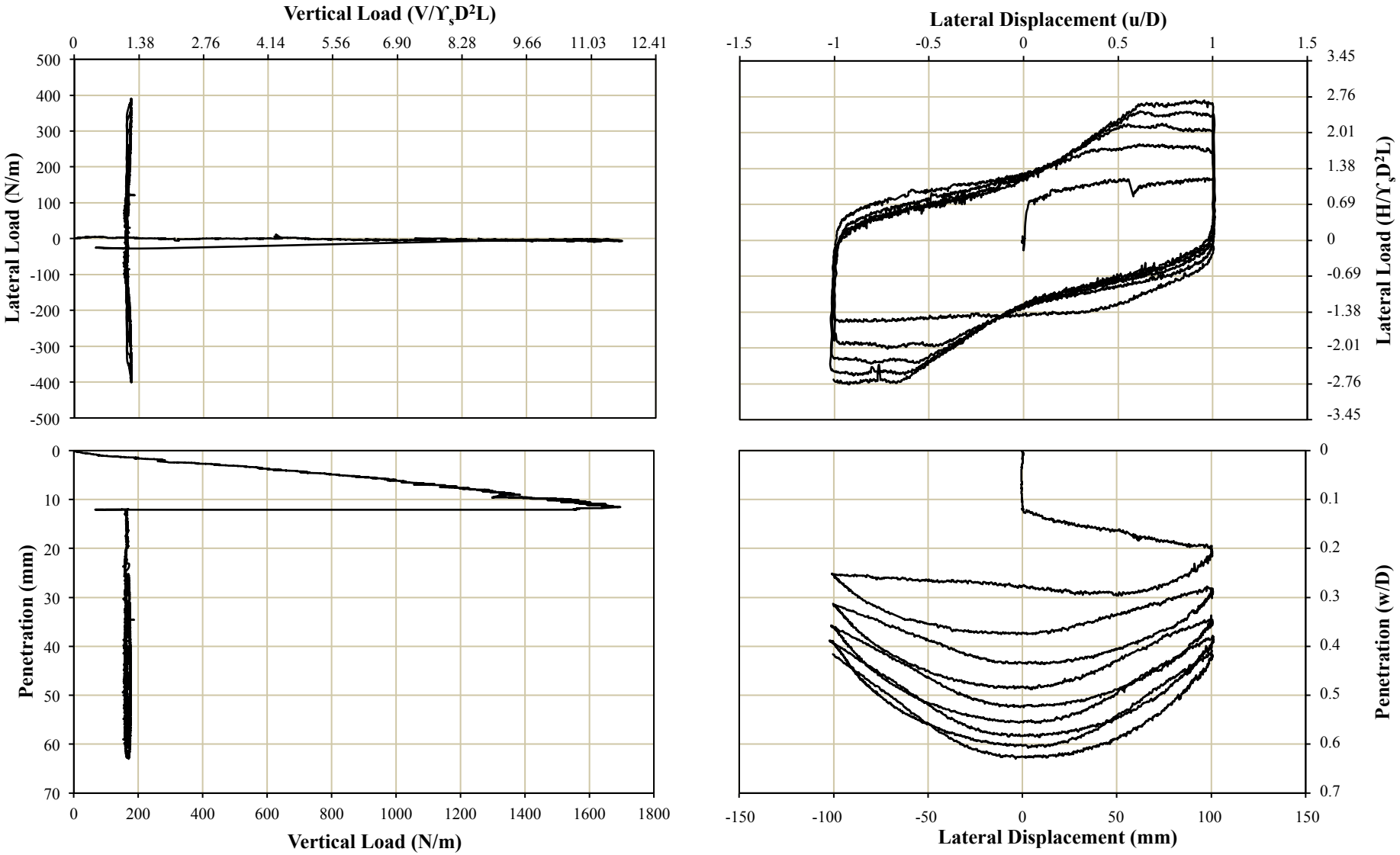

Figure 4.15. Test result of cyclic constant loading test PC02

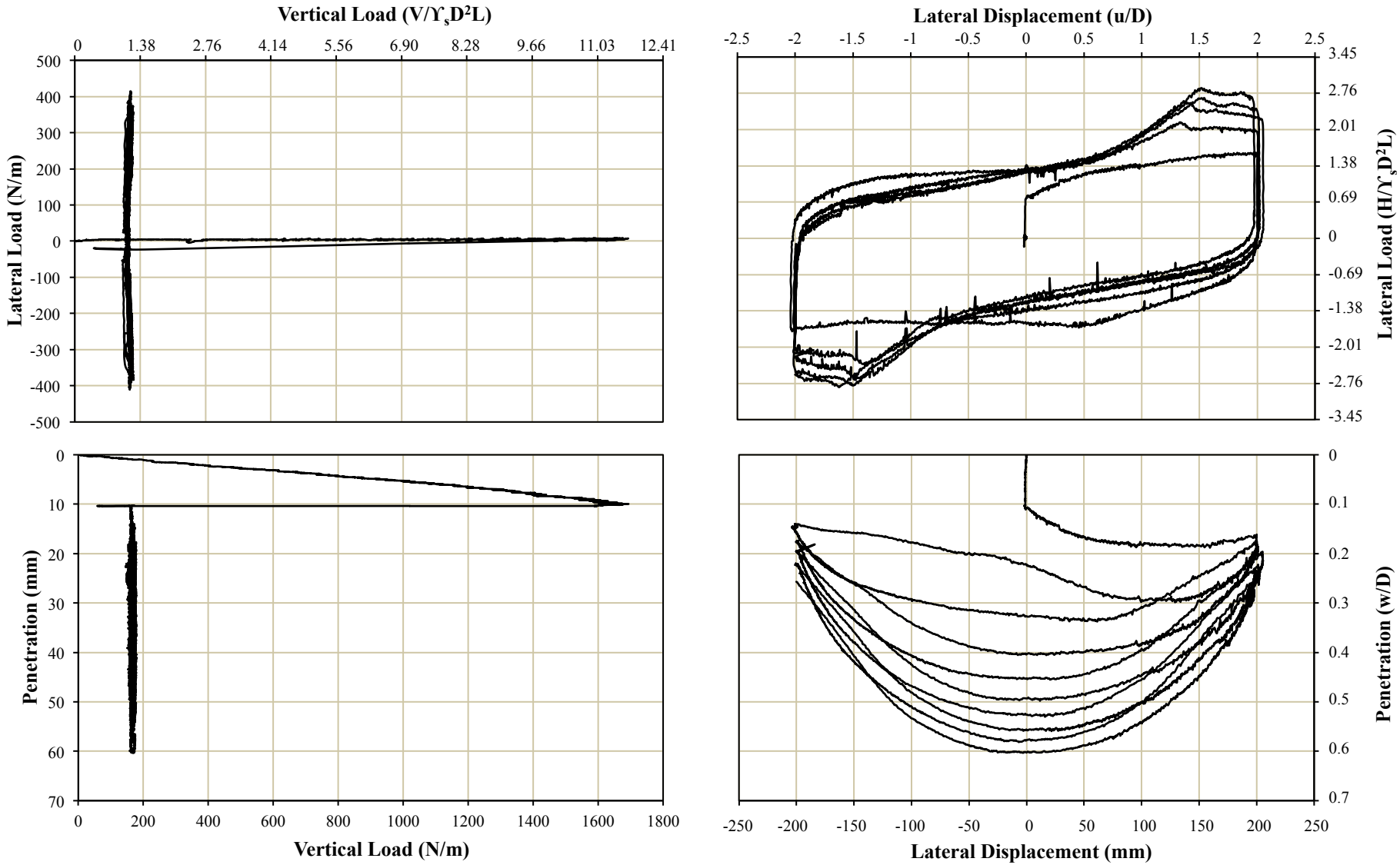

Figure 4.16. Test result of cyclic constant loading test PC03

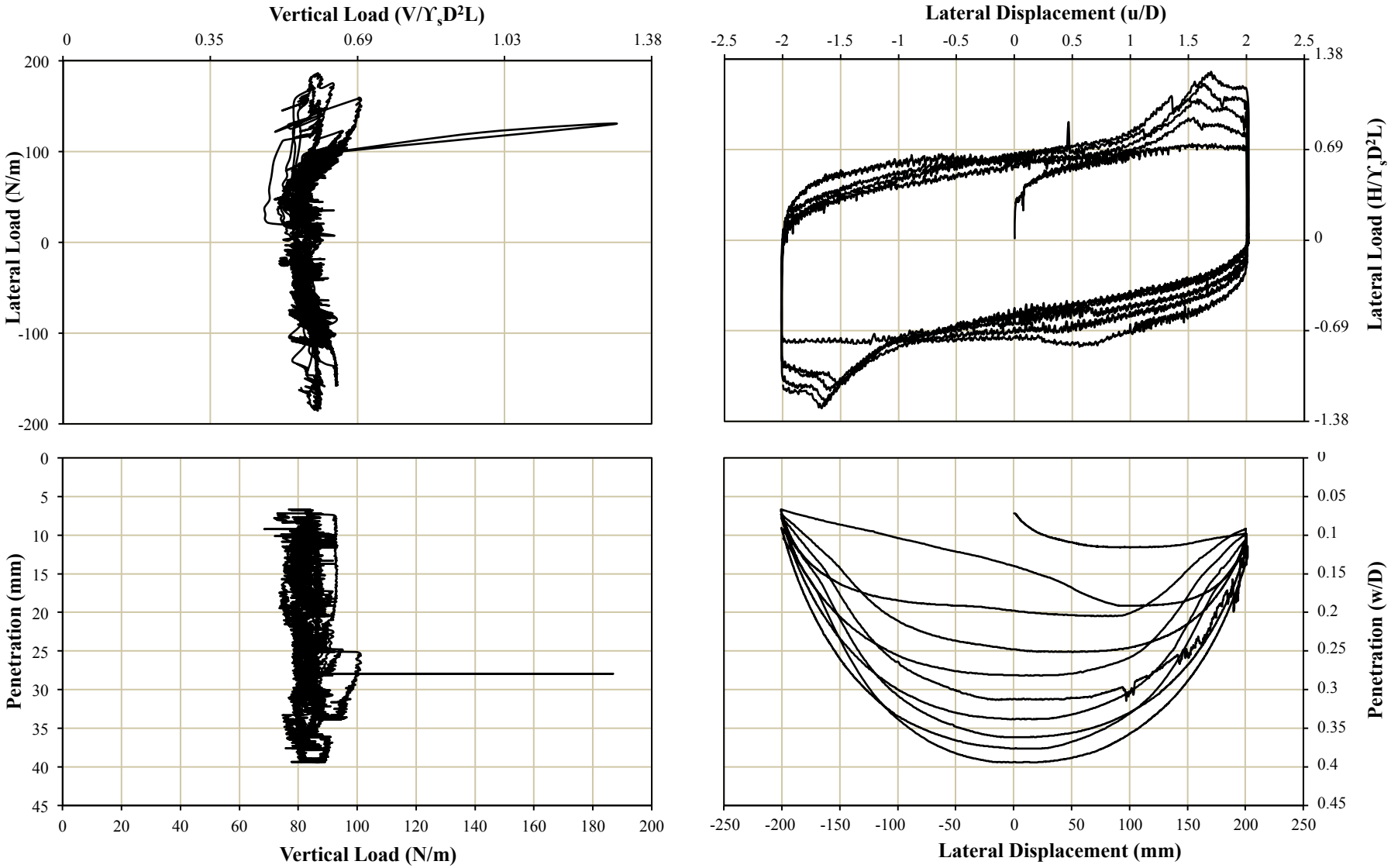

Figure 4.17. Test result of cyclic constant loading test PC04

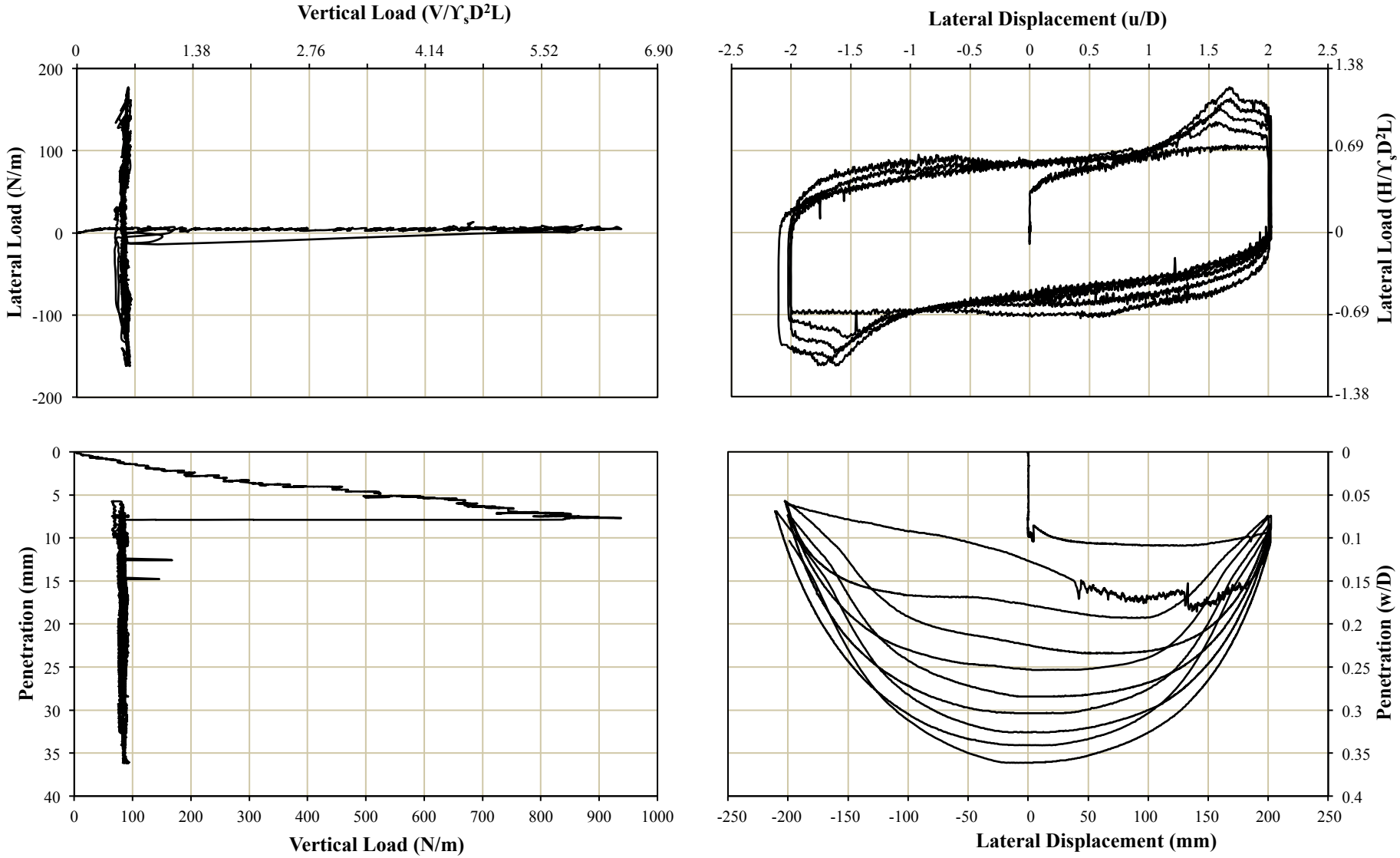

Figure 4.18. Test result of cyclic constant loading test PC05

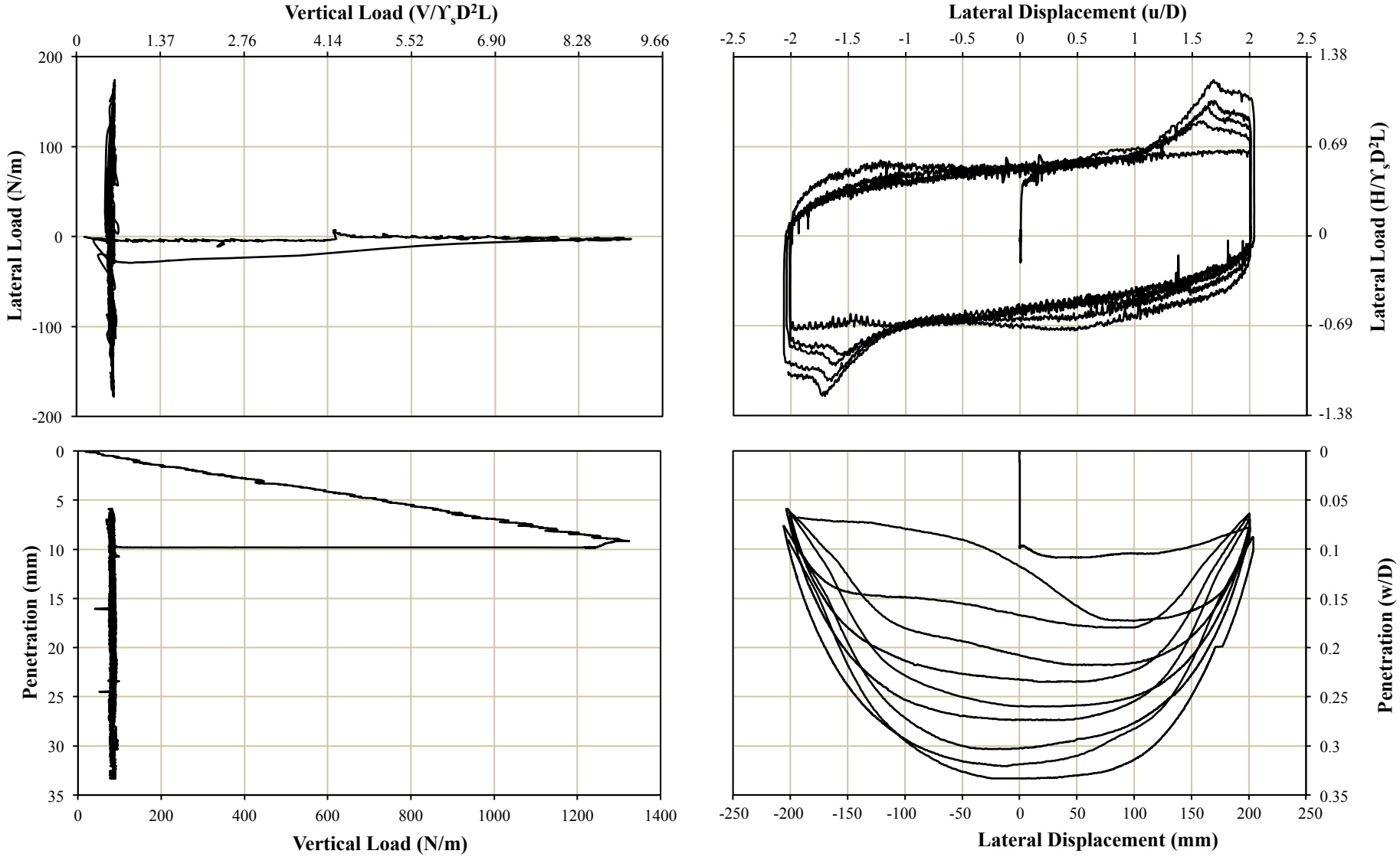

Figure 4.19. Test result of cyclic constant loading test PC06

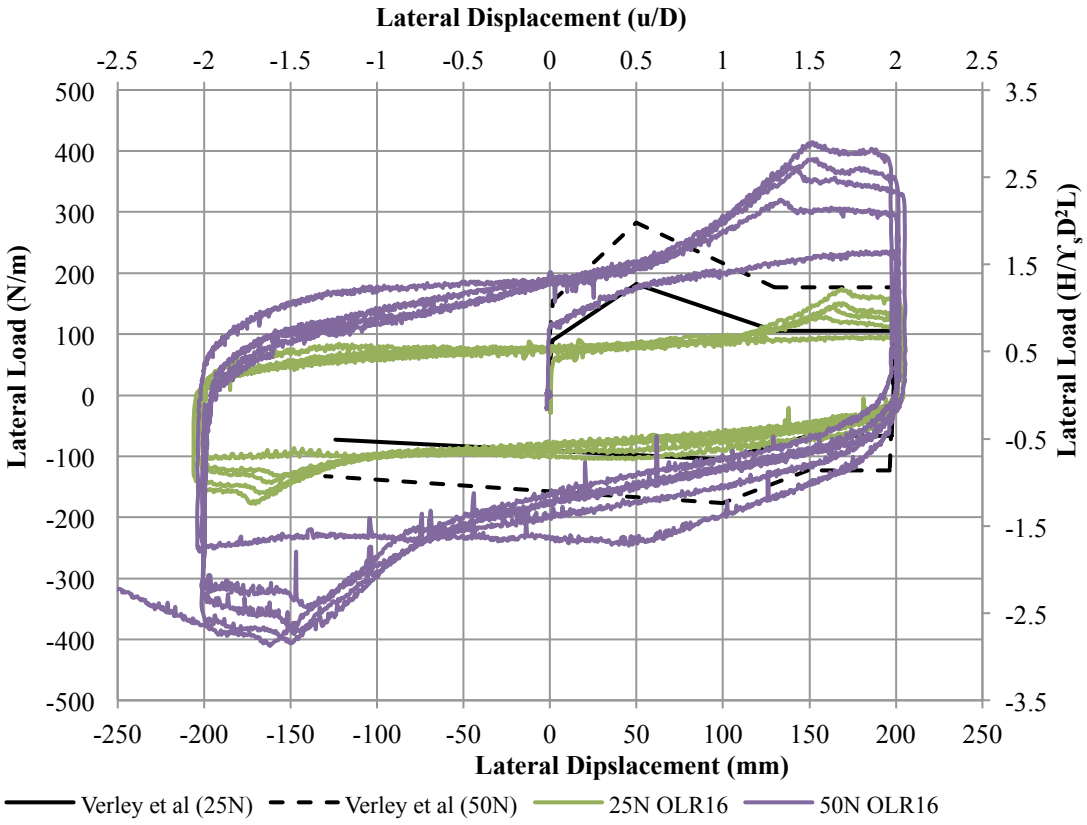

Figure 4.20 Comparison between vertical load levels

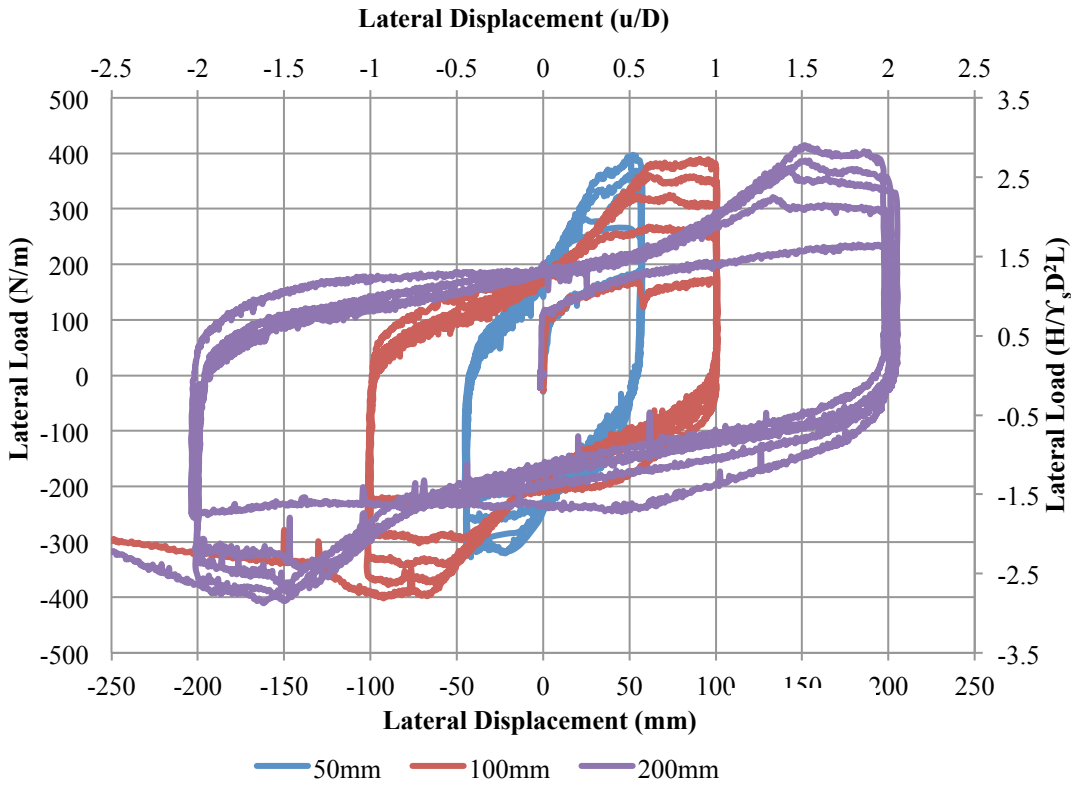

Figure 4.21 Comparison of lateral resistance between maximum lateral displacements

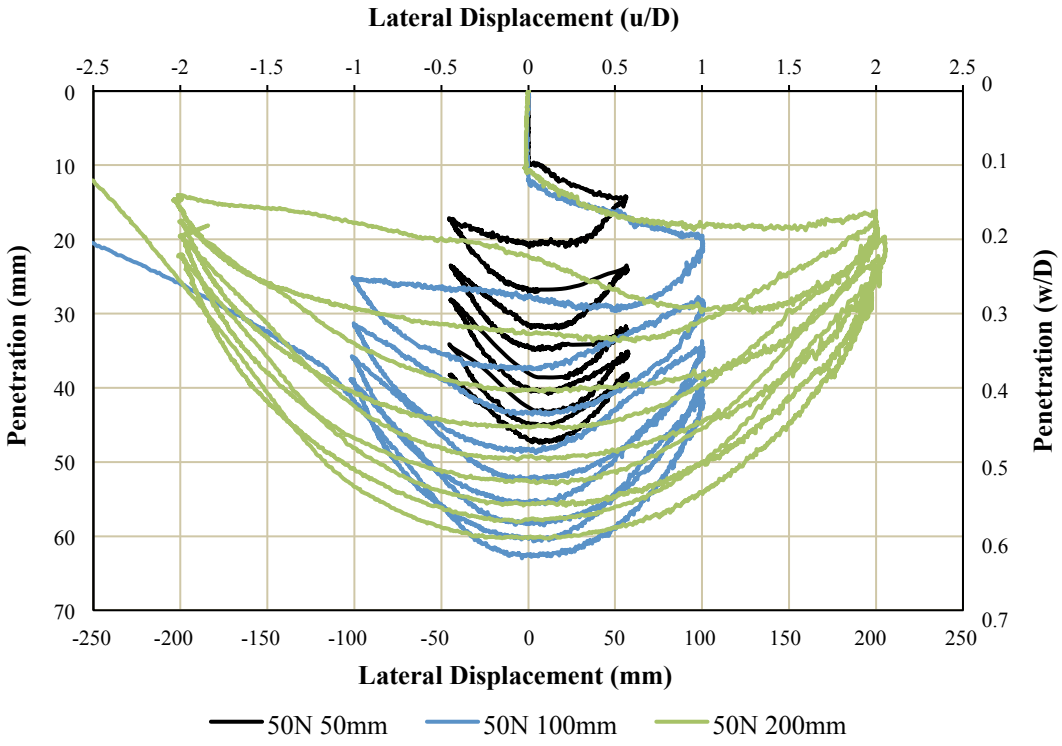

Figure 4.22 Comparison of pipe penetration between maximum lateral displacements

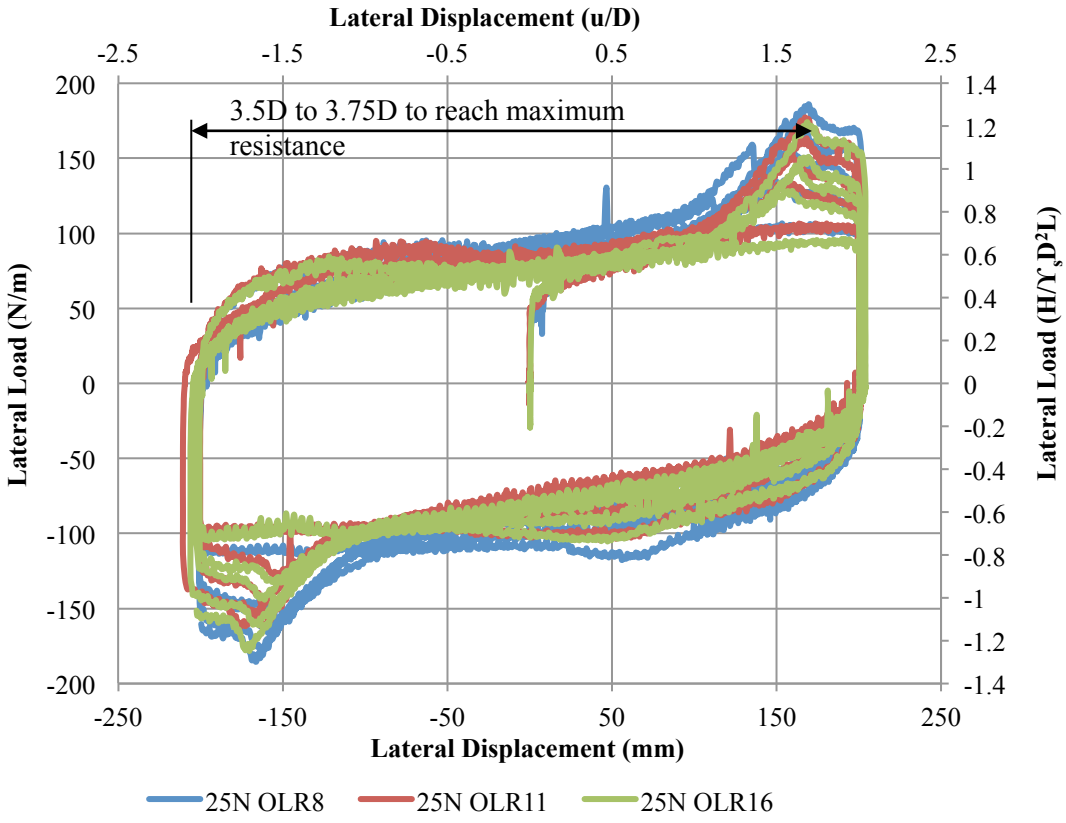

Figure 4.23 Comparison between overloading ratio

Table 4.6 Maximum friction factor

Test / Cycle	PC03 (V_0 = 165.5N/m)		PC05 (V_0 = 82.7N/m)	
	H_{max} (N/m)	H_{max}/V_0	H_{max} (N/m)	H_{max}/V_0
1	235.2	1.42	106.6	1.29
2	246.3	1.49	103.4	1.25
3	316.1	1.91	126.8	1.53
4	346.9	2.10	132.8	1.61
5	370.6	2.24	145.2	1.76
6	385.0	2.33	144.1	1.74
7	385.1	2.33	149.7	1.81
8	403.7	2.44	160.1	1.94
9	412.4	2.49	174.1	2.11
10	414.2	2.50	177.3	2.14

The maximum friction factor is found to increase with each cycle, which may due to the growing dominant berm at the side of the trench created by the pipe movement. At higher cycle number the pipe created a relatively deep trench, and consequently a larger dominant berm grew as the pipe displaced more soil at the end of each cycle. This may lead to subsequent change in the ground surface. Therefore more work was required to be done by the pipe on the sand, not only to push the sand laterally into the collected berm, but also to push the berm upwards when approaching the edge of the created trench.

Figure 4.21 compares test results with different maximum lateral displacement. The results presented were recorded from tests under similar level of vertical loads (50N) but with a maximum lateral displacement of 50mm (0.5D), 100mm (1D) and 200mm (2D) respectively. The responses of the three tests were very close before the pipe travelled to the maximum lateral displacement, and it seems that the lateral resistance would be constant at a lateral displacement of 2D. In the followed cycles a peak lateral load can be observed, and the

required lateral displacement to reach this peak load was found to increase with the maximum lateral displacement. Moreover, the development of lateral resistance was found to match with the pipe trajectories as plotted in Figure 4.22 in the first cycle (from y/D = 0 to y/D = 1). It is clear that the pipe penetration in the first cycle reached a maximum value at a lateral displacement of 1D, after which then only a small change was observed. However in higher cycles the maximum penetration was retained at about origin, where the corresponding lateral resistance was still rising. This is due to the active berm was still growing, which results in an increase in the depth of soil being ploughed away. The effect of ploughed depth will be discussed in the next chapter. The maximum penetration after ten cycles for the test with a lateral displacement of 50mm is found to be about 48mm, which is less than that obtained in the tests with lateral displacement of 100mm and 200mm respectively. However, the maximum penetration of pipe after ten cycles of lateral loading seems not to change much with maximum lateral displacement over 100mm.

The lateral resistance obtained for tests with different overloading ratio is compared in Figure 4.23. The results are similar, indicating that the overloading ratio is a minor factor to obtain the lateral displacement. In addition, the figure demonstrates that the lateral resistance seems to reach a steady value of approximately 100N/m regardless of cycles, both for positive and negative direction of lateral movement. This constant lateral resistance was found to be reached after the pipe has been laterally displaced by 0.5D. Other test results with doubled constant vertical load (50N in Test PC04 to PC06) show a linearly greater mobilised lateral load of around 200N/m. However the difference in the lateral resistance over cycling was observed after the pipe was laterally displaced by 3D, where the lateral resistance showed a further increase. A maximum lateral resistance at about 3.5D to3.75D of lateral displacement was observed. Moreover, in the pipe trajectories plotted in Figure 4.17 to 4.19 the test result

with a higher overloading ratio tends to develop an upward movement even in the first cycle. Moreover, the pipe under higher overloading ratio penetrated less into the sand bed during cyclic loading, and the maximum pipe penetration was found to decrease from 39.42mm to 33.34mm with increasing overloading ratio (Table 4.4).

4. 1 Constant Penetration Swipe Tests

A series of swipe tests were performed under constant embedment through lateral movement. The results of the constant penetration sideswipe tests are summarised in Table 4.7. In each test the pipe was first allowed to penetrate into the soil to a target depth, z_{ini}, after which lateral movement was commenced. This creates a normally loaded condition and hence the overloading ratio of the pipe-soil interaction is 1.0.

Table 4.7 Summary of constant penetration swipe tests results

Test	**Max. measured vertical load** V_{max} **(N/m)**	**Initial embedment** z_{ini} **(mm)**	**Maximum measured lateral load** H_{max} **(N/m)**	**Vertical load at max H reached** V_1 **(N/m)**	H_{max}/V_{max}
TS1	2318.2	5.19	286.8	1048.7	0.12
TS2	2121.0	5.08	201.1	850.1	0.09
TS3	5282.0	15.01	875.1	3135.3	0.17

Results of the normally loaded pipes are shown in Figures 4.24 to 4.26. The vertical load dropped and the horizontal force initially increased rapidly in the first 2.5mm where the peak lateral load was found to increase with initial embedment. This may have resulted from the larger amount of soil that is required to be moved by the pipe and therefore requiring a larger breakout force. Beyond this stage the horizontal force reduced to a lower resistance, after which it increased moderately as the pipe moved horizontally. The breakout event (Figure 4.25) was observed to take place at an estimated lateral displacement at 2-2.5mm where the lateral resistance reached a maximum value. The residual horizontal force which is the lateral

resistance after the breakout event was observed to account for approximately 35% of the maximum lateral resistance at breakout.

In addition, a gradual increase was observed in the conducted tests after the breakout event due to the build-up of soil berm in front of the pipe, and thus increasing the passive pressure. The residual horizontal resistance is found to be significantly affected by initial embedment depth. Shown in Figure 4.24, the horizontal stiffness of sand is related to the initial embedment depth such that deeper initial embedment resulted in a slightly larger horizontal stiffness after the breakout event.

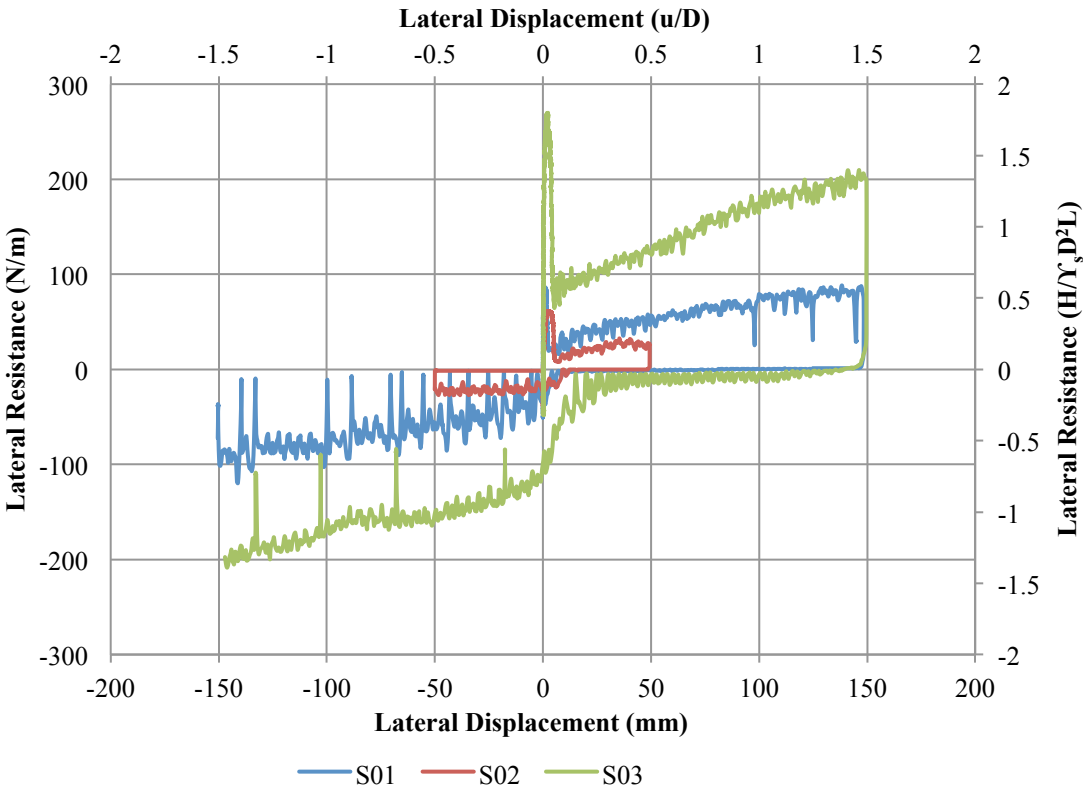

Figure 4.24 Lateral load measured in constant penetration tests

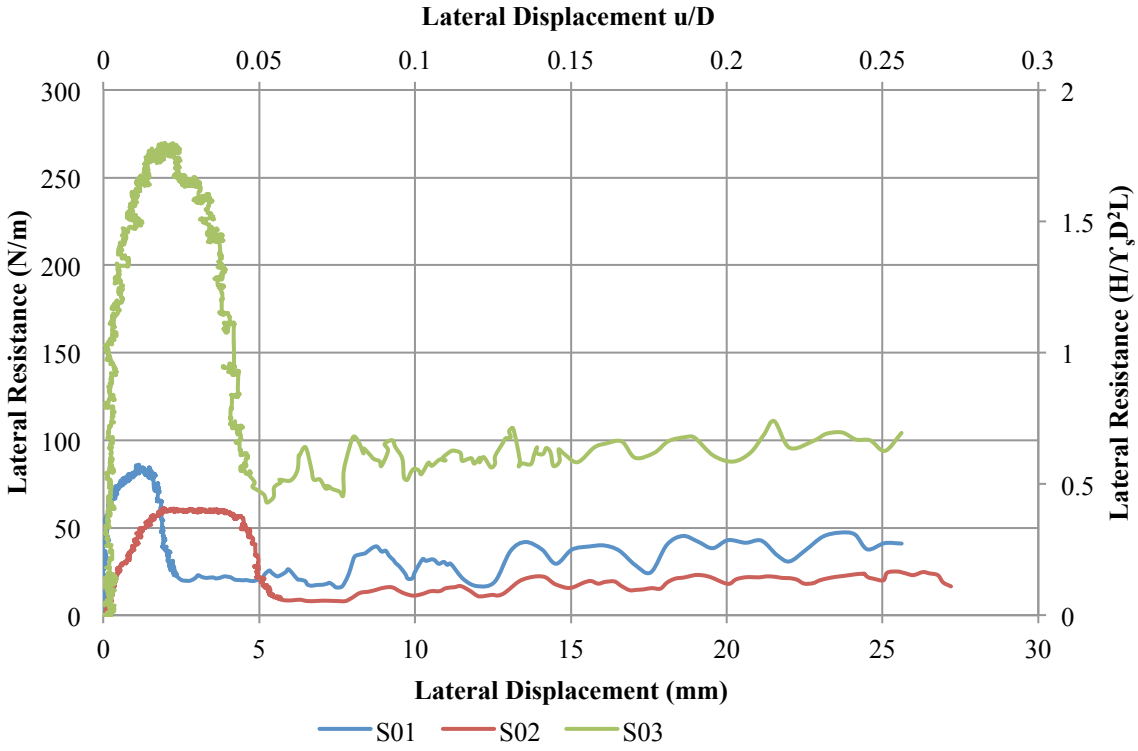

Figure 4.25 Initial break-out of pipe

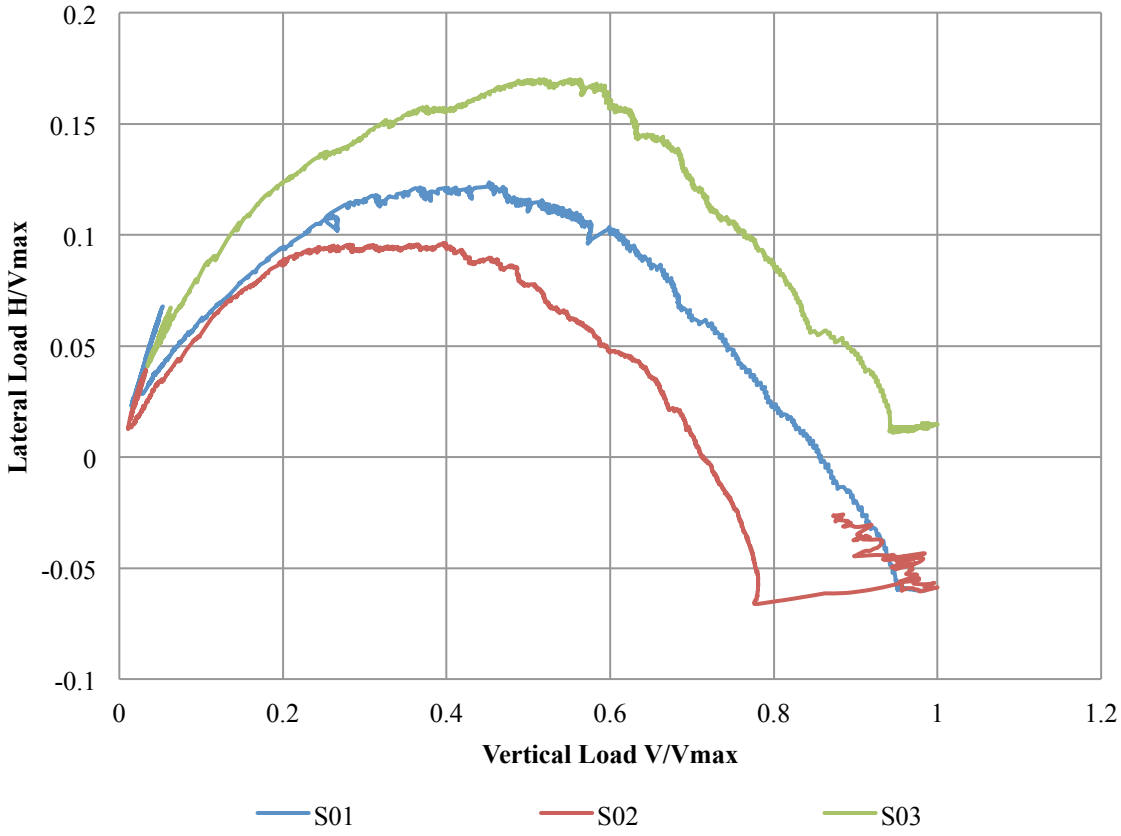

Figure 4.26 Normalised lateral load plot in V-H plane

The normalised V-H envelopes for normally loaded tests are shown in Figure 4.26. In a sideswipe test, vertical load plotted against horizontal load effectively traces out the yield envelope in V-H plane (Tan, 1990). The results and the associated plots indicate a parabolic shaped yield surface for the pipeline under combined V-H loading. The peak horizontal forces ranged from 13% to 17% of the maximum vertical force, all of which took place at approximately 40% of the maximum vertical load. This indicates a negative intersection of the yield envelope on the horizontal axis, which may due to the passive soil resistance on the partially embedded pipe, even for zero vertical loads that was applied on the pipe. In addition, the effect of initial embedment depth can be evaluated, in which the normalized horizontal load increased from 13% to 17% according to different initial embedment due to more soil to be removed as the pipe moves laterally for deeper embedment.

4. 2 Concluding Remarks

A series of lateral loading tests were conducted under a highly controlled program, which captures the pipe-soil interaction behavior at either small or large lateral displacement. The aim of these tests is to investigate the lateral loading response by conducting numerous parametric analyses to assess the key factors that govern pipeline lateral stability. Key conclusions from the tests are as follows:

i. The initial lateral resistance of a laterally loaded pipeline is mainly governed by vertical load level applied to the pipe while moving laterally. The initial embedment and overloading ratio are found to have less influence in the initial development of lateral resistance for a pipe travelling on loose sand. The lateral resistance in the initial cycles (before a trench is formed due to cyclic movement) increased monotonically to the maximum lateral displacement. The peak in the following cycles is reached when approaching the edge of the self-created trench,

typically at 0.5D before moving to the maximum displacement.

ii. The breakout displacement to obtain the peak lateral resistance was found to vary with the maximum lateral displacement. The passive component of the total lateral resistance was found to be related to the size of the berm. When the pipe moves to a deeper penetration a larger berm is created, and hence a greater passive resistance is observed. The increase in the size of the berm, which can be expressed as a function of the ploughed depth, is found to be smaller at high cycles, indicating that a converged maximum resistance could be achieved after 10 cycles of lateral movement.

iii. A series of yield surfaces were obtained from the constant penetration swipe tests. The results traced a parabolic failure envelope for the V-H relationship when buckling occurs. The maximum lateral resistance before break-out was reached at a lateral displacement of approximately 0.02D. The size of the yield surface was found to expand with larger initial embedment. The growth of the active berm caused further increase in the lateral resistance after break-out, which is again affected by the initial embedment.

CHAPTER 5 MODEL EVALUATION AND ANALYSIS

5.1 Introduction

The recent focus of substantial research in the subsea pipeline stability design and analysis has been on the on-bottom stability problems, in particular on the topic of developing a sound and solid pipe-soil interaction model. Numerous attempts of alternatives have been proposed and studied, trying to explain and predict the patterns of the plastic behaviour of the on-bottom pipelines under different combined loading scenarios. One of these models is recommended by Det Norske Veritas (DNV), and is broadly accepted and applied in the on-bottom subsea pipeline system design and analysis – the energy based model developed by Verley and Sotberg, 1994. This model is applicable to pipelines taking loads on Calcareous sand, which is a common composition of seabed soil.

5.2 Soil Resistance Model by Verley and Sotberg

5. 2. 1 Model Description

Verley and Sotberg soil resistance model is mainly based on Coulomb friction law and an introduced passive resistance:

$$H = H_f + H_p \qquad 5\text{-}1$$

where H_f is the friction component, and H_p is the passive component of the total lateral resistance. For a sand base with a constant Coulomb friction coefficient u, the friction component of this model H_f can be written into the form as follows.

$$H_f = \mu(W_s - F_L) \qquad 5\text{-}2$$

where W_s is the self-weight of the pipeline and F_L is the hydrodynamic lift force. Note that for a certain segment of pipeline laid on the seabed, the friction component of the model could be

considered as a constant value when the loading system has reached a steady state.

The passive component of the soil resistance model is mainly due to the pipe lateral displacement under combined loading (Verley *et al.*, 1994; Youssef *et al.*, 2014), which builds up a soil berm that holds up the pipeline while moving. The Verley and Sotberg model is based on the assumption that the penetration of the pipeline and hence the accumulated lateral resistance is caused by the work done by the pipe. A multi-linear model is proposed to describe the development of the passive resistance, shown in Figure 5.1. The model assumes that development of the vertical displacement and lateral resistance as the pipe moves to one side applies exactly to the reverse direction of movement, which indicates a symmetric behaviour of the passive force-displacement about the origin.

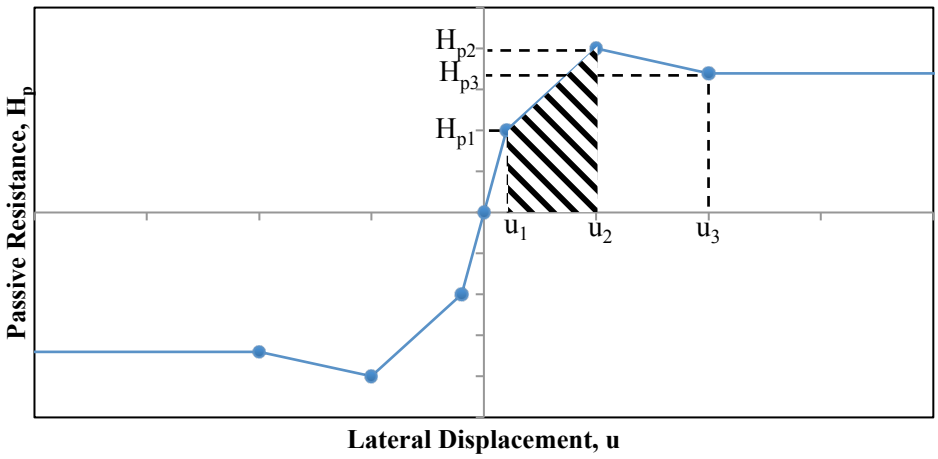

Figure 5.1 Passive Force-displacement Model

The passive force-displacement model explains the formation of the passive lateral resistance by dividing the lateral loading process by the following four regions (note that the model is symmetric about the origin, the four regions explained are only considered in the positive direction):

1) An elastic region that defined with lateral displacement of less than y_1 ($0 < u \leq u_1$). Pipe movement within this region is considered as elastic behaviour. Particularly, no work is done and the vertical displacement w_1 of the pipeline remains constant and equals to its initial penetration w_0. u_1 is assumed to be 0.02D in this model.

2) In the region of $u_1 < u \leq u_2$, the passive resistance continues to increase while the pipe accumulates vertical displacement, which reaches a maximum at $u = u_2$. This lateral displacement u_2 is termed as "breakout displacement" and is assumed to be 0.5D in the model. The "breakout penetration", w_2 is referred to the maximum penetration that the pipe achieves at breakout.

3) A breakout region, where the accumulated work is set to zero and no work is done for $u_2 < u \leq u_3$. The penetration is linearly reduced to w_3 and the passive resistance is decreased accordingly.

4) A residual region where both pipe penetration and the passive resistance remain constant with lateral displacement exceeding u_3. w_3 is taken to be 1.0D in the Verley and Sotberg model.

The model proposed an equation to define the peak breakout passive resistance, F_{r2}:

$$\frac{H_{p2}}{\gamma_s' D^2} = (5.0 - 0.15\kappa_s)\left(\frac{w_2}{D}\right)^{1.25} \quad for\ \kappa_s \leq 20, \qquad 5\text{-}3(a)$$

$$\frac{H_{p2}}{\gamma_s' D^2} = 2\left(\frac{w_2}{D}\right)^{1.25} \quad for\ \kappa_s \geq 20, \qquad 5\text{-}3(b)$$

where γ_s' is the effective unit weight of soil, and κ_s is the dimensionless vertical load parameter:

$$\kappa_s = \frac{\gamma_s{}' D^2}{W_s - F_l}. \qquad 5\text{-}4$$

Additionally, the peak elastic passive resistance H_{p1} is assumed to be taken as $0.3H_{p2}$, and the residual passive resistance H_{p3} can be calculated using the above equation by replacing w_2 with the residual penetration, w_3.

The maximum vertical displacement, referred to the breakout penetration z_2, is calculated based on an estimation of the work done (E) during lateral movement:

$$\frac{(w_2 - w_i)}{D} = 0.23 \left(\frac{E}{\gamma_s{}' D^3} \kappa_s{}^{-1} \left(\frac{u_{max}}{D} \right)^{-0.5} \right)^{0.31}, \qquad 5\text{-}5$$

where $E = \int H_p dy$ stands for the work done with pipe movement in region (2) defined above, which can be calculated by estimating the shaded area shown in Figure 5.1, and u_{max} represents the maximum lateral displacement inside the current cycle of pipe movement.

The residual penetration, w_3, can be obtained through the following empirical equations:

$$\frac{w_3}{w_2} = 0.82 - 3.2 \left(\frac{w_2}{D} \right), \ for \ \left(\frac{w_2}{D} \right) \leq 0.1, \qquad 5\text{-}6(a)$$

$$\frac{w_3}{w_2} = 0.5, \qquad for \ \left(\frac{w_2}{D} \right) > 0.1. \qquad 5\text{-}6(b)$$

The total lateral resistance can therefore be calculated.

5. 2. 2 Maximum Lateral Load at Breakout

The conventional model to analyse the interaction between the pipe and the seabed is based on the coulomb friction theory. The model assumes that the total resistance provided by the soil against lateral load in a pipeline lateral buckling event consists of two parts: i) a friction component which is calculated by applying a friction coefficient to the vertical load that is

applied to the pipeline, and ii) a passive component which is an additional resistance due to the formation of a soil berm accumulated during lateral movement. The proposed modified friction model is written in terms of the friction factor, μ, penetration and soil strength of the surrounding seabed. The total resistance can be therefore expressed in the following form:

$$H = H_f + H_p \qquad 5\text{-}7$$

Where H is the ultimate (total) lateral resistance of pipeline; H_f is the friction component which is given by $H_f = \mu \times V$; and H_p is known as the passive component of the total lateral resistance that is related to the penetration of the pipeline. This analysis focuses on studying the modeling of the passive resistance provided by the soil berm.

Verley and Sotberg (1994) have developed an empirical model to simulate the lateral load-displacement relationship. In this approach a tri-linear force-displacement model was adopted to estimate the passive component of lateral resistance, H_p. It assumes that the lateral load on a model pipe will increase to a peak value at a breakout displacement ($y_2 < D$) before falling to a residual value.

According to the assumptions made in the conventional model, the lateral resistance of a pipeline under constant vertical loading, especially its passive component is governed by the maximum penetration within each cycle. The friction component of lateral resistance is estimated based on an assumed friction factor, μ = 0.6. Therefore the passive component of lateral resistance can be calculated with the following equation:

$$H_p = H - \mu V, \qquad 5\text{-}8$$

where H_p = passive component of lateral resistance, and V = constant vertical load applied on the pipe during the test. Maximum H_p is denoted as H_{p2}. The passive term, H_p, was calculated

from several test results and plotted in terms of different vertical load (Figure 5.2) and maximum lateral displacement (Figure 5.3) respectively.

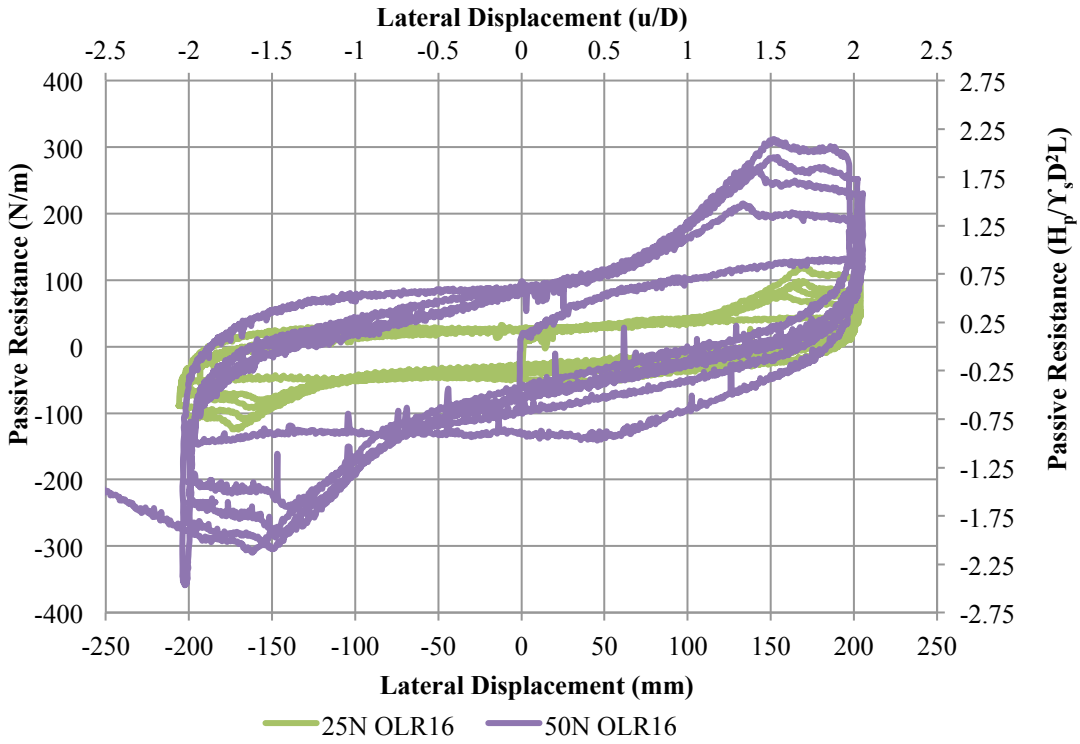

Figure 5.2 Comparison of berm resistance between vertical load levels

The results show that the vertical load determines the passive resistance of pipeline. It also reveals that the passive resistance at very small lateral displacement is almost zero. This indicates that the friction mainly provided the resistance at the beginning of lateral movement.

The normalised berm resistance subtracted from each cycle in the cyclic constant loading tests was then calculated and plotted in Figure 5.4 against normailised maximum penetration achieved in the corresponding cycle in terms of the constant vertical load level.

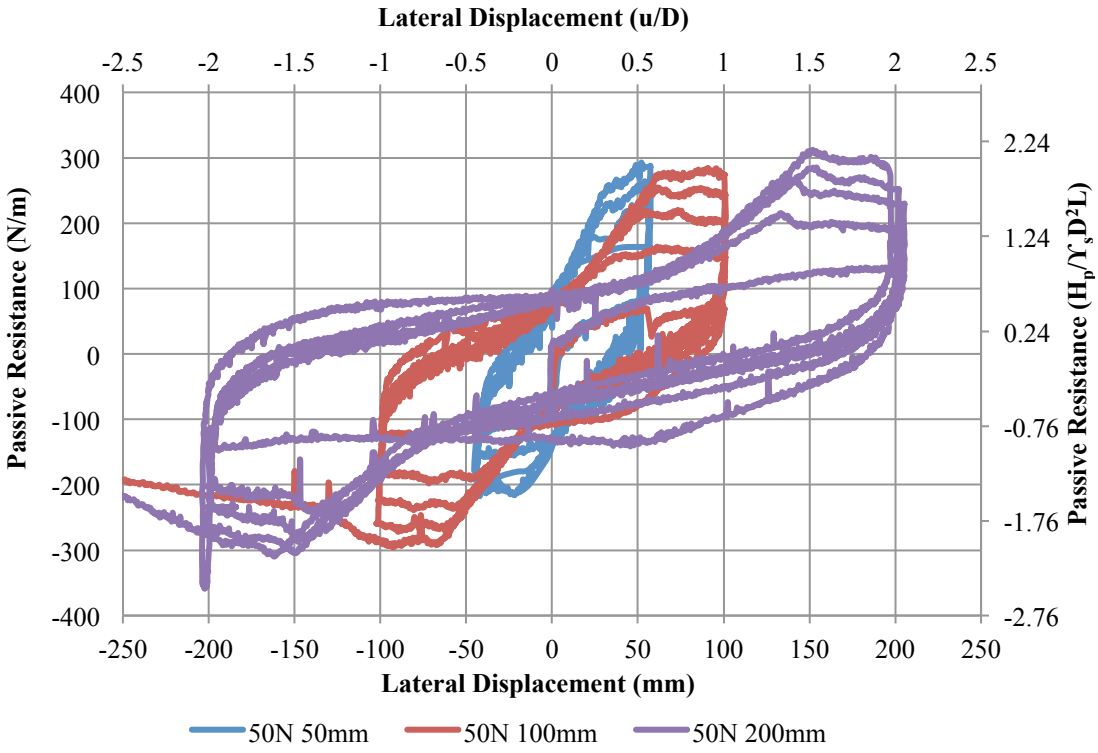

Figure 5.3. Comparison of berm resistance between maximum lateral displacements

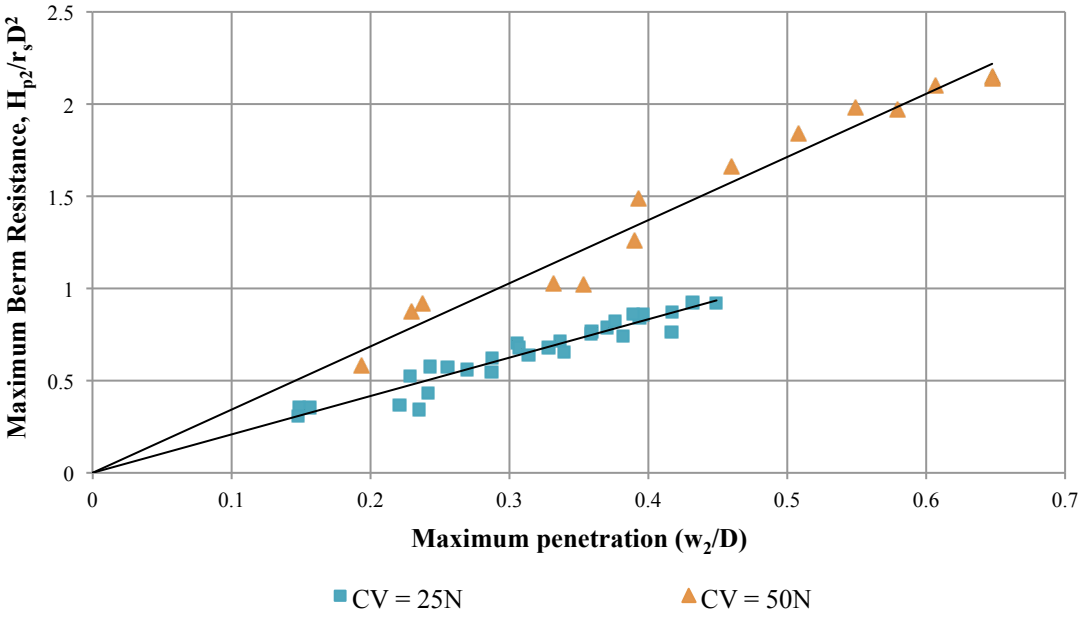

Figure 5.4. Effect of Maximum penetration on Maximum berm resistance

The following equation gives a good fit to the data:

$$\frac{H_{p2}}{\gamma_s D^2} = (4.8 - 1.65\kappa)\left(\frac{w_2}{D}\right)^{0.87}, \qquad 5\text{-}9$$

where H_{p2} = break-out passive term of lateral resistance, and w_2 = maximum penetration within each loading cycle.

5. 2. 3 Penetration Development

The penetration occurring during lateral movement is assumed to be the result of the work done by the pipe, and can be calculated as the integral of $H_p(s)ds$ (Verley and Sotberg, 1994). Dimensionless analysis suggests that the final vertical displacement could be linked to the following factors.

$$\frac{w}{D} = f(\xi, \kappa, u/D), \qquad 5\text{-}10$$

where y is the current lateral location of pipe, and ξ is a dimensionless group for the work done by the pipe to move the sand, i.e. $\xi = \frac{E}{\gamma' D^3}$. The work, E, can be calculated based on the lateral load-displacement response:

$$E = \int H_p ds = \sum \overline{H_p} \Delta y. \qquad 5\text{-}11$$

The model assumes that only work done prior to the break-out event can contribute to the increasing penetration. Assuming that no energy was consumed during the elastic deformation region (roughly in the first 5% to 10% of pipe-diameter), E is calculated based on work done between y_1 (elastic displacement) and y_2 (break-out displacement).

Figure 5.6 shows the plot of calculated dimensionless factors for the work done to cause further penetration. The data shows that the maximum penetration does vary with the initial overloading ratio (OLR) in each data set; in particular z_2 was found to increase with the decreasing OLR. This may due to the higher loading that the soil experienced in its loading

history prior to the test. The soil beneath is therefore compacted and results in an increasing the bearing capacity. However, the influence of initial overloading is found to be small that it may be neglected in the simplified model. The following equation can best fit the data plotted above:

$$\frac{w_2 - w_{ini}}{D} = 0.2\left(\xi \times \kappa^{-0.5} \times \alpha^{-0.5}\right)^{0.45} \qquad 5\text{-}12$$

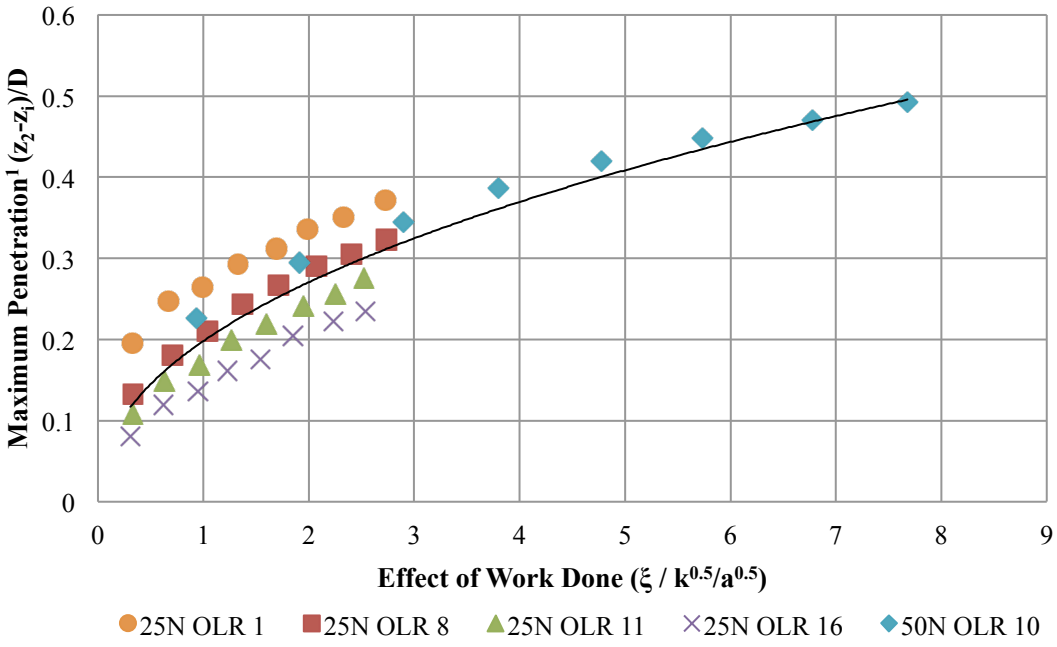

Figure 5.5. Effect of work done by the pipe on the soil

The Verley and Sotberg model is used to back-analyses the testing results and to perform some parametric studies to investigate the sensitivity of various factors.

The geometry and variables of the model were similar to that in the first chapter (Figure 1.3). The pipeline is assumed to be a rigid body that does not deform under the combined loadings during lateral movement. The soil berm that accumulated during movement is simplified to be a rectangular with a length of l and a height of h_r, as shown in Figure 5.11.

[1] Maximum penetration plotted in Figure 5.5 has eliminated the effect of initial embedment, i.e. using $\frac{z_2 - z_i}{D}$ instead of $\frac{z_2}{D}$.

The model in this study is established from an iteration process that starts from an initial condition, i.e. the initial embedment. The maximum breakout force F_{r2} can then be calculated, and therefore the force-displacement relationship can be plotted for the current cycle of movement. The vertical displacement at the end of the current cycle is then input as an initial embedment of the next cycle of lateral movement.

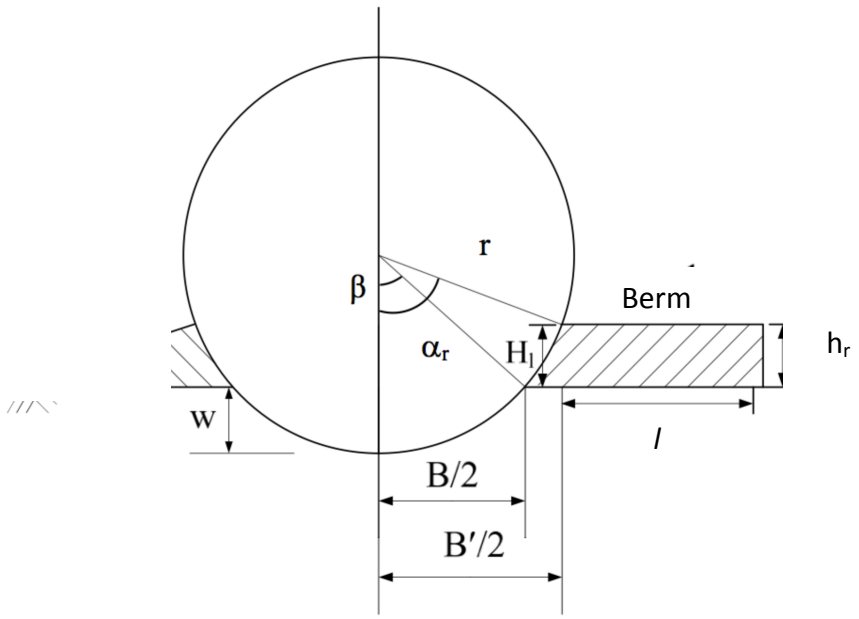

Figure 5.6 Modelling of Soil berm (Lee, 2012)

A total of 8 analyses were conducted to perform the back-analysis and to compare with the experiment results. The comparison of the initial cycle is shown in Figure 5.12 a) and b). In these tests, the pipe was modelled with an initial embedment ratio (w/D) from 0.02 to 0.12, and the maximum lateral displacement was varied from 0.5D to 2.0D. The comparison results showed a good match in the elastic region with a lateral displacement of y = 0.01D, afterwhich the pipe enters the yield zone and the lateral passive resistance accumulates slowly.

However in all the tests, breakout event is not clearly observed during the first cycle of lateral

movement, and the peak breakout load obtained from the model does not match the testing results. The breakout displacement seems to be underestimated as the passive resistance kept increasing after 0.5D of lateral displacement. For example with test P08 (light green line in the plot) in Figure 5.12, the vertical displacement reached a maximum of y = 1.53D, which indicates the occurrence of a breakout event. Similar observations can also be found in the results of test PC02 and PC04, where the breakout occurred at y = 1.2D and 1.44D. The result of pipe penetration agrees with the theory that maximum lateral load was achieved at maximum penetration depth, but these peak loads generally occurred at a lateral location of 1.5D to 2D, which is over-estimated by the model.

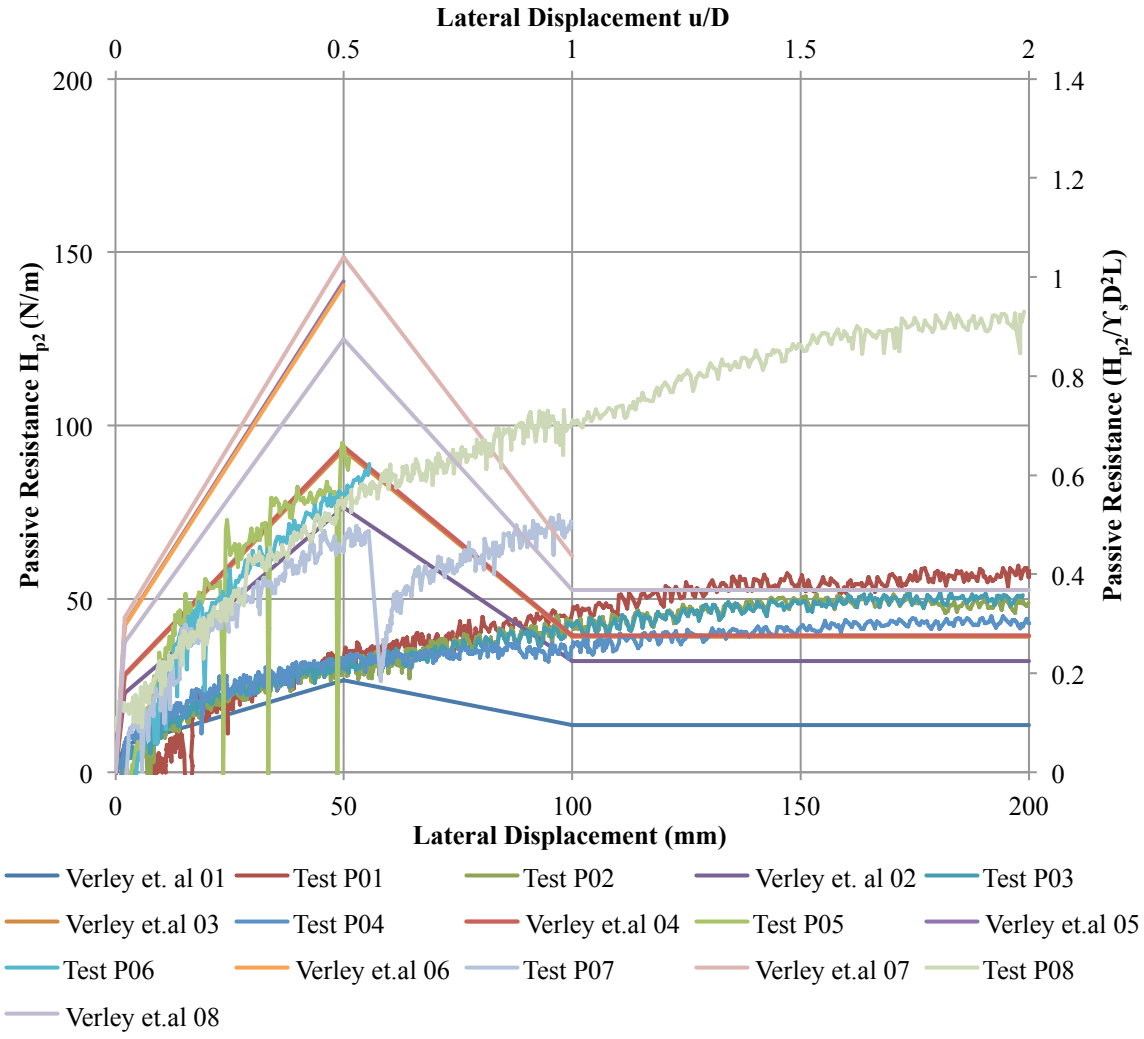

Figure 5.7a Comparison of passive resistance calculated from the Verley and Sotberg model and tests PC01-PC08

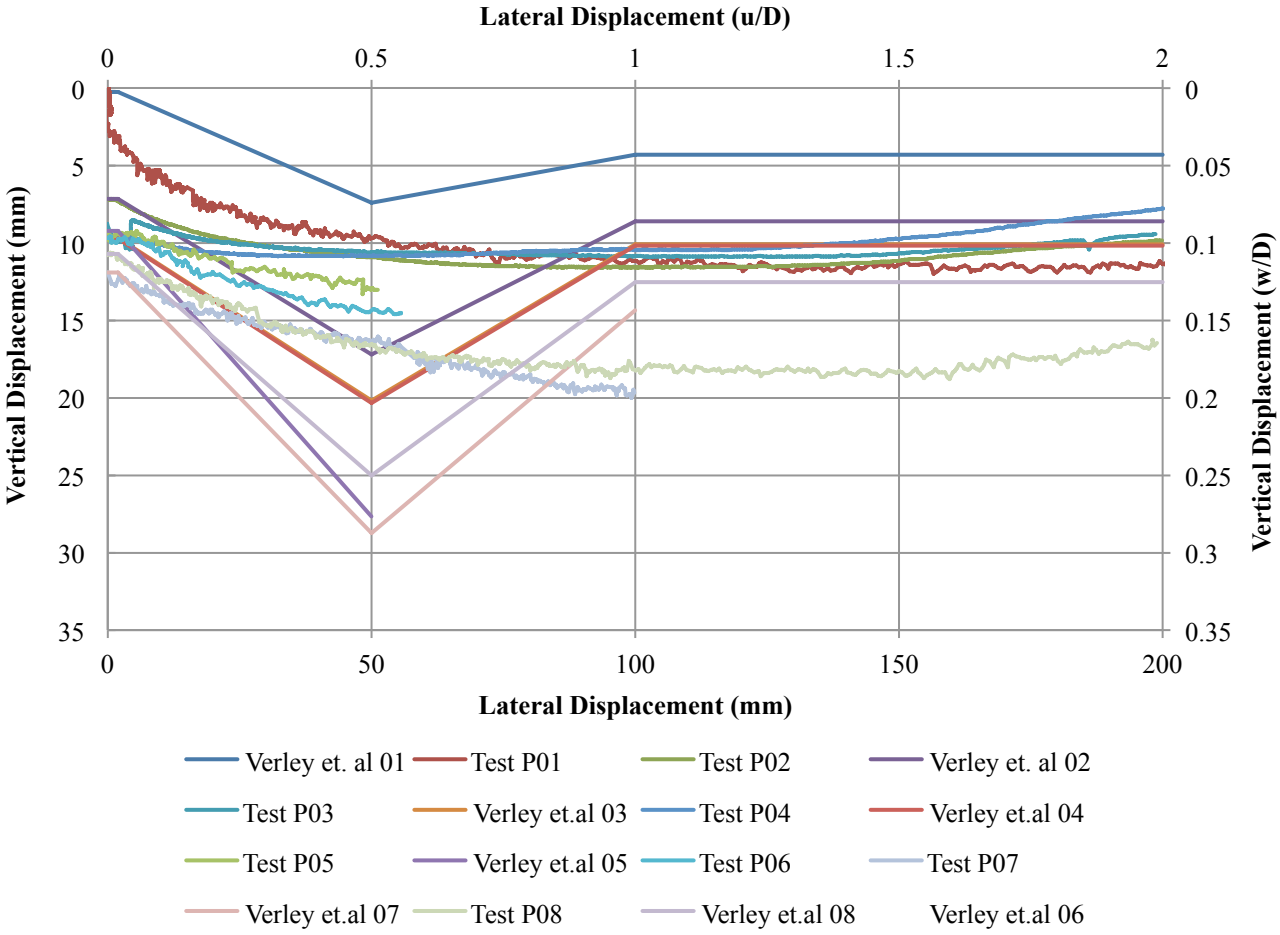

Figure 5.7b Comparison of vertical displacement calculated from the Verley and Sotberg model and tests PC01-PC08

5. 2. 4 Soil Berm

Results show that the passive component of lateral resistance of pipelines is mainly dependent on the size of the soil berm created ahead of pipe in the direction of movement. Before each test, the sand was carefully poured into the sand box as uniformly as possible to create a uniform loose bed. With the assumption of volume conservation in loose sand, the size of soil berm is able to be estimated by considering the volume of sand being ploughed away by the model pipe during movement. The ploughed depth, t_{plough} is defined as the vertical difference between the current position of a pipe and the surface of the trench which is created by the pipe during its previous lateral movement (Figure 5.13). By considering conservation of volume, the growth of a berm is related to the thickness of soil t_{plough} that is swiped away by

the pipeline during lateral movement.

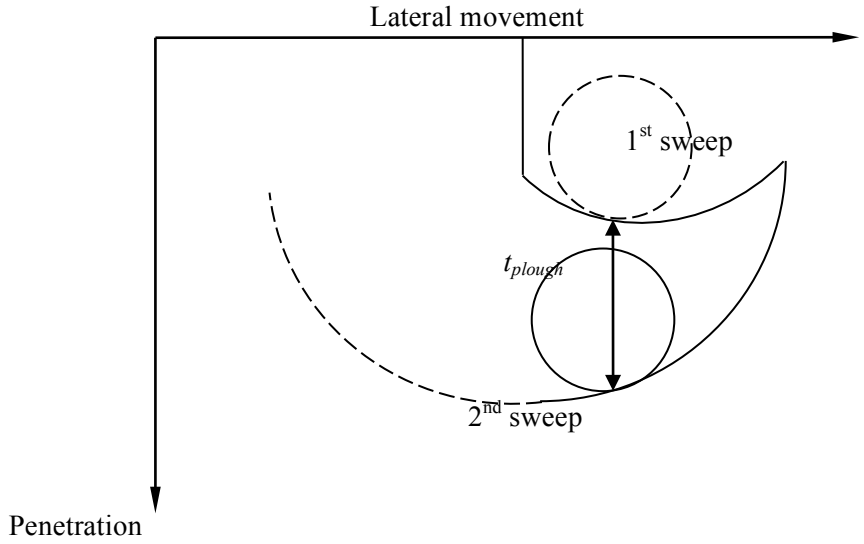

Figure 5.8. Definition of ploughed depth

Therefore the ploughed depth can be defined as follows:

$$t_{plough} = w_{current} - w_{previous}, \quad 5\text{-}13$$

where $w_{current}$ and $w_{previous}$ are the current pipe penetration and the pipe penetration at the same lateral displacement in the previous sweep, respectively. The sign convention defines the direction of the vertical movement of model pipe. A plus sign means that the pipeline penetrates deeper into the soil, while a negative sign indicates the pipeline break-out of the current ground surface.

The area of a berm (cross-sectional area in the vertical plane perpendicular to the direction of lateral movement) can then be estimated using the following equation:

$$A_{berm} = \int t_{plough} du, \quad 5\text{-}14$$

where A_{berm} is the cross-sectional area of the soil berm (assuming a segment of pipeline having a unit length) and y is the lateral displacement. The size of the active berm can be then

calculated based on the length of the pipe segment and therefore it is directly linked to the ploughed depth during a lateral sweep.

Figure 5.14 shows a plot of the ploughed depth during a cyclic lateral loading event. The test was controlled such that the model pipe moved laterally under a constant vertical load of 25N to a lateral displacement of 200mm (2D). To compare between different cycles of sweeps, a sign factor of -1 was applied to the horizontal displacement of even cycles (i.e. the 2nd, 4th, 6th, 8th and 10th cycle of sweeps) so that all plots start at a lateral displacement of -200mm. The initial overloading ratio is measured to be 8, and the initial embedment is measured at around 10mm. The plot is constructed by subtracting the ploughed depth, t_{plough}, from each cycle using the above equation. The ground surface is set to be of 0 levels in the vertical penetration axis, which means that the ploughed depth in the first cycle equals the current penetration depth. From the second cycle the ploughed depth is calculated based on the above equation. Since in the second cycle the pipe will travel to the negative zone of the lateral displacement axis where the ground surface is still at 0 vertical penetrations, there is an abrupt increase in the ploughed depth in the 2nd cycle. It can be shown that other than the first and second cycle, the plot tends to converge to a steady state. Even in the first half of the 2nd cycle, the ploughed depth showed a similar trend as the followed cycles.

In the first cycle, the ploughed depth can be simplified to a parabola which is vertically symmetric at a lateral displacement $u = a/2$, a being the cycle amplitude of cycle:

$$t_{plough} = f(u) = c(u - \frac{a}{2})^2 + C_0. \qquad 5\text{-}15$$

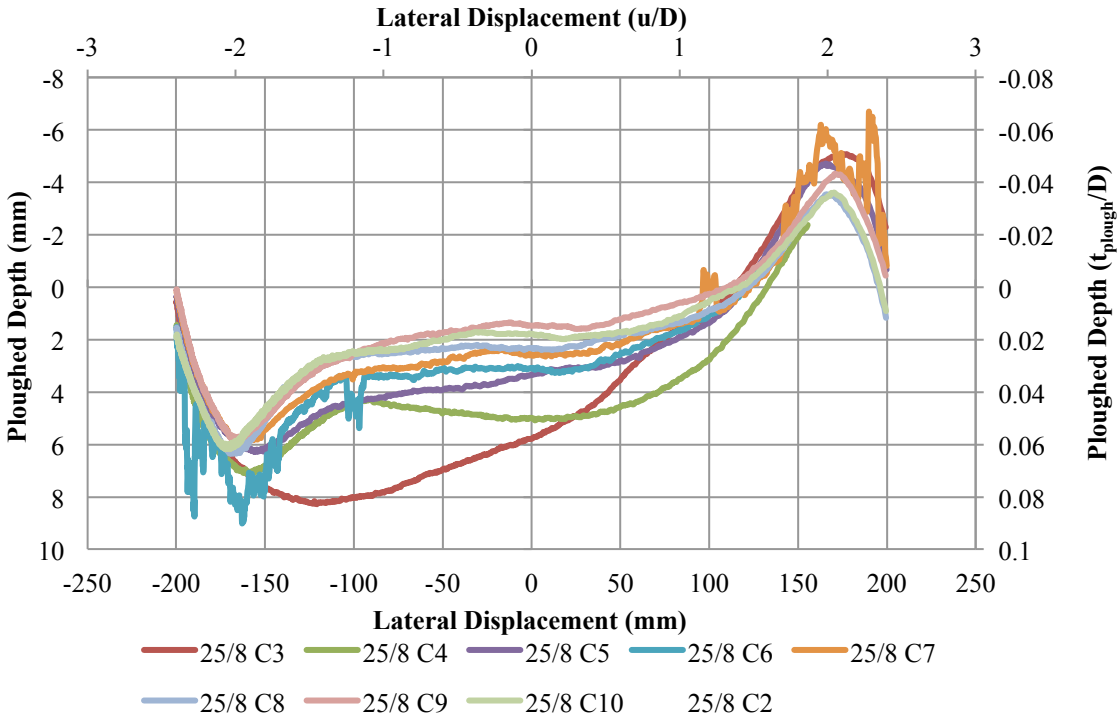

Figure 5.9 Ploughed depth for test under constant vertical load of ~25N

In the installation process of an on-bottom pipeline, the pipeline is laid freely on the seabed to bury itself in the sand, or is pushed into the ground. Either way the pipeline is initially restrained by its embedment caused in this process. In an event of lateral loading, the pipeline starts to travel laterally back and forth, and pushes the soil away to create a trench. It can be imagined that an initial trench forms when the number of cycles is larger than 2, after which it will keep sweep soil away and deepen the trench. White and Check (2007) suggested that the passive resistance (for clay) of pipeline due to the formation of active berm could be expressed as follows:

$$H_{berm} = \lambda \, A_{berm}{}^{\delta}, \qquad 5\text{-}16$$

where λ and δ are the shape coefficients. Considering the sand is in a loose state, the slope angle of the berm created should therefore be governed by its friction angle. Hence the area of berm will be proportional to the square of its base length, given that the angle of the berm slope is maintained constant. If the berm resistance is assumed to be attributed to the shearing

force across its base, i.e. $H_{berm} = \tau_{shear} \times l_{base}$, which is proportional to the square root of the berm area and hence indicates a suggest value of 0.5 for the index δ. The test result also suggests a value of 0.52 for δ, which is close to the assumption.

Figure 5.15 shows the corresponding passive component of total lateral resistance against lateral displacement within one cyclic test under a constant vertical load of ~25N (83.3N/m). It is clear that the passive resistance follows a similar trend as in the 1st and 2nd cycle and in the lateral displacement is less than 3D in the following cycles. The maximum resistance was thereafter achieved at a lateral displacement of about 3.5D, and was found to increase over cycles. This increase could be linked to the larger berm created when the pipe approaches the edge of the self-digging trench.

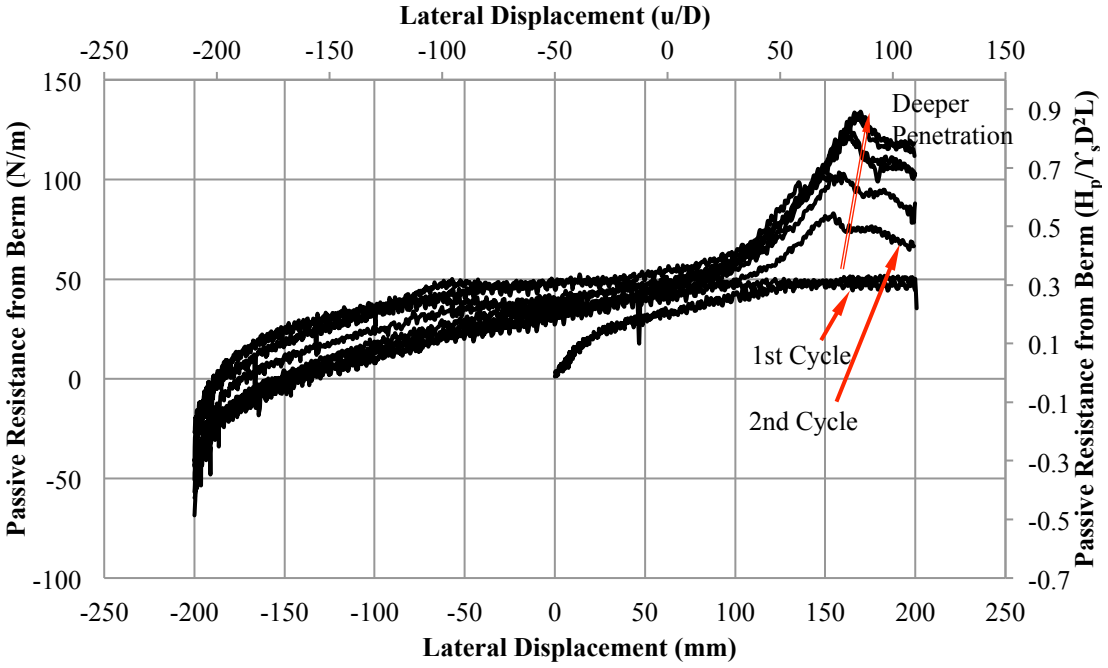

Figure 5.10 Development of passive resistance over cycles

It is observed that the development of the active berm (being the change in the area of berm across its lateral movement) is different from what was shown in the first two cycles. Figure 5.16 shows a series of plots of ploughed depth against the lateral displacement for 4 separate constant vertical load tests of a maximum lateral displacement of 200mm. The tests vary in

different vertical load during lateral movement and in the initial overloading ratio.

Interestingly, the results show that the change in berm size is interestingly similar for the 4 test results, despite that they are not subject to the same loading conditions. At the beginning of each cycle when the pipe starts to travel back, the embedment in the direction of its movement (opposite to its previous moving direction) is trivial, and hence the pipe penetrates into the soil at a higher rate. This explains the rapid increase in the first 25% pipe-diameter of lateral displacement. The size of berm grows and the lateral resistance increases accordingly as the pipe penetrates deeper into the soil. After the ploughed depth reaches a maximum value, the growth rate of the soil berm decreases and consequently the berm resistance increases at a slower rate. The maximum berm resistance is achieved when the ploughed depth decreases to zero at a lateral displacement of around 1.25 pipe-diameters. The pipe rises up against the current soil surface (swept by the pipe in the last cycle) and no longer penetrates into the soil. The negative ploughed depth leads to a decrease in the berm size and hence a decrease in the berm resistance. The plot contracts with higher number of cycles, which is probably because of the higher stress state of the soil at a larger depth, which strengthens the stiffness of soil that is being pushed away. A small portion of region with a constant residual berm resistance is observed at the end of higher cycles of lateral loading, where the active berm created during lateral movement joins the dominant berm at the edge of the trench.

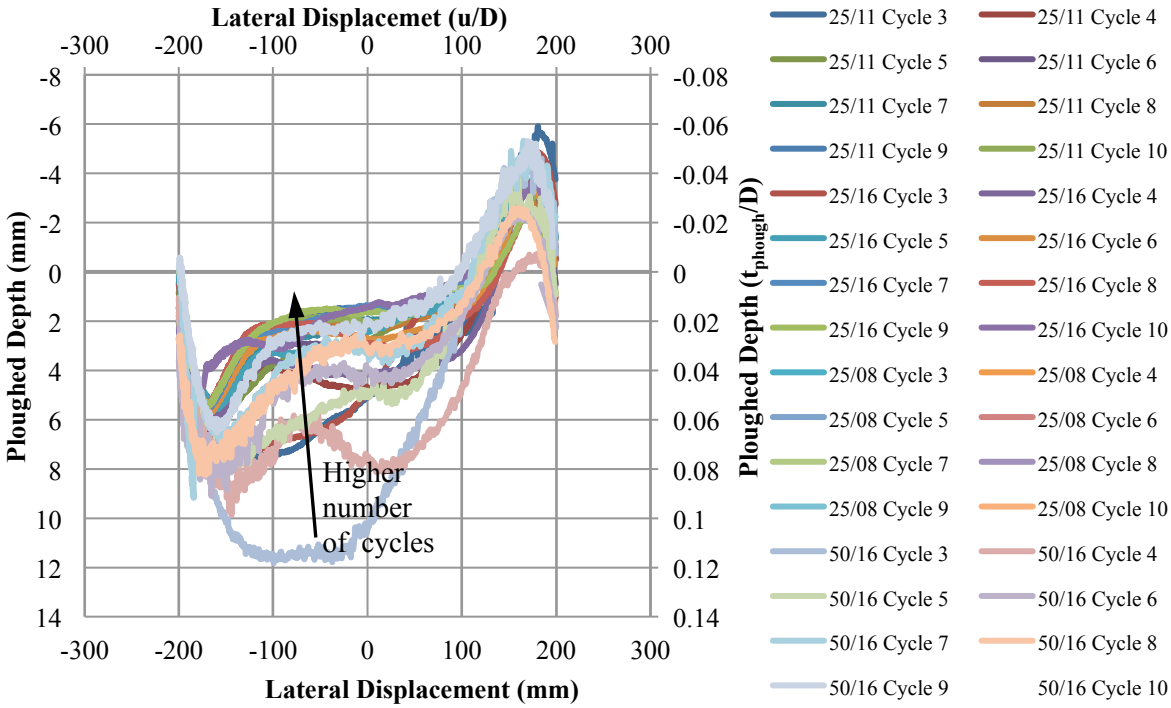

Figure 5.11 Comparison of ploughed depth in different loading conditions

CHAPTER 6 CONCLUSIONS AND FUTURE RESEARCH

6 . 1 Concluding Remarks

The purpose of this study is to investigate the vertical and lateral behaviour of the pipe-soil interface of a single pipeline segment on a sand base. By understanding the interactions between the pipe wall and the surrounding soil, a more accurate and sophisticated model can be developed and lead to a more cost-effective design guideline. 2 existing models were discussed, including a traditional friction approach developed by Verley et al. (1994, 1995) and an alternative developing plasticity model proposed by Zhang (2001). A series of laboratory tests were designed and carried out in order to verify, calibrate and evaluate these models.

6.1.1 Vertical Penetration Tests

The vertical penetration tests were carried out at different locations in the sand tank, i.e. tests were performed at 0, ±100mm and ±200mm on the lateral axis of the tank. Results have shown that the vertical behaviour along the lateral axis of the sand tank is similar. The vertical plastic modulus (ratio of vertical load to penetration) was found to be similar at these locations, and hence we can assume it to be constant in the other tests. The plastic modulus of the sand can be determined from the graph (i.e. the slope of the vertical load – displacement curve), which is an important factor in the theoretical model (Verley and Sotberg model, 1994).

6.1.2 Lateral Loading Tests

6.1.2.1 Constant Penetration Swipe Tests

Sideswipe tests of up to 1.5-pipe-diameter lateral displacement were carried out under different initial embedment. These tests have been designed such that the vertical penetration of the model pipe for each test was kept the same as the initial embedment. Results of these tests indicates a parabolic yield surface for the model pipe under combined Vertical-Horizontal (V-H) loading, similar to the results from a wide range of testing. The data suggest that the yield envelopes will intersect the vertical axis, giving a horizontal capacity for zero vertical load, due to the passive soil resistance on the partially embedded pipe. The peak load recorded in the break-out event and the residual load thereafter showed a strong relationship to the initial embedment, and vertical load level. This is to be expected as the deeper the pipe the larger the amount of soil that must be moved is. The tests are characterised by an initial break out phase followed by a gradual and linear increase, due to the build-up of soil berm in front of the pipe.

6.1.2.2 Constant Vertical Load Probe Tests

Probe tests of up to 1.5-pipe-diameter lateral displacement were performed to examine the development of lateral resistance against lateral movement under constant vertical load. A scaling analysis based on previous experiment data has been carried out to determine the design vertical load during tests such that the model tests can represent the real case. Both monotonic and cyclic tests have been carried out to study the behaviour of pipe-soil interaction system. Test results show that the lateral resistance is dependent on the vertical load level and the vertical penetration; however the effect of over-loading ratio on the lateral

response was not apparent in tests with small cycles.

Monotonic probe tests of up to 8-pipe-diameter lateral displacement have been carried out after calibration of the newly installed geared vertical actuator this year. The results have been found to cope with the existing theory. The results indicate that the break-out resistance is mobilised at approximately 1 pipe-diameter.

In the force-displacement model described by Verley and Sotberg (1994), there is a yielding point of lateral load which peak at a lateral displacement of 0.5 pipe-diameter and drops to a residual value. This is not observed in the tests with small cycles, but was observed in the tests with larger cycles (typically after the first cycle of test).

The displacement response is characterised by penetration for cycles of small lateral displacement. However as the cycles increase in distance the pipe starts to rise up out of the soil. This is due to the large embedment depth when the pipe returns to the starting point; at such point there existed some penetration on the backside of pipe, whereas the front side of the model pipe towards lateral movement still remained at its initial level. The larger embedment depth caused an increase in vertical load as the pipe moved laterally, which then was adjusted to move upwards in order to reduce the vertical load to the pre-set constant value.

6 . 2 Limitations and Future research

6.2.1 Soil Conditions

The tests involved in this study are carried out on a loose sand base in a dry environment. Therefore the analyses and conclusions were limited to this soil condition, which in reality more suitable for a shallowly embedded pipeline at smaller water depth. The database can be extended by considering denser sand in dry or partially drained conditions for a more comprehensive assessment of the current model.

6.2.2 Cyclic Effect

Prediction using a model developed by Verley et al (1994) gives an underestimation of the maximum lateral resistance (see figure below). More importantly, the breakout displacement used in the model (assumed to be 0.5D to obtain maximum lateral capacity) is found to be about 1.5D, and when applying this lateral displacement instead, the model gave an acceptable simulation of the test result in the beginning cycle, and needs to be verified. In addition, the lateral resistance is found to increase with the number of cycles. A peak can be observed after the second cycle, at which point the pipe created a trench. As the number of cycles of loading increases, an additional resistance can be observed to the lateral resistance, which is due to the active berm of sand collected in front of the pipe approaching the edge of the trench.

It is also an interesting finding that the lateral locations where these peak berm resistances were not the same as the maximum lateral displacement increased (see Figure 6.2 below) as cyclic loading build up. However they were reached at approximately a similar distance from the edge of the trench (created when the pipe moved back and forth). This may be worth looking into.

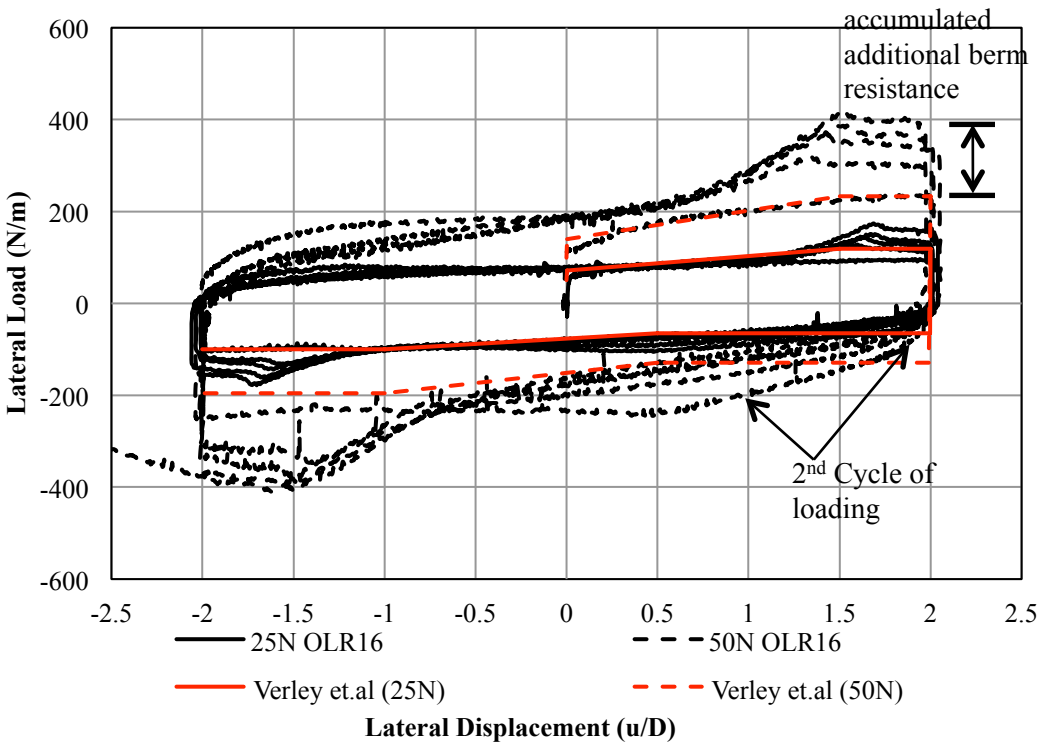

Figure 6.1 Cyclic effect of vertical load

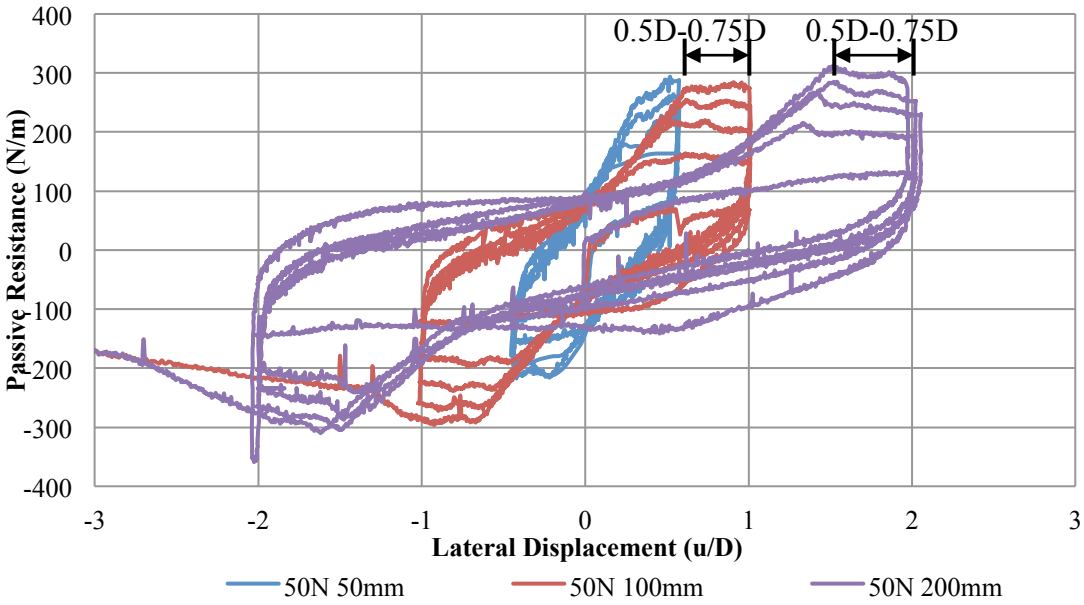

Figure 6.2. Cyclic effect of maximum lateral displacement

REFERENCE

AGA/PRC Vol.1,1993. Submarine Pipeline On-Bottom Stability. Analysis and Design Guidelines

Allen D.W., Lammert W.F., Hale J. R., Jacobsen V. 1989. Submarine pipeline on-bottom stability: Recent AGA research, OTC 6055

Arabzadeh H., Zeinoddini M. 2011. Dynamic Response of Pressurized Submarine Pipelines Subjected to Transverse Impact Loads, Procedia Engineering 14, pp 648–655

Brennodden, H., 1988, Pipe-Soil Interaction Tests on Sand and Soft Clay, SINTEF Report STF69 F887018, prepared for the American Gas Association.

Brennodden H., Lieng J.T., Sotberg T., Verley R.L.P. 1989. An energy based pipe-soil interaction model. OTC 6057

Brennodden H., Sveggen O., Wagner D.A., Murff J.D. 1986. Full-scale pipe-soil interaction tests, OCT 5338

Bruton D., White D., Cheuk C., Bolton M., Carr M. 2006. Pipe-Soil Interaction Behaviour during Lateral Bulking, Society of Petroleum Engineers, Vol 1, issue No. 03, pp 1-9

Butterfield, R. and Ticof, J. 1979. Design parameters for granular soils (discussion contribution). Proc. 7th International Conference of Soil Mechanics, Vol 4, pp 259-261

Byrne, B.W., Cassidy, M.J. 2002. Investigating the response of offshore foundations in soft clay soils, Proc. 21st International Conference on Offshore Mechanics and Arctic Engineering, OMAE2002-28057

Byrne B.W., Houlsby G.T. 1998. Model Testing of Circular Flat Footings on Uncemented Loose Carbonate Sand: Experimental Data, OUEL Report, No 2192/98, University of Oxford

Byrne, B.W., Houlsby, G.T. 1999. Drained behaviour of suction caisson foundations on very dense sand. Offshore Technology Conf., Houston, OTC 10994

Cathie D. N., Jaeck C., Ballard J-C., Wintgens J-F. 2005. Pipeline Geotechnics-State of the Art, Proc. International Symposium on Frontiers in Offshore Geotechnics (IS-FOG 2005), pp 19-21

Cheuk, C. Y. 2005. Soil-pipeline interaction at the seabed. PhD thesis, University of Cambridge

Cheuk C.Y., Take W.A., Bolton M.D., Oliveira J.R.M.S. 2007. Soil restraint on buckling oil and gas pipelines buried in lumpy clay fill, Engineering Structures, Vol. 29, pp 973–982

Churchman M. 2009. Lateral loading of buried and partially buried pipes in sands, PhD Thesis, University of Oxford

Dafalias Y.F., Herrmann L.R. 1982. A bounding surface soil plasticity model, Soil mechanics-transient and cyclic load, Pande and Aienkiewicz (eds.), pp 253-282

Hahn G. D., Sritharan S. 1994. Lateral Response of Underground Pipeline to Earthquakes, Computers & Structures Vol. 53.No. 3. pp 601-611.

Hodder M.S and Cassidy M.J. 2010. A Plasticity model for predicting the vertical and lateral behaviour of pipelines in clay soils. Geotechnique, Vol.60, issue No. 04, pp 247-263

Houlsby, G. T. & Puzrin, A. M. 1999. The bearing capacity of a strip footing on clay under combined loading. Proc. Royal Society. Vol. 455, pp 893-916

Gadre, A. D., Dobry, R. 1998. Lateral cyclic loading centrifuge tests on square embedded footing. J. Geotech. and Geoenviron. Vol. 124, issue No. 11, pp 1128-1138

Gao F.P., Gu X.Y., Jeng D.S. 2003. Physical modelling of untrenched submarine pipeline instability, Ocean Engineering. Vol. 30, pp 1283–1304

Gao F.P et. al. 2011. Steady flow-induced instability of a partially embedded pipeline: Pipe–soil interaction mechanism, Ocean Engineering Vol. 38, pp 934–942

Gottardi, G. and Butterfield, R. 1993. On the bearing capacity of surface footings on sand under general planar loads. Soils Found. Vol 33, issue No. 3, 68-79 1993

Gottardi, G., Houlsby, G. T. Butterfield, R. 1999. The plastic response of circular footings on sand under general planar loading. Geotechnique, Vol. 49, issue No. 4, pp 453-469

Green, A. P. 1954. The plastic yielding of metal junctions due to combined shear and pressure. J. Mechanics and Physics of Solids, Vol2, issue No. 3, pp 197–211

Jorgensen, M., Steensen-Bach, J.O., Steenfelt, S.S. 1988. Lateral Resistance and Displacement Patterns for Cyclically loaded pipelines in Sand Inferred from Model Testing. Proc. Modelling Soil-Water-Structure Interactions, pp 33-42

Kassimali, A. 1983. Large Deformation Analysis of Elastic-Plastic Frames, J. Structural Engineering, Vol. 109, Issue No. 8, pp 1869-1886

Kennedy J. L. 1993. Oil and Gas Pipeline Fundamentals, Second edition, PennWell Books

Lambrakos, K.F., Remseth, S., Sotberg, T., Verley, R.L.P. 1987. Generalised Response of Marine Pipeline, OTC5507

Lee Y. S., Smith C. C., Cheuk C. Y. 2011. Lateral Breakout Resistance of Shallowly Embedded Offshore Pipelines, Procedia Engineering, Vol. 14, pp 1690–1695

Lyons C.G. 1973. Soil Resistance to Lateral Sliding of Marine Pipelines OffshoreTechnology Conf., Houston, OTC 1876

Martin, C.M. 1994. Physical and Numerical Modelling of Offshore Foundations Under Combined Loads. D.Phil thesis, University of Oxford

Martin, C.M., Houlsby, G.T. 1999. Jack up units on clay: structural analysis with realistic modelling of spudcan behaviour, Offshore Technology Conf., Houston, OTC 10996

Merifield R., White D. J., Randolph M. F. 2008. The ultimate undrained resistance of partially embedded pipelines, Geotechnique, Vol. 58, issue No. 6, pp 461–470

Montrasio, L., Nova, R. 1997. Settlements of shallow foundations on sand: geometrical effects, Geotechnique, Vol. 47, issue No. 1, pp 49-60

Murff J.D., Wagner D.A., Randolph M. F. 1989. Pipe penetration in cohesive soil, Geotechnique, Vol. 39, issue No. 2, pp 213-229

Palmer A.C., Steenfelt J.S., Steensen-Bach J.O., Jacobsen V. 1988. Proc. 20th Offshore Technology Conference, OTC 5853

Randolph MF, Houlsby GT. 1984. The Limiting Pressure on a Circular Pile Loaded Laterally in Cohesive Soil, Geotechnique, Vol. 34, issue No. 4, pp 613-623

Randolph, M. F., White, D. J. 2008. Upper bound yield envelopes for pipelines at shallow embedment in clay. Geotechnique, Vol. 58, issue No. 4, 297-301

Sandford R. J. 2009. The Lateral Resistance of On-Bottom High Pressure and Temperature Pipelines, PhD Thesis, University of Oxford

Stimpson P. 2010. Lateral loading of buried and partially buried pipelines, PhD Thesis, University of Oxford

Taylor N., Gan A.B. 1986. Refined Modelling for the Lateral Buckling of Submarine Pipelines, J. Construct. Steel Research, Vol. 6, pp 143-162

Taylor N., Tran V. 1996. Experimental and Theoretical Studies in Subsea Pipeline Buckling, Marine Structures, Vol. 9, pp 211-257

Tørnes K., Zeitoun H., Cumming G., Willcocks J. 2009. A Stability Design Rationale -A Review of Present Design Approaches, OMAE2009-79893

Verley, R.L.P. and Lund, K. M. 1995. A Soil Resistance Model for Pipelines Placed on Clay Soils, International conference on offshore mechanics and arctic engineering, Copenhagen (Denmark), pp 18-22

Verley R. L. P., Sotberg T. 1994. A Soil Resistance Model for Pipelines Placed on Sandy Soils, J. Offshore Mechanics and Arctic Engineering, Vol. 116, pp 145-153

Wagner, D.A., Murff, J.D. 1987. Pipe-Soil Interaction Model, Offshore Technology Conf., OTC 5504

Weerasinghe M. 2011. Lateral Loading on Pipelines, 4th Year Project, University of Oxford

White D.J., Cheuk C.Y. 2007. Modelling the soil resistance on seabed pipelines during large cycles of lateral movement, Marine Structures, Vol. 21, issue No. 1, pp 59-79

White, D. J., Take, W. A., Bolton, M. D. 2003. Soil deformation measurement using particle image velocimetry (PIV) and photogrammetry. Geotechnique, Vol. 53, issue No. 7, pp 619-631

Zhang J. 2001. Geotechnical Stability of Offshore Pipe-line in Calcareous Sand, Doctoral Thesis, University of Western Australia

Zhang, J., Erbrich C.T. 2005. Stability design of untrenched pipelines–geotechnical aspects. Frontiers in Offshore Geotechnics: ISFOG – Gourvenec & Cassidy (eds), pp 623-628

Zhang J, Stewart DP, Randolph M.F. 2002. Modelling of shallowly embedded offshore pipelines in calcareous sand. Journal of Geotechnical and Geoenvironmental Engineering, Vol. 128, issue No. 5, pp 363-371